Università degli Studi di Palermo

AREA QUALITÀ, PROGRAMMAZIONE E SUPPORTO STRATEGICO
SETTORE STRATEGIA PER LA RICERCA
U. O. DOTTORATI

D067 - TECHNOLOGIES AND SCIENCES FOR HUMAN HEALTH

Dipartimento di Scienze e Tecnologie Biologiche Chimiche e Farmaceutiche (STEBICEF)

SSD: BIO/18

STUDY OF SMALL MOLECULES IN THE FIGHT AGAINST NONSENSE AND SPLICING MUTATIONS THAT CAUSE CYSTIC FIBROSIS

Ph.D. STUDENT:
Dr. Riccardo Perriera

COORDINATOR:
Prof. Vincenzo Cavalieri

TUTOR:
Prof. Laura Lentini

CYCLE - XXXV
2019/2023

CONTENTS.

INTRODUCTION.

1. Cystic fibrosis: one of the most common genetic diseases.

Cystic fibrosis (CF) is one of the most common genetic pathologies (around 89000 cases in 43 countries, in 2020) associated with multiorgan defects, especially in the lungs and pancreas [Bell S.C., et al. 2020]. CF is an autosomal recessive genetic disease found within the Caucasian population. During the 20th century, attention to this pediatric disease increased exponentially after the discovery of its pathologic characteristics. One of the first descriptions of CF was reported in 1938 and it regarded only the infantry patients that presented pancreas fibrosis and nutrient malabsorption [Andersen D.H. 1938].

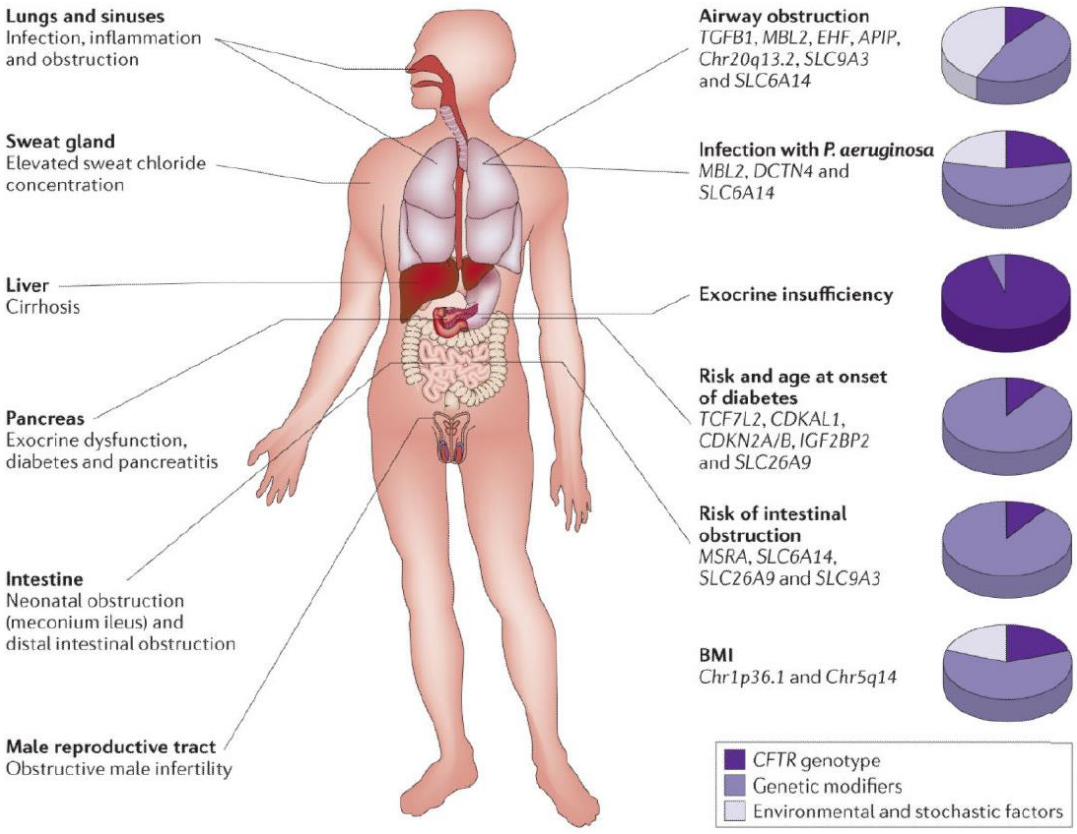

Figure 1: *Clinical features of cystic fibrosis patients (left) and the associated contribution of other genetic modifiers (right). Different organs are affected by cystic fibrosis (CF), especially the lungs and pancreas. Airways obstruction, infections, and pancreatic dysfunction are CF individuals' primary and limiting symptoms. BMI= body mass index. Cutting G.R. 2015.*

The presence of abnormally viscous secretion in the airways and the ducts of different organs of patients with CF causes nutrient absorption defects, inflammation, duct obstruction, and tissue damage, principally in the pancreas and lungs (fig. 1).

In the second part of the previous century, the *Cystic Fibrosis Transmembrane conductance Regulator* gene (*CFTR*) was identified as responsible for CF [Riordan J.R., et al. 1989; Kerem B., et al. 1989; Rommens J.M., et al. 1989]. The *CFTR* gene maps in the

long arm of chromosome 7 and contains 27 exons. The gene encodes for a channel protein (1480 amino acids, 168142 Da), that regulates the anionic flux (Cl^-) through the plasma membrane and the hydration of the organ ducts and some surface of epithelia [Gentzsch M., et al. 2018].

More than 2100 mutations of *CFTR* (CFTR1 database; http://www.genet.sickkids.on.ca) were identified and classified based on dysfunctions that affect the protein [Laselva O., et al. 2022].

Through the improvement in the quality of therapies, in the last years, the life expectancy of people with CF is increased. Based on 2019 American Registry data, the life expectancy of people with CF born between 2015 and 2019 is predicted to be 46 years (fig. 2).

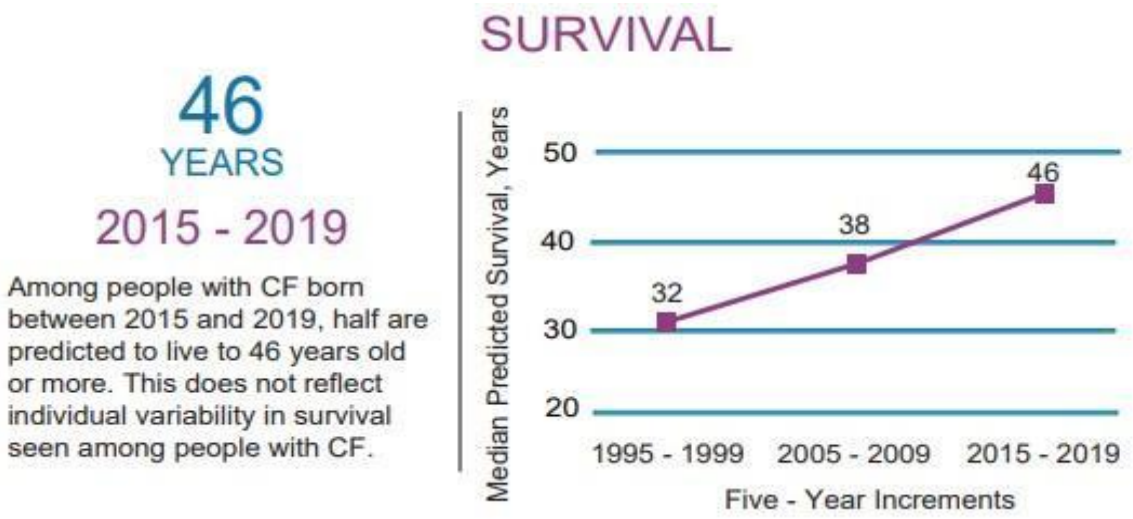

Figure 2: *Survival statistics for the year 2015 through 2019. Cystic Fibrosis Foundation. https://www.cff.org/managing-cf/understanding-changes-life-expectancy.*

2. CFTR physiology and the pathophysiological cascade of cystic fibrosis.

The CFTR protein is an anionic transmembrane channel involved in the regulation of ions transport (Cl^- and HCO_3^-) and in maintaining water flow through the plasma membrane of numerous secretory epithelia (airway, intestines, pancreas, kidney, sweat gland, and male reproductive tract).

Additional functions of CFTR are the bicarbonate secretion for the pH regulation of airway surface liquid (ASL) and the inhibition of epithelial sodium channel (ENaC) that has an important role in the preservation of the osmotic pressure in the cellular secretion/absorption mechanism. The clinical consequences of CFTR alterations are related to the organs and tissues where this channel is expressed [Saint-Criq V., et al. 2017].

2.1 Role of CFTR in the airways.

The principal function of the lungs is to concentrate the oxygen in the blood favoring its transport in all body districts. Simultaneously, the carbon dioxide is removed from blood cells and released outside in the atmosphere.

The lungs include the conducting airways and the respiratory airways. The conducting airways have the function of preventing the access of any noxious matter into the alveolar gas exchanging sites. Moreover, the ciliated cells remove the particles trapped into the mucus layer, produced by mucous cells [Knowles M.R., et al. 2002].

In the conducting airways, CFTR has the fundamental role to maintain the correct hydration of airway surface liquid (ASL) [Saint-Criq V., et al. 2017]. The ASL is a thin liquid layer (around 10 μm) composed of mucus and water in which the inhaled particles and pathogens are trapped and successively removed by the ciliated cells. The secretion of Cl^- by apical CFTR channels generates a water flux that hydrates the mucus layer and preserves the correct density of the ASL and mucociliary clearance (fig. 3A). On the apical surface of conducting airways, CFTR drives Cl^- and HCO_3^- secretion and regulates Na^+ absorption by inhibiting the ENaC. This chemical concentration in the luminal area increases the ASL hydration and pH.

In CF patients the absence of the CFTR or the not correct function of the channel causes ASL depletion and the formation of a thick mucus layer (fig. 3B-D).

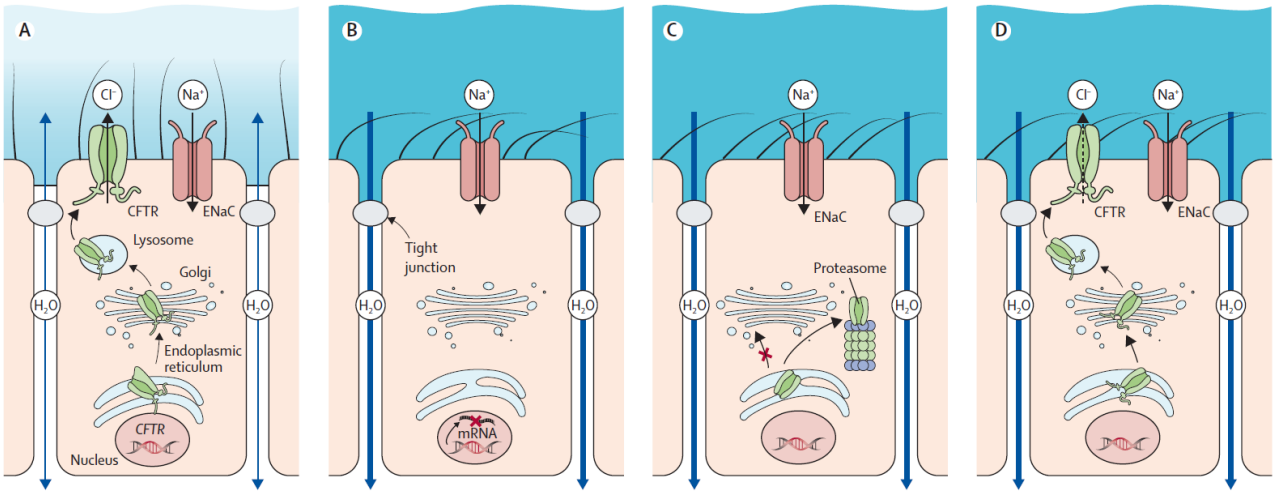

Figure 3: *Role of CFTR in airways and molecular mechanisms involved in cystic fibrosis. A) In physiological conditions CFTR is expressed on the apical membrane of airway cells and maintains the correct mucociliary clearance. (B-D) In cystic fibrosis, according to the mutation, the protein is absent (B), the incorrect folding retains the protein in the endoplasmic reticulum (C), or the channel is not fully functional. Bell S.C., et al. 2020.*

In these conditions, the cilia beat does not remove the inhaled particles and pathogens leading to the establishment of chronic and recurrent lung infections (mainly *Pseudomonas aeruginosa* and *Staphylococcus aureus*). The absence of ENaC inhibition by CFTR activity increases the Na^+ absorption and consequently, the water passes into the basolateral versant, generating a dehydrated mucus layer.

Moreover, the maintenance of correct ASL pH is an important factor for the immune response and the eradication of pathogens trapped in the mucus layer. The alteration of ASL pH modifies the production and activity of antimicrobial peptides (AMPs). Thus, the antibiotics become ineffective in the long term and do not reach the pathogens because the ASL density is too high and bacteria produce biofilm, resulting in lung destruction and respiratory failure. To prevent lung infections, CF people eject the excess airways mucus through specific physiotherapy and aerosol therapy, and take antibiotics everyday for a lifetime [Elborn J.S., 2019].

2.2 Role of CFTR in the pancreas.

The pancreas is constituted of endocrine and exocrine glands. The exocrine part of the pancreas is composed of glands that produce pancreatic juice (containing HCO_3^- and digestive enzymes), and ductal cells for the transport of the secretions into the intestine. Acinar cells excrete a NaCl-rich secretion with different types of digestive enzymes in an inactive form. However, ductal cells assemble the tubular ducts that link pancreas secretions with the intestine [Argent B.E., et al. 2012].

The apical membrane of ductal cells highly express CFTR, which is fundamental for the fluid secretions of the pancreas and the integrity of the gland system (fig. 4). Cl^- and HCO_3^- secretions from the duct cells generate also a flux of Na^+ and water from paracellular versant in order to establish an HCO_3^--rich isotonic fluid. CFTR regulates this HCO_3^- transport in two ways: CFTR regulates the activity of SLC26A, responsible for Cl^-/HCO_3^- exchange, and a direct exit pathway for HCO_3^- [Saint-Criq V., et al. 2017].

A lot of evidence has indicated that insufficient HCO_3^- and less fluid secretion leads to the destruction of pancreas glands. An altered HCO_3^- concentration decreases the pH of pancreatic juice (less than 6,5) and increases the mucus viscosity, causing difficulties in the solubility of digestive enzymes [Hegyi P., et al. 2016].

CFTR defects and structural alterations disrupt completely the electrolyte homeostasis and in consequence the water release into the pancreas ductal area. This condition generates pancreas obstruction and pancreatic insufficiency. CF people are predisposed to the formation of mucin plugs and cysts within the ductal tree [Saint-Criq V., et al. 2017].

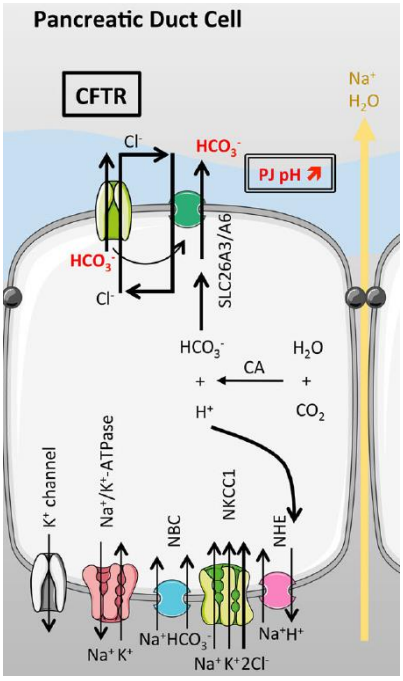

Figure 4: *Ion transport and electrolyte homeostasis of pancreatic duct cells. Cl^- and HCO_3^- are accumulated inside the cell and the other transporter maintains an electrical driving force for the efflux of the ions across the apical membrane. PJ= pancreatic juice, CA= carbonic anhydrase, NBC= Na^+-bicarbonate cotransporter, NHE= Na^+/H^+ exchanger. Adapted image, Saint-Criq V., et al. 2017.*

The enzyme-secreting capacity and the structural integrity of the pancreas degenerate in CF condition, already during the child age. For these reasons, CF people take drugs and pancreatic enzymes to prevent the malabsorption of nutrients for a lifetime. Strategies to improve CF pancreas HCO_3^- secretion are limited because most people present a marked pancreas tissue destruction at birth.

2.3 Role of CFTR in the sweat gland, intestine, and male reproductive tract.

CFTR protein is also expressed in the sweat gland, gastrointestinal tract, and male reproductive tract.

The sweat gland is a tubular exocrine gland that is located in the lower part of the dermis, and it is connected to the surface of the skin by a duct. The gland is divided into two functional parts: the secretory coil that produces the primary sweat and the absorptive straight duct that absorbs NaCl but not water. CFTR is expressed in both functional parts of the gland [Wine J.J., 2022]. In the sweat gland, CFTR activity permits the re-uptake of salt (NaCl) and ions during the regulation of the whole temperature of the body in response to a hot environment. The sweat is secreted by eccrine glands, and it consists of a hypotonic solution of water and salt, compared to the interstitium. Other functions of sweat are the production and secretion of antimicrobial peptides (AMPs) and skin lubrication. Sweat gland disorders, such as CF, lead to abnormal NaCl absorption and in consequence

excessive salt loss, to decrease of secreted volume, and uncontrolled and excessive sweat secretion [Saint-Criq V., et al. 2017].

Cells of the intestinal tract highly express CFTR (fig. 5), especially in the crypt cells, with respect to the stomach in which this protein is not too present.

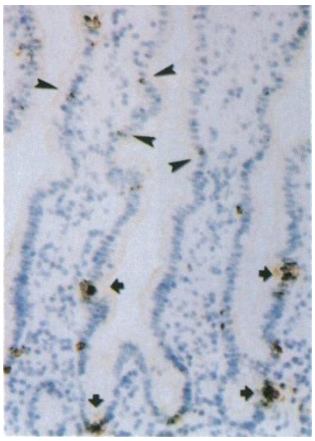

Figure 5: *Localization of CFTR mRNA in the small intestine. Using an anti-sense probe specific for CFTR mRNA, the duodenal section image shows highly positive cells for CFTR mRNA (indicated by the arrowheads). An antibody specific for endocrine protein was used to identify enteroendocrine cells (arrows). Adapted image from: Strong T.V., et al. 1994.*

The principal role of this channel protein is the secretion of bicarbonate and fluid to digest and absorb nutrients. When CFTR function is reduced, the digestion and absorption do not work correctly and the dehydrated luminal environment generates an accumulation of mucus [Gabel M.E., et al. 2019]. The most serious complication is the obstruction of the intestine (terminal ileum or proximal large intestine) that causes rupture and sepsis of the tissue. In addition, all these symptoms lead to microbial dysbiosis and chronic inflammation.

Obstruction of the male reproductive tract is the first cause of CF male infertility. *CFTR* mutations are correlated with oligospermia, epididymal obstruction, congenital bilateral absence of the vas deferens (CBAVD), and idiopathic ejaculatory duct obstruction (EDO). Seminal vesicles do not secrete a normal amount of fluid and that is associated with CFTR defects, in analogy to the obstruction of the pancreas ducts or the intestine lumen [Yoon J.C., et al. 2019].

3. CFTR protein structure and function.

Cystic fibrosis transmembrane conductance regulator is a member of the ATP-binding cassette (ABC) transporter proteins, but it is an anionic channel. CFTR is composed of 1480 amino acids that constitute an anionic pore with gating regulation.

The ABC transporters have the function to move substrates across the plasma membrane, into the cells, or in the extracellular domain. Generally, the ABC transporter structure is composed of two transmembrane-spanning domains (TMDs) and two nucleotide-binding domains (NBDs). The TMDs represent the core of the transporter while the NBDs are the regulatory domains that interact with ATP and protein kinase for transport activity. CFTR is a unique ABC transporter in which the TMDs form an ion channel, and possess a particular regulatory domain, named R region (fig. 6). The two TMDs are composed respectively of 6 alpha-helices that are located inside the phospholipid bilayer of the plasma membrane, while the two NBDs are a mix of alpha-helices and beta-sheets, that are placed in the cytoplasm. NBD1 and NBD2 are linked through the R region, an alpha-helix domain that prevents the interaction between the two NBDs. The TM8 is a different alpha-helix because it is more flexible compared to the other TM domains. This transmembrane helix is fundamental for the conformational change during the open-close process of the channel, as well as the TM6, TM7, and TM12 [Liu F., et al. 2017].

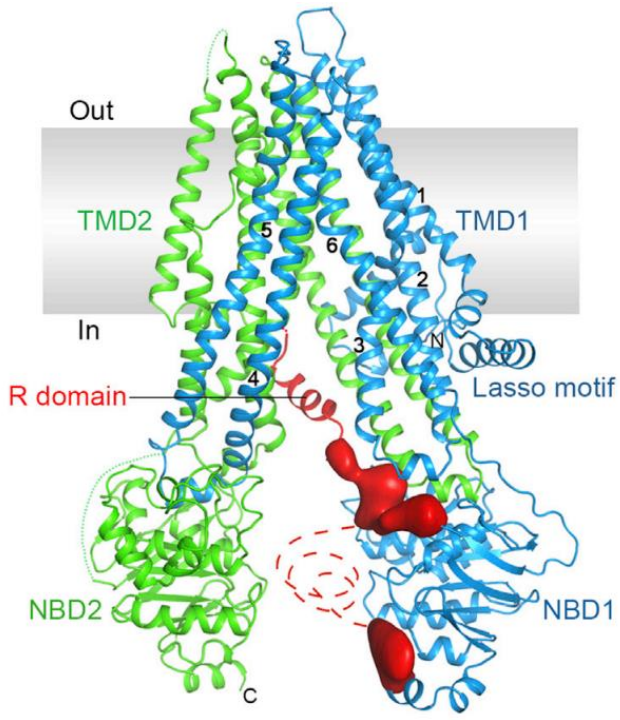

Figure 6: *Structure of human CFTR in the dephosphorylated and ATP-free conformation. The electron densities in red correspond to unstructured regions. The numbers represent the helix region of the TMD1. Liu F., et al. 2017.*

TMDs and NBDs are linked with the intracellular loop and when the regulatory domains bind ATP, the two NBDs form a dimer that induces the TMDs pore opening.

Based on the most recent kinetic model of allosteric modulation, CFTR is found in a dynamic state between closed and opened conformation in presence of both ATP and phosphorylation by protein kinase A (PKA) [Mihályi C., et al 2020].

The channel contains a large number of positively charged amino acids such as arginine and lysine, that have a role in attracting anions into the pore through electrostatic interactions. Other positive charged amino acids are presented in the extracellular side of the TMDs in order to attract anions inside CFTR [Linsdell P., 2017].

The R region is an unstructured/alpha-helix domain that has multiple sites of phosphorylation by protein kinase A (PKA). The unphosphorylated form of the R domain has an inhibitory effect on CFTR because this R loop prevents the NBDs dimerization and in consequence the chloride channel opening [Liu F., et al. 2017; Kleizen B., et al. 2020].

In general, the unphosphorylated state of CFTR increases the probability of a closed conformational state, otherwise, in a phosphorylated state and in presence of ATP, the opening state is favored.

The catalytic subunit of PKA (around 30 kDa) can interact easily with the R region's multiple serine sites during channel activation because there are no steric obstacles during phosphorylation.

When the multiple sites of the R domain are phosphorylated by PKA (in presence of ATP), this domain moves from the inhibitory position, and the NBDs can interact to generate a dimer, inducing the pore opening (fig. 7).

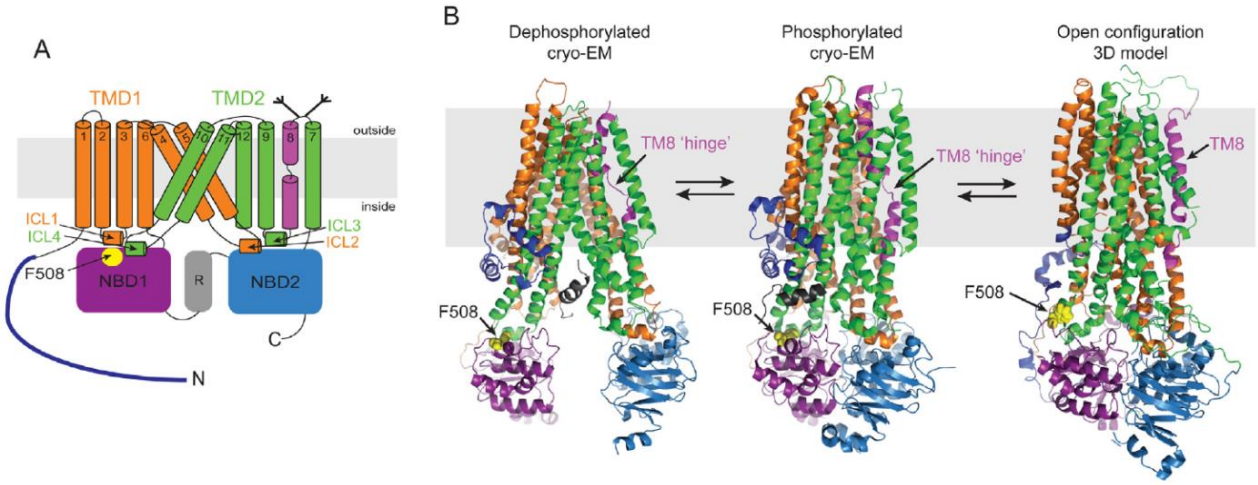

Figure 7: *Opened and closed conformation of CFTR. A) Schematic representation of CFTR domains. B) Cryo-EM models of CFTR in a dephosphorylated and phosphorylated form. The position of the TMDs reflects the open and closed conformation of the channel protein. ICL= intracellular loop, Cryo-EM= electron cryomicroscopy. Kleizen B., et al. 2020.*

4. CFTR mutations and classification.

Nowadays, over 2100 different variants of *CFTR* are identified (CFTR1 database, http://www.genet.sickkids.on.ca) but not all molecular consequences are clarified for each different mutation. The classification was made according to the mechanism of CFTR

synthesis reduction, impaired trafficking, function or stability, and alterations that are caused by various mutations (fig. 8) [Bell S.C., et al. 2020].

The most diffuse *CFTR* mutation is the F508del (Phe508del, around 70% of the worldwide CF people), a deletion of a triplet codifying for a phenylalanine amino acid in position 508 (polypeptide chain).

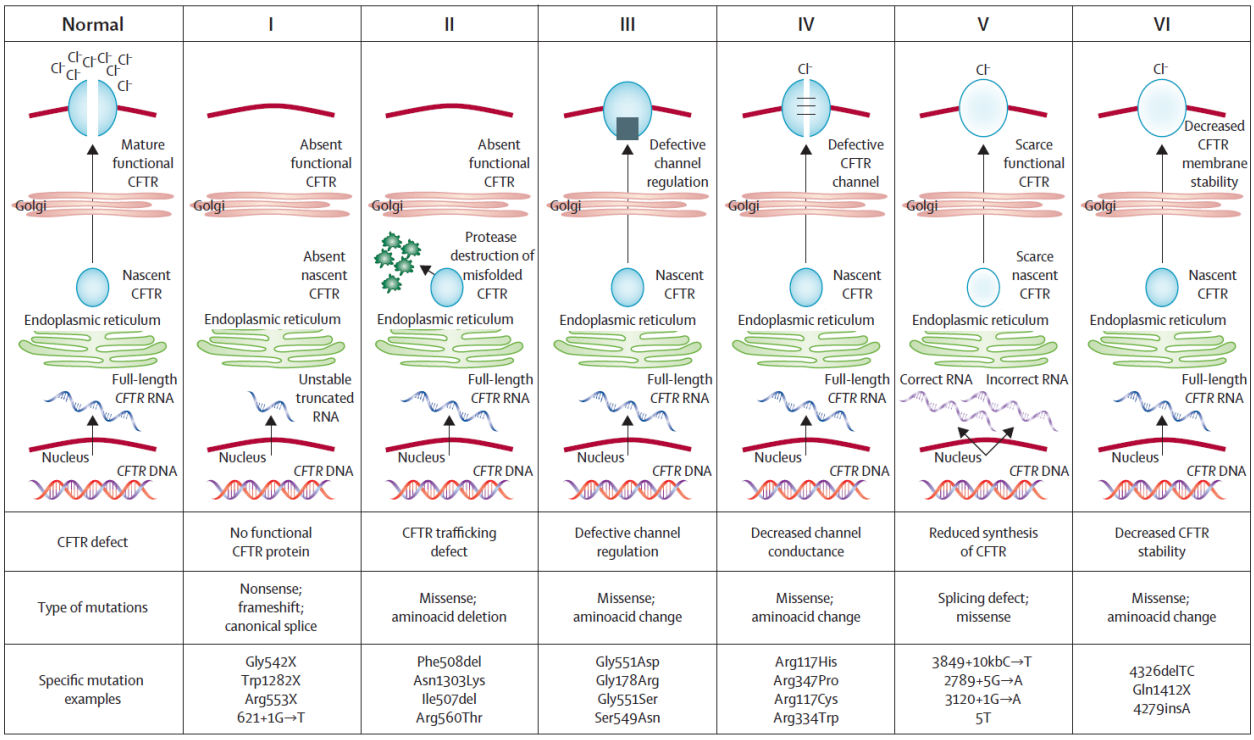

Figure 8: *Classification of CFTR mutation. Class I results in no protein. Class II causes retention of misfolded protein and degradation. Class III defects consist of impairing channel opening. Class IV mutations reduce pore conductance. Class V leads to decreasing in mRNA or protein. In class VI mutations CFTR is less stable in the plasma membrane. Boyle M.P., et al. 2013; Bell S.C., et al. 2020.*

In general, class I, II, and III are associated with poor or no CFTR function and result in a severe CF phenotype, such as exocrine pancreas insufficiency and recurrent lung infections. The class IV and V mutations have residual CFTR functions. The class VI variants are the less severe, with a decrease in CFTR stability. Another classification group (class VII) exists, and it includes the unrescuable *CFTR* mutations (e.g. dele2,3) characterized by the absence of CFTR mRNA [De Boek K., 2020].

The classification of *CFTR* mutations:

- **Class I** mutations include nonsense, frameshift, and canonical splice site mutations that lead to the formation of premature termination codon (PTC). The substitution of a coding triplet with a PTC or the translation reading shift generates an in-frame stop codon that induces the premature termination of the translation process.

The consequence is the production of a truncated polypeptide, which is not functional and it will be degraded by the proteasome.

In addition, mRNA harboring PTCs are prematurely degraded by the nonsense-mediated mRNA decay pathway (NMD), a quality surveillance system of the cell. For this reason, two subclasses of this group of mutations exist: class 1a precludes CFTR synthesis, and class 1b generates a truncated form of the protein [Laselva O., et al. 2022].

Nonsense mutations have a frequency of around 10% (CFTR2 database, https://cftr2.org/) and include the most prevalent G542X, W1282X, and R553X mutations [Laselva O., et al. 2022]. In Italy, the percentage reaches 20% of CF patients (REG. ITA. CF Report 2018).

The G542X is the most diffuse nonsense mutation and it is common in a Mediterranean population. This mutation generates a completely not functional CFTR channel. Besides, the W1282X is diffuse in the Jewish populations and it is the second most common nonsense mutation. The presence of the PTC in position 1282, deletes part of the NMB2 domain preventing NBD dimerization and the proper CFTR folding.

However, spontaneous or induced translational readthrough (a molecular mechanism that leads to the overcome of PTC) allows to the translation of a complete channel that will contain a non-conservative amino acid [Xue X., et al. 2017].

Nonsense mutations are extremely adverse for CF patients because the absence of CFTR protein limits the use of drugs that increase CFTR activity (CFTR modulators). The only strategy to restore nonsense *CFTR* mutations is gene therapy using the CRISPR/Cas9 approach or similar DNA/RNA modifications, and the pharmacological approach by translational readthrough-inducing drugs (TRIDs) [Pranke I., et al. 2019].

Gene therapy is an emerging method to treat genetic pathology, but nonsense suppression therapy with TRIDs is a promising, more accessible, and specific clinical management for nonsense-related CF care.

- **Class II** mutations are characterized by defects in the trafficking and processing of CFTR protein that does not reach the apical membrane of the cells. The protein is retained in the endoplasmic reticulum (ER) and degraded by the ubiquitin-proteasome pathway. The F508del mutation is the most representative mutation of

this class. The altered folding of F508del CFTR causes the activation of ER quality control pathway and the elimination of this defective protein [Fukuda R., et al. 2020].

Today, many promising compounds named "CFTR correctors" are able to correct the folding defect of F508del and prevent CFTR degradation [Tewkesbury D.H., et al. 2021]. In the last years, many CFTR modulators have started the "target therapy era" in order to correct CFTR defects in a specific way. One of them, Ivacaftor (VX-770), induces an allosteric correction of CFTR function increasing the open conformation probability of the channel and its functionality. Ivacaftor binds CFTR in a state-dependent manner, it has a higher affinity for the open state and lower for the closed state.

This is a method to favor the achievement of functional conformation of CFTR with respect to the mutated one [Yeh H.I., et al. 2017].

Ivacaftor induces improvements in ions transport, ASL height, and ciliary beating *in vitro*, but only modest clinical benefit. However, a combination with the potentiator Ivacaftor and two correctors, Elexacaftor (VX-445) and Tezacaftor (VX-661), generates an increase of F508del mutated CFTR protein function resulting in an improved chloride ion transport [Middleton P.G., et al. 2019; Ridley K., et al. 2020]. Results derived from studies of this triple combination of CFTR modulators have allowed the synthesis of a single compound that contains Elexacaftor, Tezacaftor, and Ivacaftor. This new molecule, approved by Food and Drug Administration (FDA), is known as Trikafta™ (also known as Kaftrio®; Vertex Pharmaceutical) and its clinical use showed better symptoms improvement than single CFTR modulators treatment, in patients with mutations related to CFTR trafficking and gating defects [Heijerman H.G.M., et al. 2019].

- **Class III** mutations are represented by gating defects of the channel protein. Mutations such as G551D alter the activity of NBD1 and the resulting CFTR protein exhibits a much lower opening probability than wild-type (WT) channels. The ATP binding pocket is localized in NBD1 and it is not accessible for the ATP. This condition is associated with severe CF phenotype [Laselva O., et al. 2022]. Some molecules are known as "CFTR potentiators" restore or enhance the channel activity of CFTR. Normally the resulting phenotype is severe CF form, but the care with CFTR potentiators (e.g. Ivacaftor and GLPG1837) help to keep the channels in the open conformation for longer [Davies J.C., et al. 2019].

- **Class IV** variants lead to a similar effect to class III mutations, showing a reduced chloride conductance of the CFTR protein [Laselva O., et al. 2022]. The quantity of ions passing through the pore is decreased but the chloride flux is not completely deleted, generating a less severe form of CF. Examples of this class of mutation are R117H and R334W. The class IV defects are also restorable by the treatment with CFTR potentiators [Laselva O., et al. 2022].

- **Class V** mutations are often splicing mutations in which the quantity of the CFTR protein is not sufficient to work on the cell surface. Alternative splicing or errors during the maturation of CFTR mRNA generate a reduced amount of the protein [Deletang K., et al. 2022]. Splicing mutations represent 12% of all reported CFTR mutations, and some of these are 3849+10kb C>T and the polymorphism T_nTG_m. This frequent polymorphism located at the end of intron 9 (formerly known as intron 8) is known to influence the splicing efficiency of exon 10 [Pierandrei S., et al. 2019].

  Alleles bearing less T and more TG repeats are associated with a lower rate of exon 10 inclusion. The CFTR transcript with exon 10 skipping encodes for a misfolded and non-functional protein lacking 21% of the N-terminal end of the NBD1 region [Deletang K., et al. 2022]. Expression of this protein isoform in combination with a CF-causing mutation in trans can be associated with monosymptomatic forms of CF, like the congenital bilateral absence of the vas deferens (CBAVD) or chronic airway diseases [Deletang K., et al. 2022].

  Moreover, the 5T allele is also known to modify the expressivity of the p.Arg117His mutation when this is in cis [Deletang K., et al. 2022]. Usually, splicing mutations result in a less aggressive CF phenotype, however, if the mutation alters the splicing site around exons fundamental for the functionality of CFTR or generates the formation of a PTC, the resulting phenotype is more severe and the mutation is included in another class (class I) [Bergougnoux A., et al. 2019; Deletang K., et al. 2022].

  Ideally, compounds that selectively modify RNA splicing, would represent a better option to correct splicing defects. Recent studies reported the successful use of small molecules modulating splicing in different Mendelian conditions like familial dysautonomia (FD) [Salani M., et al. 2019]. Among effective compounds, *kinetin* (fig. 9), a plant cytokinin used topically for its antiaging properties, was shown to

modulate splicing in mutated *ELP1* and *IKBKAP* genes [Salani M., et al. 2019; Ajiro M., et al. 2021].

Figure 9: *Kinetin and RECTAS structures. RECTAS differs for Cl substituent (red part), compared to kinetin.*

More importantly, *kinetin* was successfully administered to 8 FD homozygotes for splicing mutation leading to a significant increase in wild-type IKBKAP mRNA in leukocytes. Recently, also a *kinetin* synthetic analogue RECTAS (fig. 9, red part) was shown to promote better exon 20 inclusion in the same gene [Ajiro M., et al. 2021].

Overall, the encouraging results obtained in FD suggest that splice-modulating drugs have the potential to become valuable future therapeutics for the treatment of different genetic diseases, including CF. Splicing mutations may cause serious CF phenotypes in patients and a specific cure for all splicing variants (more than 200) does not exist [Deletang K., et al. 2022]. Evaluation of *kinetin* and RECTAS efficacy in CF research models is an important challenge to find a future target therapy for *CFTR* splicing mutation.

- **Class VI** includes *CFTR* variants associated with the production of functional CFTR protein but unstable, leading to quick degradation (lysosome mediated degradation) once on the cell apical membrane [Strub M.D., et al. 2020]. This class includes Q1412X and 4326delTC and these are considered also less severe CF diseases. CFTR correctors work in class VI mutations [Yeh J.T., et al. 2019].

According to researchers, another classification could be done, composed of mutations for which there are no drug treatments at present [De Boeck K., 2020]. This is a new class, class VII or class zero, which is associated with severe disease and the only methodology to target these alterations is gene therapy (e.g. dele2,3 mutation).

The principal aim of CF mutation treatment is the restoration of CFTR function to approximately 25% with respect to the WT value. In this case, the probability to confer a tangible clinical benefit increases [Laselva O., et al. 2022].

5. Nonsense mutations and translational readthrough mechanism.

Translation of messenger RNA (mRNA) into protein is a necessary molecular mechanism for the decoding of genetic information in all cells. Translation starts at an initiation codon (AUG codon) and continues up to one of the three stop codons UAA, UAG, or UGA, generating a full-length polypeptide chain. Sometimes, ribosomes may ignore the stop signal overcoming the point in which the translation should be concluded, and generating a protein that will have an extra C-terminus portion compared to the normal one. This event, in which the ribosomes bypass the stop codons is named "translational readthrough" [Palma M., et al. 2021]. The absence of termination codon recognition can constitute a decoding error but also represents a system to express protein isoforms (programmed translational readthrough) or a therapeutic approach for some pathologies (induced translational readthrough) [Palma M., et al. 2021].

5.1 Translation termination.

Translation termination is an efficient process in which the nascent polypeptide chain is released from the translation complex (ribosome and tRNA) when the ribosome reaches a stop codon.

Translation termination takes place when A site of the ribosome achieves one of the three stop codons (UAA, UAG, or UGA). In this case, the translation termination complex and the near-cognate tRNAs compete to bind two of the three stop codon bases (fig. 10) [Palma M., et al. 2021].

The translation termination complex is composed of two protein factors named eukaryotic release factors 1 and 3 (eRF1 and eRF3). The eRF1 factor mimics a tRNA and enters into the A site to bind and recognize the stop codon (all of the three stop codons). The eRF3 protein is a GTPase that is stimulated by the interaction with polyA-binding protein (PABP) during the translation termination at the physiological stop codon (also known as natural termination codon, NTC), or it is stimulated by the nonsense-mediated mRNA decay (NMD) factor UPF3B at a premature termination codon (PTC) [Neu-Yilik G., et al. 2017]. After the conversion of GTP to GDP, eRF3 modifies the conformation of eRF1 promoting the release of nascent polypeptide and the termination of translation. eRF3 was replaced by the ATPase ABCE1 (ATP binding cassette subfamily E member 1) that induces the recycling of the two ribosome subunits after the hydrolyzation of ATP to ADP [Palma M., et al. 2021].

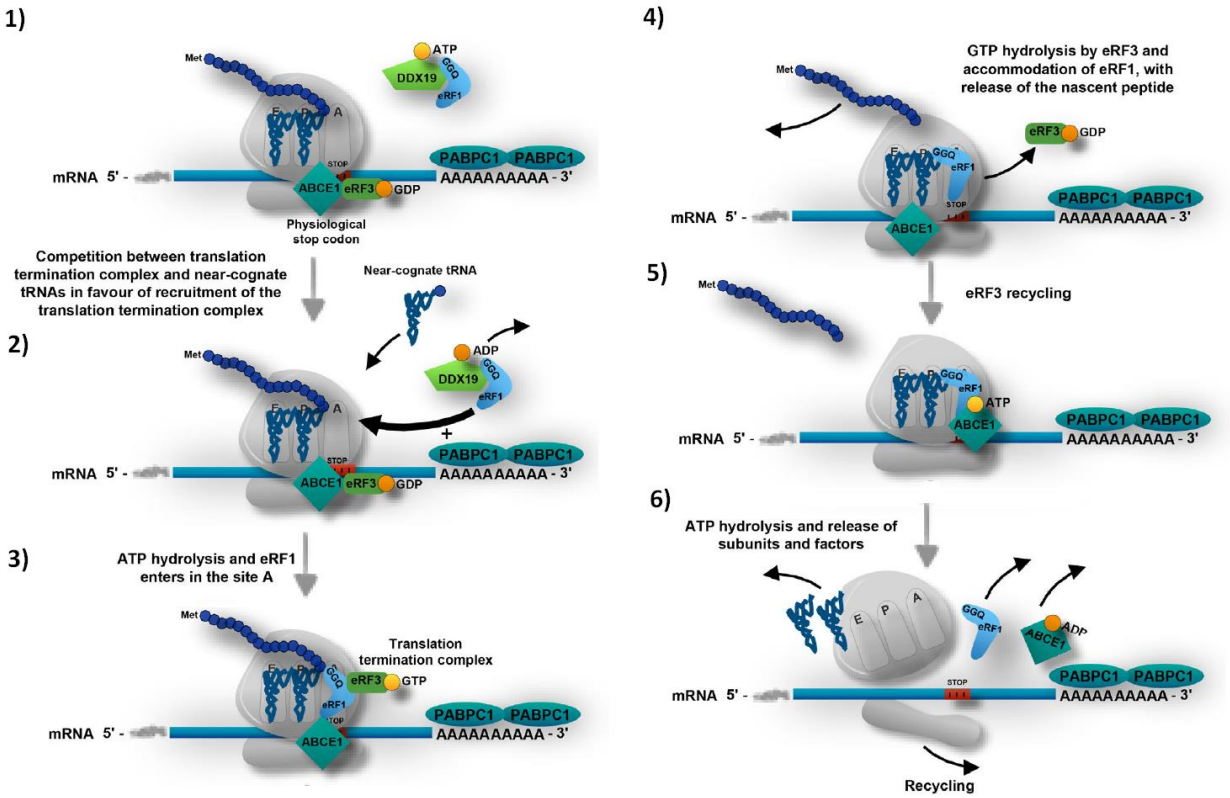

Figure 10: *Translation termination mechanism. When the ribosome covers the stop codon in the A site, eRF3 and ABCE1 interact with the ribosome. ABCE1 recruits the DDX19-eRF1 complex (DEAD-box helicase 19B). eRF3 hydrolyzes GTP and modifies the structure of eRF1, with subsequent dissociation of the peptide. Adapted image from Palma M., et al. 2021.*

5.2 Translational readthrough.

There is a low probability that a near-cognate tRNA can be inserted in the A site of the ribosome during translation termination instead of release factors. In this case, the translation continues until a next stop codon promoting the termination of the process. This mechanism is named “stop codon readthrough”, a molecular event divided into three typologies depending on the presence of regulatory elements or readthrough-inducing drugs [Palma M., et al. 2021].

Stop codon readthrough efficiency can be influenced by different kinds of factors such as stop codon identity, the nucleotides surrounding it (genetic context), proteins, and RNAs.

The first nucleotide immediately next to the stop codon strongly influences the termination efficiency. A purine in this position helps the translation termination in 90% of the most expressed genes, indeed a pyrimidine near-stop codon facilitates translational readthrough [Wangen J.R. and Green R. 2020].

-Induced translational readthrough:

Translational readthrough of the PTCs can be promoted by molecules and compounds generating the misreading during translation (fig. 11). The ribosome does not stop at the premature termination codon in presence of translational readthrough-inducing drugs (TRIDs). In this case, the recruitment probability of near-cognate tRNA is favored with respect to the introduction of release factor (eRF1) into the ribosome A site on the PTC position. Aminoglycoside antibiotics are the first molecules that showed the capacity to induce translational readthrough (such as geneticin, paromomycin, gentamicin, and neomycin). These compounds bind the ribosome minor subunit inside the decoding center and generate a conformational rigidity of the ribosome complex during the recognition of the stop codon [Prokhorova I., et al. 2017]. This mechanism increases miscoding errors and the recruitment of near-cognate tRNA.

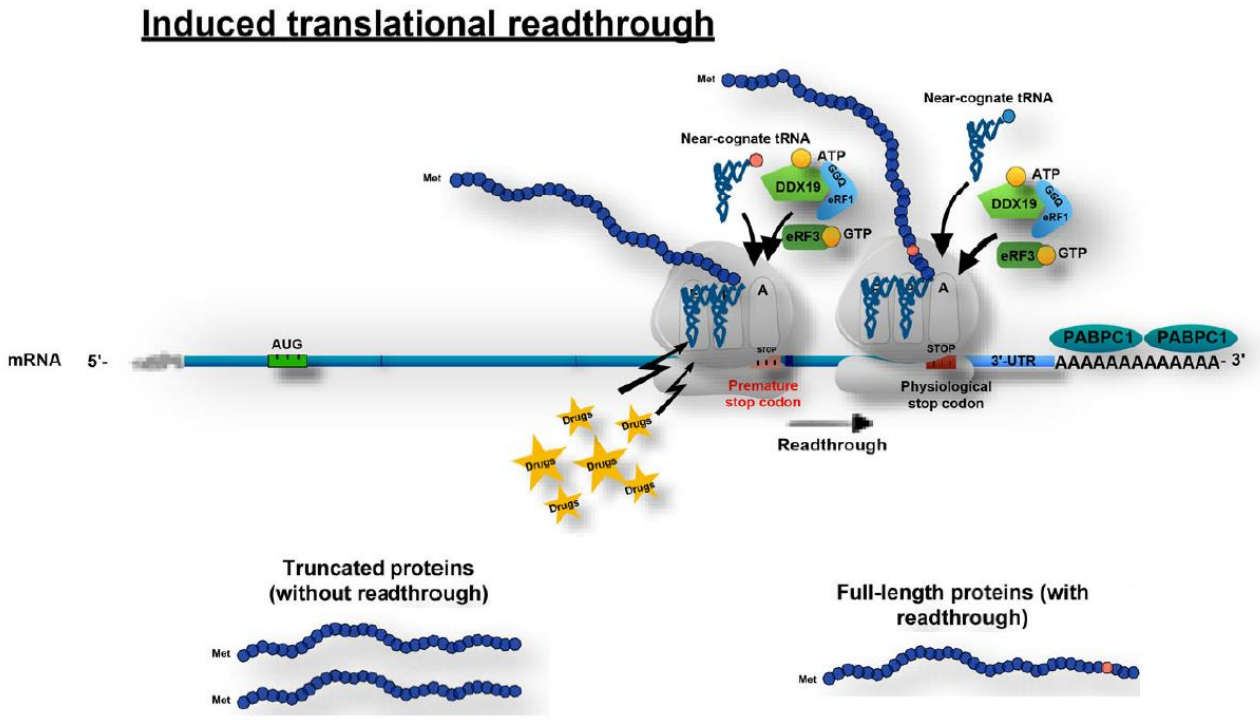

Figure 11: *Induced translational readthrough is promoted by molecules and compounds that force the misreading of the stop codons. UTR= untranslated region. Adapted image from Palma M., et al. 2020.*

However, evidence suggests that new-generation TRIDs do not induce translational readthrough of NTCs but only the readthrough of the PTCs. This specificity is possible thanks to the nucleotides surrounding the NTC, which allow to establish efficiently the translation termination, with respect to PTC [Benhabiles H., et al. 2017].

The induced translational readthrough has two specific limits:

- The quantity of the nonsense mRNAs is less than the normal one because the nonsense-mediated mRNAs decay (NMD) degrades nonsense mRNAs;

- The near-cognate tRNA that is inserted during translational readthrough could deliver a different amino acid in chemical characteristics compared to the original one, influencing negatively CFTR folding and/or functionality. In this case, the nonsense mutation is converted into a missense mutation (as regards the effect on CFTR protein).

6. Nonsense-mediated mRNA decay (NMD) mechanism and inhibitor molecules.

Nonsense-mediated mRNA decay (NMD) is a surveillance pathway used by eukaryotic cells to degrade viral and nonsense mRNAs. NMD activation limits the induced translational readthrough efficiency.
The complex of this surveillance pathway consists of several proteins factors: up-frameshift proteins (UPF), suppressors with morphological effects on Genitalia proteins (SMG), and the exon-junction complex (EJC) with specific subunits [Mailliot J., et al. 2022].
During a translation event, the slow termination at the PTC allows the formation of a ribosome-associated complex with the SMG proteins, UPF1, and the release factors eRF1 and eRF3. This complex interacts with EJC and other UPF proteins (UPF2 and UPF3B), forming the decay-inducing complex (DECID). At this point, the factors responsible for mRNA deadenylation and mRNA-5'-cap removal can modify the nonsense mRNA. mRNAs without 5'-capping result unprotected and susceptible to RNA-exonuclease degradation [Mailliot J., et al. 2022].

6.1 NMD-inhibitor compounds and combination with readthrough agents.

The quantity of the mRNA is a limiting factor for the induced translational readthrough. Some compounds are both TRIDs and NMD inhibitors, for example, Amlexanox^{TM} or Escin, and in theory, these work better to suppress nonsense mutation [Banning A., et al. 2018]. Otherwise, this rule is not absolute because other TRIDs without NMD inhibition capacity promote greater synthesis of full-length proteins than to dual-action molecules, such as 2,6-diamino purine (DAP) [Trzaska C., et al. 2020].
Compounds that inhibit only the NMD pathway as SMG1i or NMDI14 (also known as NMD-14) increase the rescue level in cellular or organoid systems harboring nonsense

mutations using a combination treatment with TRIDs, but generally the inhibition of the NMD pathway could induce a variety of off-target effects [McHugh D.R., et al. 2020]. However, the synergy between TRIDs and NMD inhibitors requires more research efforts in order to understand the clinical benefit of nonsense-related pathologies.

7. Nonsense suppression therapy: Translational Readthrough Inducing Drugs (TRIDs) to treat nonsense mutations.

Several readthrough compounds have been identified during the last decades. According to the general classification, these are divided into two classes: aminoglycosides and non-aminoglycosides readthrough agents.

7.1 Aminoglycoside antibiotics and derivatives.

The capacity to induce PTC readthrough is a potential therapeutic strategy for every nonsense-correlated pathology. For this reason, many studies are focused on the identification of efficient readthrough molecules.
Already in 1985, researchers had observed the readthrough effect of the aminoglycoside antibiotics in mammalian cells [Burke J.F., et al. 1985]. Among the aminoglycosides, there are geneticin (also known as G418) gentamicin, paromomycin, and neomycin (fig. 12), however, other antibiotics do not show readthrough action (e.g. hygromycin, streptomycin, kanamycin, tobramycin).

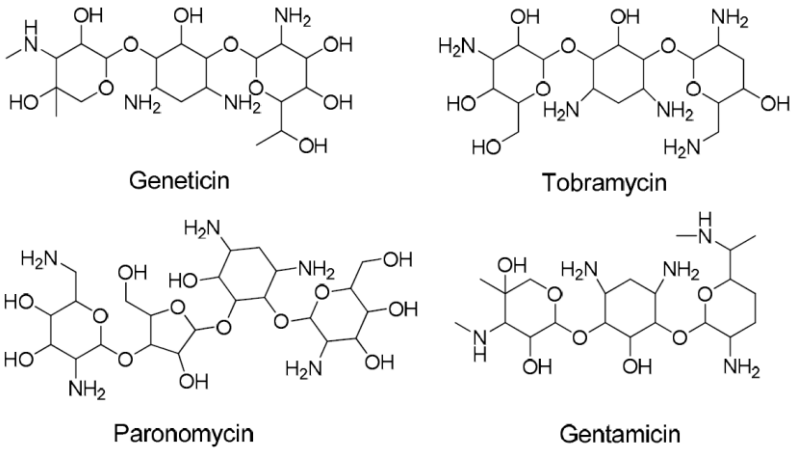

Figure 12: *Molecular structure of the aminoglycoside antibiotics. Geneticin, gentamicin, and paronomycin show readthrough activity, however, tobramycin is an aminoglycoside without the same readthrough effect. Adapted image from Pibiri I., et al. 2020.*

Unfortunately, long-term treatment with aminoglycoside antibiotics causes oto- and nephrotoxicity, and these cannot be used as a treatment for nonsense pathologies (e. g. CF and Duchenne muscular dystrophy, DMD).

ELX-02 (Eloxx Pharmaceuticals; fig. 13) is a synthetic aminoglycoside that shows readthrough activity similar to G418 and the absence of nephrotoxicity [Leubitz A., et al. 2019].

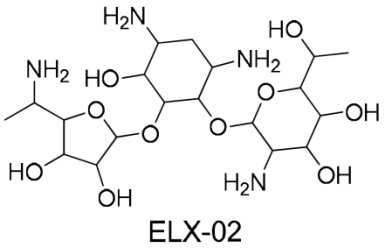

ELX-02

Figure 13: *ELX-02 chemical structure. This compound is composed of sugar substituted with one amino group, a typical aminoglycoside component. Adapted image from Pibiri I., et al. 2020.*

It showed the rescue of nonsense CFTR mutation in CF organoids, but it did not present the same results in CF patients [Crawford D.K., et al. 2021; Venturini A., et al. 2021].
Currently, the phase-II clinical trial using ELX-02 (ClinicalTrials.gov Identifier: NCT04135495) to evaluate the effect on CF patients with G542X nonsense mutation, is concluded (31 July 2022). This clinical trial failed to rescue pulmonary capacity, measured by FEV1 (forced expiratory volume in the 1st second), in G542X CF patients (ClinicalTrials.gov Identifier: NCT04135495).

7.2 Non-aminoglycosides: Ataluren (PTC124) and oxadiazole derivatives.

The necessity to develop a safe and efficient readthrough agent allowed us to identify several non-aminoglycoside molecules that have been shown to promote translational readthrough. The PTC124 (also known as Ataluren or Translarna) is an oxadiazole derivate synthesized to treat nonsense-related diseases such as CF and Duchenne Muscular Dystrophy (DMD). This compound is a readthrough agent that restores CFTR expression and function in cells and transgenic mice [Roy B., et al. 2016].
PTC124 was approved by FDA and EMA (European Medicines Agency) for the treatment of patients with DMD, an X-linked recessive genetic pathology caused by mutations in the dystrophin gene (*DMD*) such as nonsense mutation [Morkous S.S., 2020]. In addition, this TRID is the only molecule that has reached the clinical trial II-III phase for the treatment of CF patients [Kerem E., et al. 2014]. Unfortunately, it showed no significant improvement in CF patients with nonsense mutations. The mechanism of action remains unclear but recent evidence suggest that PTC124 binds two different targets: the 18S portion proximal to the ribosome decoding center and the PTC in the mRNA [Huang S., et al. 2022].

Among the oxadiazole derivatives that promote the induced translational readthrough, there are three new molecules identified by Pibiri I. et al. using a virtual screening of public and in-house libraries and tested by luciferase (FLuc) activity assays [Pibiri I., et al. 2018; Pibiri I., et al. 2020]. The identified compounds are three synthetic 1,2,4-oxadiazole derivatives (NV848, NV914, and NV930; PTC Int. Appl. WO 2019/101709 A1 20190531) with an accessible chemical structure to the synthesis and with readthrough activity (fig. 14) [Pibiri I., et al. 2020].

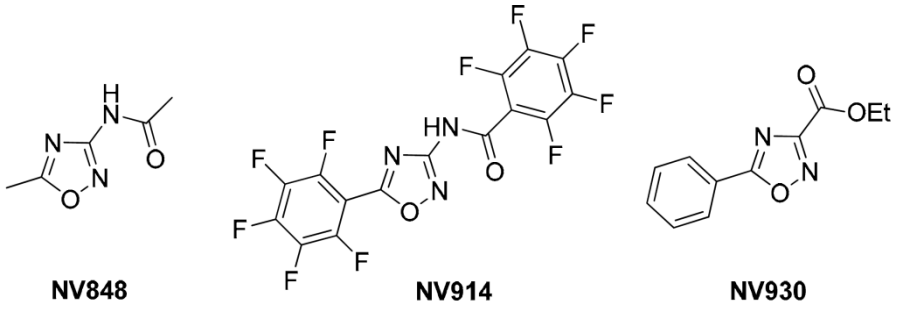

Figure 14: *Oxadiazole derivative structures. These compounds are newly developed TRIDs.*

The oxadiazole compounds NV848, NV914, and NV930 present significant structural differences compared to PTC124: NV848 has acidic and aryl substituents, NV914 presents a maximized fluorine content while NV930 has an organic alcohol moiety. These three TRIDs were tested in CF cellular model system (Fischer rat thyroids cells, FRT) transfected by a vector harboring nonsense mutated (G542X or W1282X) CFTR cDNA. The compounds showed high readthrough efficiency restoring CFTR protein expression and channel functionality [Pibiri I., et al. 2020].

Considering the limits of the pharmacological approach to suppress nonsense mutations, this hopeful evidence must be verified in more complicated CF experimental systems to confirm the readthrough efficacy and molecule specificity of the target (inducing the PTC readthrough and not the NTC readthrough).

8. Advanced *in vitro* systems to evaluate CFTR functionality.

Different model systems were proposed to study CFTR functionality *in vitro* [Ramalho A.S., et al. 2022]. Animal cells that overexpress human mutated *CFTR*, can be used to measure the amount of protein rescue and the channel chloride transport after treatment with specific drugs.

Fischer rat thyroid cells (FRT), suitable transfected with appropriate vectors harboring human wild-type or mutated human CFTR cDNA, are used in the following experimental

studies such as electrophysiology, western blot, compounds screening, immunofluorescence, and others [Sheppard D.N., et al. 1994]. This kind of animal cell is a good system in order to perform a screening of compounds library for all *CFTR* mutations. Otherwise, primary human bronchial epithelial cells (HBE), derived from CF patients, are a more similar biological *in vitro* system, concerning human physiology [Awatade N.T., et al. 2018]. Primary HBE cells are considered the "gold standard" for the analysis of CFTR rescue in all CF research fields.

However, colon (intestinal) organoids contain all of the distinct cell types present in the *in vivo* epithelium. CFTR activity analyzed through organoids 3D cultures has an important utility for the diagnosis and prognosis of CF patients [van Mourik P., et al. 2019]. Organoids derived from CF patient's biopsies (as well as HBE cells) have high CFTR expression at the apical membrane and that allows to study the activity of the channel in a personalized manner.

8.1 Human intestinal organoids and forskolin-induced swelling (FIS) assay.

The intestine is characterized by various kinds of differentiated cells with highly specialized functions [Taelman J., et al. 2022]. *In vivo,* the intestinal surface is structurally organized in villi and crypt domains. The villi are finger-like protrusions of intestinal tissue with the function of increasing the total absorbent area and need to facilitate the passage of fluid and nutrients during digestion.
Besides, the crypts are small domains located in the bottom of villi in which the multipotent stem cells (ISCs) lineage reside for the periodic renewal of the tissue (fig. 15A). Human intestinal epithelium undergoes renewal every 5-7 days thanks to ISCs. ISCs are localized in the bottom of the crypts and can be identified by the expression of the receptor LGR5 for R-respondin (RSPO). Plus, Paneth cells are interspaced with ISCs and they are specialized in the secretion of antimicrobial molecules. Differentiation factors like Notch signaling are secreted by secretory lineage precursor cells and others are produced by specialized mesenchymal cells (Trophocyte and Telocyte) for the maintenance of differentiation factor gradient inside the crypt. However, the absorptive progenitor cells give rise to absorbing enterocytes in the villi, while secretory precursor cells generate enteroendocrine cells, mucus-producing cells, and Paneth cells. The apical cells residing in the apical portion of the villi undergo spontaneous apoptosis.

Intestinal organoids, which are generated from crypt biopsies and ISCs, are self-organizing three-dimensional (3D) structures consisting of both multipotent stem cells and their differentiated progeny.

Generally, organoids recapitulate *in vivo* tissue architecture, cell heterogeneity, and interaction, but it constitutes an *in vitro* model (fig. 15B).

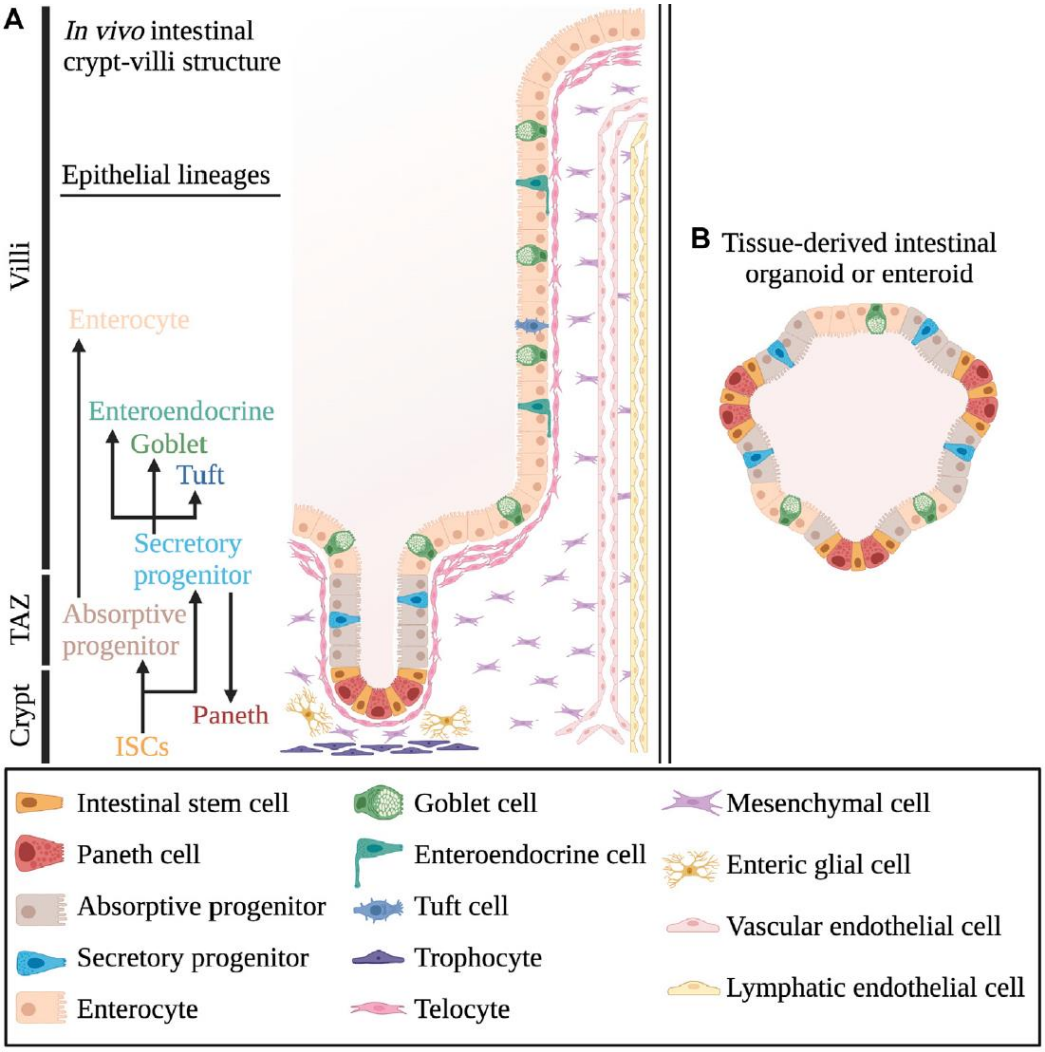

Figure 15: *Cellular organization of intestinal domains and organoids. A) Different cellular types constitute the intestinal epithelium. The cellular heterogeneity reflects the complexity of the tissue function. B) Cellular organization of the organoids is similar to in vivo structures. Adapted image from Taelman J., et al. 2022.*

Organoids could be propagated like human stem cells (bi-dimensional culture; 2D), from which they are derived, but they are more precise than cellular culture and, in some cases, animal models too. When intestinal organoids are completely mature, they present budding crypts and villi, similar to *in vivo* intestinal tissue [Guiu J., et al. 2022]. Intestinal organoids appear as a sort of hollow sphere in which the different cellular types constitute the surface, while inside the sphere there is a cavity named the lumen of the organoids.

Cellular lineage consists of ISCs and progenitor cells, differentiated enterocytes, globet cells, and Paneth cells.

For all these characteristics, intestinal organoids are an innovative and hopeful *in vitro* system to study intestinal function, intestinal-related diseases, and drug discovery screening.

One of the most affected organs in CF is the gastrointestinal system. CFTR is highly expressed in colon tissue and intestinal organoids are an excellent *in vitro* system to study the functionality of the channel through specific assays like the "swelling assay".

The forskolin-induced swelling (FIS) assay permits to quantify CFTR function in intestinal organoids derived from CF patients, especially after treatment with specific compounds. When CFTR is opened by forskolin the chloride enters through the channel in the luminal region of the organoids, together with water, thanks to the osmotic pressure that is generated inside the organoids. The water flow increases the dimension and the luminal area of the organoids after a relatively short period (e.g. 60 min), compared to the initial organoid state. Immediately after the addition of forskolin (t0) or if CFTR is mutated (fig. 16 A-B on top) the organoids appear thin and not swollen.

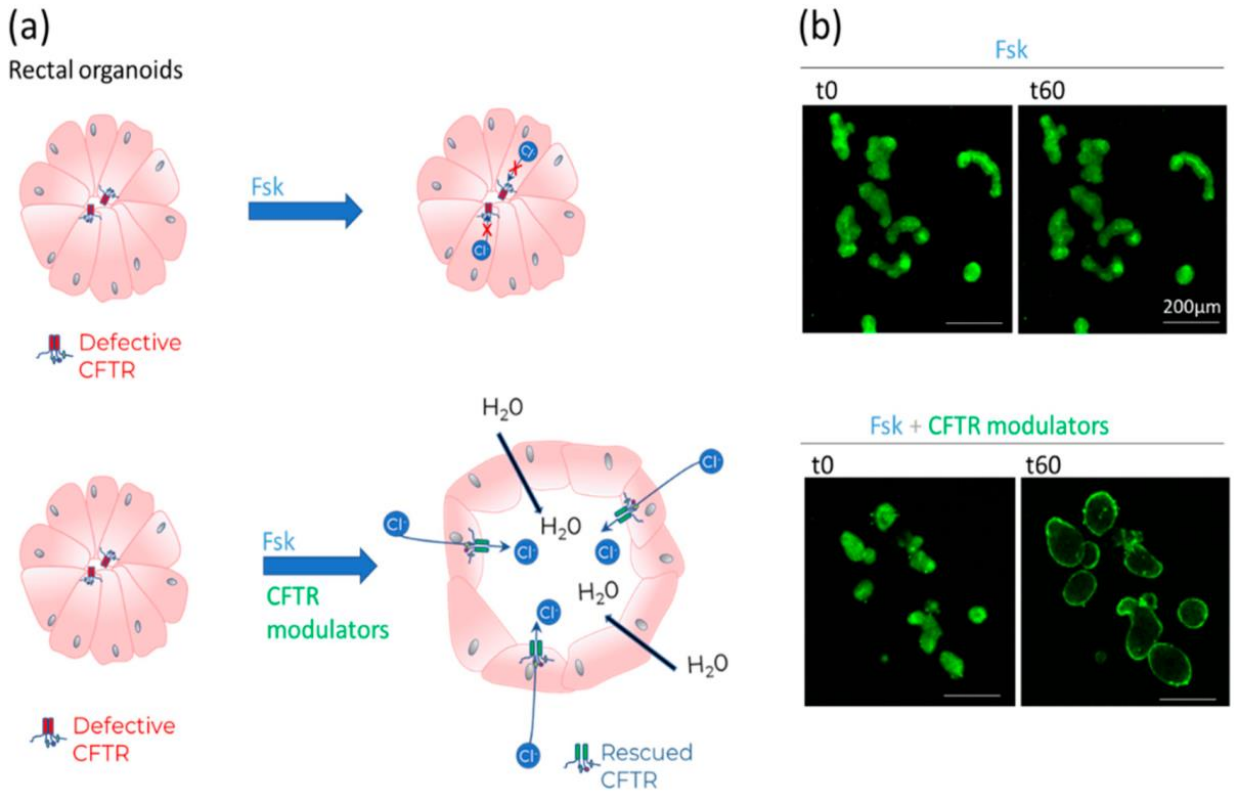

Figure 16: *Schematic representation of forskolin-induced swelling (FIS) assay. A) When the CFTR channel is altered by mutations, the luminal secretion of chloride is absent and also water, resulting in an absence of luminal organoids increasing. Rescue of CFTR by treatment with mutation-specific drugs (e.g. CFTR modulators for F508del) restores the chloride flux and the water entrance inside the lumen increases the organoids area. B) confocal images at time=0 min and time= 60 min (t=0 and t=60) with calcein staining. Adapted image from Ramalho A.S., et al. 2022.*

On the other hand, after a period of time incubation with forskolin (t60, one hour) and if mutated CFTR activity is restored by compound treatment, the organoids appear more or less swollen depending on the rescue level of protein expression/channel activity.

This increasing luminal area is named “swelling of the organoids” and its quantification during time is an indirect measurement of CFTR activity. A positive response in the FIS assay, using CF-derived organoids, predicts clinical response to treatment (readthrough agents, CFTR modulators, gene therapy) [Berkers G., et al. 2019]. The patient-specific sample is the great advantage of this technique, especially for the analysis of rare CF genotypes and personalized clinical approach. However, the organoids model and FIS assay is a really expensive methodology and requires a high level of expertise.

AIMS OF THE PROJECT.

CF is one of the most widespread genetic diseases in the world. Although it is an aggressive and adverse genetic pathology, thanks to progress in both clinical treatments and biomedical research, CF patients' quality of life and their age have improved in recent years [Bell S.C., et al. 2020; Laselva O., et al. 2022].

Currently, only CF patients harboring at least one allele with the F508del mutation are allowed to receive an FDA- and EMA-approved pharmacological therapy (CFTR modulators Trikafta™ or Kaftrio®; Vertex Pharmaceutical) [Zaher A., et al. 2021]. Other CF people carrying different kinds of mutations, such as nonsense and splicing mutations, do not benefit from any target therapy.

For these reasons, biomedical studies are focused on finding target treatments for every *CFTR* mutation' category.

Based on these observations the aims of the present project were focused on the rescue of CFTR protein expression and functionality using different small molecules to fight splicing and nonsense mutations.

Splicing mutations alter mRNA splicing sites and compromise the efficiency of correct maturation of the mRNA. This condition leads to different splice events such as exon skipping, modification of splice sites, and intron retention [Deletang K., et al. 2022].

Today, a specific target therapy to modulate splicing alterations of the CFTR mRNA does not exist and all the treatments are experimental [Deletang K., et al. 2022]. A promising, proposed strategy, used in other genetic diseases characterized by splicing defects, is the use of small molecules that restore abnormal splicing processes. To this aim, the first objective of this Ph.D. project was centered on the rescue of the CFTR protein expression by two small molecules *kinetin* and its synthetic analogous named RECTAS [Salani M., et al. 2019; Ajiro M., et al. 2021].

A specific vector harboring a CFTR *minigene* with the polymorphism T_5TG_{12} (pcDNA3.1-CFTR$^{N59+N510+5T12TG}$), and two regions of the intron 9 and intron 10 was used to produce a cell model system to evaluate *kinetin* and RECTAS ability in the rescue of CFTR expression.

The following step was to clone the CFTR *minigene* into a retroviral vector in order to produce CFTR$^{N59+N510+5T12TG}$ stably expressing cells to obtain a greater number of cells for the analysis. These cells were also used to test *kinetin* and RECTAS capacity to restore the CFTR protein expression.

An important class of CFTR mutations is represented by nonsense mutations. They are a severe genetic defect that leads to the introduction of a premature termination codon (PTC) into the codifying sequence causing the complete absence of the CFTR protein. An innovative therapeutic approach for this genetic defect is nonsense suppression therapy by translational readthrough-inducing drugs (TRIDs). Despite numerous studies, there is not a molecule that resulted efficient in CF nonsense-related clinical trials [Laselva O., et al. 2022; e.g. Elox-02, ClinicalTrials.gov Identifier: NCT04135495]

Recently, three new TRIDs named: NV848, NV914, and NV930 were identified by virtual screening and orthogonal assays by Pibiri I., et al. These molecules showed promising results in different nonsense cell model systems and resulted well tolerated in the murine model [Pibiri I., et al. 2020; Corrao F., et al. 2022].

Therefore, the second part of the project was focused on the rescue of CFTR expression in nonsense-CFTR cell model systems and in human intestinal organoids from CF patients using the three new TRIDs [Pibiri I., et al. 2020].

Moreover, another object of the study was to establish: I) the metabolic stability of the NV molecules by human liver microsomes (HLM), II) the specificity of the PTCs readthrough, and III) the hypothetical mechanism of action (MOA)/biological target of the three molecules.

In particular, the experimental plan is summarized in these main tasks:

TASK#1 Study of CFTR expression in the rescue of splicing mutation defects after treatment with the small molecules *kinetin* and RECTAS.

TASK#2 Rescue of the CFTR expression and functionality by translational readthrough inducing drugs (TRIDs) in nonsense cystic fibrosis (CF) model systems.

TASK#3 NV848, NV914, and NV930 molecule metabolic stability and mechanism of action (MOA) studies.

MATERIALS AND METHODS.

-*Compounds*.

Compounds were prepared and purchased as reported in **table 1**:

Compound	Solvent	Concentration	Manufacturer
Kinetin	DMSO	10 mM	MedChemExpress MCE
RECTAS	DMSO	25 mM	*
Geneticin (G418)	H_2O	200 mg/mL	Gibco
ELX-02	H_2O	8 mM	MedChemExpress MCE
PTC124	DMSO	100 mM	MedChemExpress MCE
NV848	H_2O	100 mM	**
NV914	DMSO	100 mM	**
NV930	DMSO	100 mM	**
NV2899	DMSO	100 mM	**
NV2909	DMSO	100 mM	**
NV2907	DMSO	100 mM	**
NV2913	DMSO	100 mM	**
VX-445 (Elexacaftor)	DMSO	10 mM	Selleckchem
VX-661 (Tezacaftor)	DMSO	20 mM	Selleckchem
VX-770 (Ivacaftor)	DMSO	20 mM	Selleckchem
NMDI14	DMSO	6,25 mM	MedChemExpress MCE

Table 1: *Compounds were dissolved in DMSO (dimethyl sulfoxide, Sigma Aldrich) or sterile water (H_2O) at the indicated stock concentrations. (*) kindly provided by Prof. Duga S, Humanitas University, Milan. (**) TRIDs are produced by Prof. Ivana Pibiri (STEBICEF department), University of Palermo, Palermo. All compound stocks were stored at -20°C.*

-*Cell culture and conditions.*

All cells were cultured in a humidified incubator with an atmosphere of 5% CO_2 at 37°C. HCT116, HeLa, and Phoenix cells were cultured in DMEM (Dulbecco's modified eagle medium, Gibco) supplemented with 10% FBS (fetal bovine serum, Gibco) and 1% Streptomycin and Penicillin antibiotics (Corning). Antibiotics were removed 24 hours before treatments.

Fisher rat thyroid (FRT) cells were cultured in powder Coon's modified Ham's F-12 medium dissolved in 1 L of sterile water for injection (WFI, Gibco) supplemented with 2,68 g/L sodium bicarbonate (AnalytiCals Carlo Erba). The medium was filtered by a specific membrane filtration system (CytoOne® bottle filtration unit 0,20 μm, StarLab) and 10% FBS was then added (fetal bovine serum, Gibco), along with 1% Streptomycin/Penicillin antibiotics (Corning) and 1% glutamine (Corning). Antibiotics were removed 24 hours before the addition of every compound for the experiments.
FRT cells are characterized by the absence of CFTR protein expression and are considered a good model for FC studies.
The FRT-CFTR^{G542X} and FRT-CFTR^{W1282X} cells express human CFTR cDNA (p-TRACER plasmid) harboring the nonsense mutations G542X or W1282X.

Human bronchial epithelial cells (16HBE) were cultured in MEM (minimum essential medium, Gibco) supplemented by 10% FBS (fetal bovine serum, Gibco) and 1% Streptomycin/Penicillin antibiotics (Corning). Before plating, every plate was coated with rat tail collagen (1:100). Antibiotics were removed 24 hours before treatments.
16HBE cells represent a superior *in vitro* system compared to FRT cells for the study of CF.

-Human intestinal organoids.

CF human rectal mucosa tissues were obtained by suction biopsy during a routine clinic visit at the UZ Leuven University Hospital (Herestraat 49, 3000 Leuven, Belgium) by Dott. F. Vermeulen's group. The biopsies were stored in ice-cold phosphate buffer and kept in ice until crypt isolation.
Crypts were isolated from the rectal biopsies and subsequently mixed with 70% matrigel and plated on 24-well plates; human organoid expansion medium (A83-01 500 nM, SB202190 p38 inhibitor 10 μM, EGF 50 ng/ml, Nicotinamide 10 mM, N-Acetylcysteine 1.25 mM, B27 supplement 2%, Wnt3A conditioned medium 50%, fcNoggin conditioned medium 10%, RspoI conditioned medium 20%, ADF+++ 20%) was added after the solidification of matrigel (1 ml for wells) [Vonk A.M., et al. 2020]. The medium was changed every day. Organoids were split by mechanical disruption after 7 days in culture.
Organoids samples used in the experiments were characterized by two different CFTR genotypes: CFTR$^{G542X/G542X}$ and CFTR$^{W1282X/dele2,3}$. In particular, in CFTR$^{W1282X/dele2,3}$ genotype one allele shows a nonsense mutation, and the other allele the dele2,3 class VII

mutation, a large deletion of the *CFTR* gene that results in severe CF phenotype and no CFTR protein expression [De Boeck K. 2020].

-Plasmids and vectors.

pcDNA3.1 plasmids (**fig. 17**; previously provided by Prof. Duga S, Humanitas University) are characterized by the human CFTR wild-type cDNA (pcDNA3.1-CFTR^{WT}) and the human CFTR *minigene* harboring the specific polymorphism (T_5TG_{12}) localized at the 3' end of intron 9 (pcDNA3.1-CFTR$^{N59+N510+5T12TG}$).

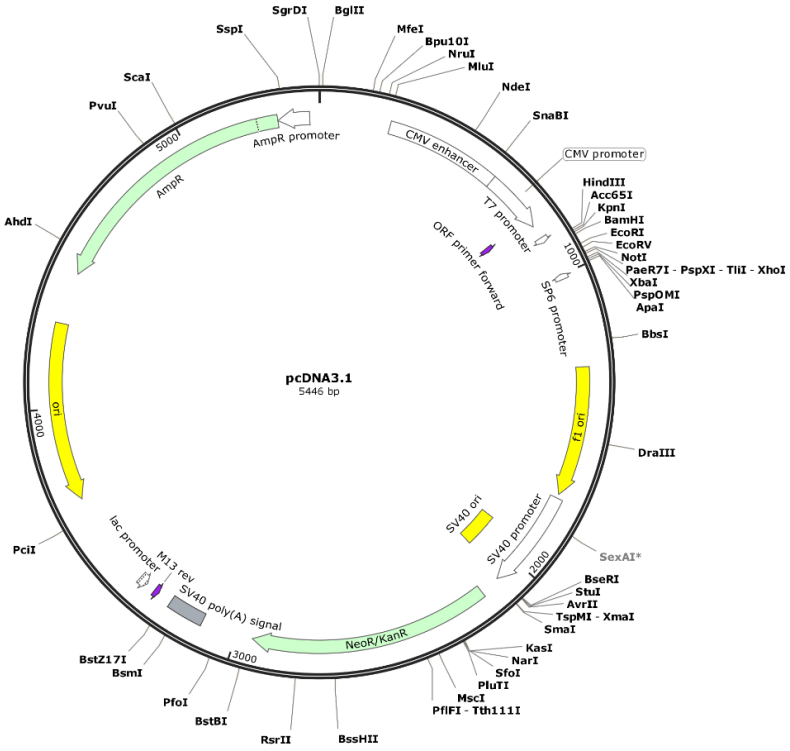

Figure 17: *pcDNA3.1 plasmid backbone map.*

In addition, pcDNA3.1-CFTR$^{N59+N510+5T12TG}$ contains two intron (9 and 10) parts localized at the extremities of exon 10, fundamental for splicing activation (**fig. 18**). The intron 9 and intron 10 fragment sizes are respectively 298 pb and 300 pb in the pcDNA3.1-CFTR$^{N59+N510+5T12TG}$.

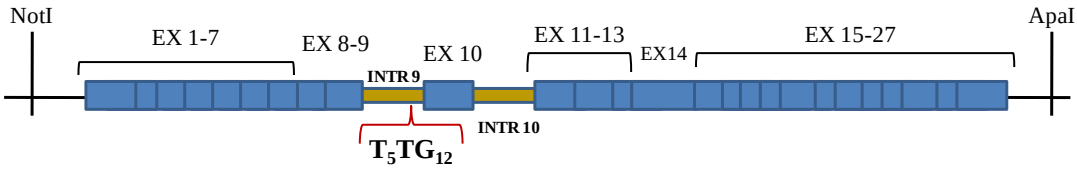

Figure 18: *Schematic representation of CFTR minigene (CFTR$^{N59+N510+5T12TG}$). The polymorphism T_5TG_{12} located in the intron 9 constitutes the CFTR mutation that alters mRNA splicing. In this picture, there are*

also displayed the restriction enzyme (NotI and ApaI) sites used for the cloning. EX, blue: exon; INTR, yellow: intron.

The pcDNA3.1-CFTR$^{\Delta EX10}$ contains the human CFTR cDNA without the sequence of the exon 10, in order to simulate the skipping of the exon 10 caused by CFTR T_5TG_{12} mutation.

-Cloning protocol.

CFTR$^{N59+N510+5T12TG}$ *minigene* and CFTR^{WT} cDNA were recovered from pcDNA3.1 plasmids by NotI-ApaI restriction enzymes and cloned under the control of the tetracyclin-inducible (Tet) system of retroviral vector pBPSTR1, digested with NotI and PmeI (**fig. 19**; Invitrogen) [Paulus W., et al. 1996]. pcDNA clones were first digested with ApaI and 3' protruding ends were removed by T4 DNA polymerase (ThermoScientific). Fragments were then released by NotI restriction and they were dephosphorylated to favor ligation with pBPSTR1/NotI-PmeI (Rapid DNA Dephos & Ligation Kit, Roche). Ligation products were transformed into *E. coli Top10* competent cells. Recombinant clones were screened by colony PCR with primers pBPSTR1-Fw (Fwd: 5'-CCAGACGACGAGGCTTGC-3') and CFTR 6dw (Rev: 5'-CAATAACTTTGCAACAGTGG-3'). The thermal cycle used for the PCR was: (step 1) 3 min, 94°C; (step 2) 20 sec, 94°C; (step 3) 30 sec, 54°C; (step 4) 1 min, 72°C; (step 5) 5 min, 72°C. Steps 1 to 3 were repeated for 30 cycles. Finally, PCR products were separated with agarose gel (1%) electrophoresis in order to verify the correct size of the amplicons.
The two final vectors are the following: pBPSTR1-CFTR$^{N59+N510+5T12TG}$ and pBPSTR1-CFTR^{WT}.
The extremities of pBPSTR1-CFTR$^{N59+N510+5T12TG}$ and pBPSTR1-CFTR^{WT} produced after NotI digestions were then sequenced using Sanger-sequencing methodology by an external company (BMR Genomics). The primers used for the sequencing mapped in the retroviral vector pBPSTR1 (Fwd: 5'-CCAGACGACGAGGCTTGC-3'; Rev: 5'-GACGCCATCCACGCTGTTTTC-3').

-Phoenix cell line and retroviral infection system.

Phoenix (ΦNX) packaging cells (provided from Stanford University, Nolan lab; Pear W.S., et al. 1993) are a human embryonic kidney cell line transformed by adenovirus, which gives rise to high titers of retroviral supernatant. These cells were transfected with the two

retroviral vectors (pBPSTR1; **fig. 19**) containing: CFTR$^{N59+N510+5T12TG}$ *minigene* and CFTR^{WT} cDNA to produce retroviral particles.

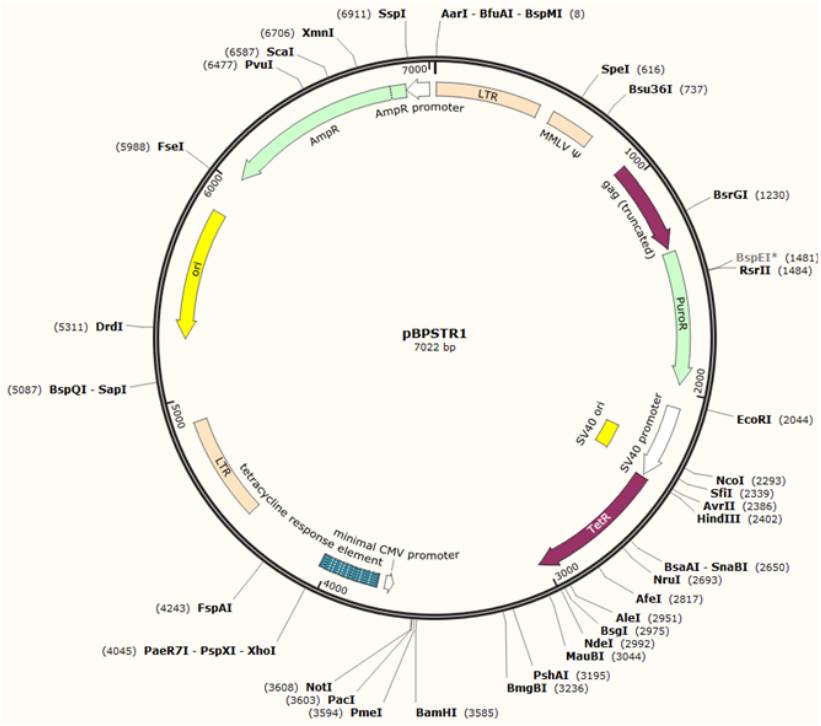

Figure 19: *Retroviral vector pBPSTR1 map. Long terminal repeat (LTR) elements, puromycin resistance cDNA (PuroR), and MMLV Ψ (retroviral psi packaging element) are displayed in the map.*

3x10^6 of Phoenix cells were plated. On the second day, cells were transfected with the above retroviral vectors. The transfections were performed by Lipofectamine^{TM} 3000 Transfection Reagent (Invitrogen) according to the manufacturer's instructions. 72 hours after transfection, the cell medium containing retroviral particles was collected and then filtered with a 0,45 µm filter.

For infection, medium containing retroviruses was added to previously plated FRT cells (3x10^6). Polybrene 1 µg/ml (a cationic polymer that neutralizes charge repulsion between virus and cell) was used in order to promote the interaction between retroviral particles and cells.

The selection of cells stably expressing the retroviral vector (harboring CFTR$^{N59+N510+5T12TG}$ or CFTR^{WT} sequences) was performed by puromycin 1 µg/ml for three weeks.

-Trypan blue assay.

FRT cells were plated onto a 6-well plate at a density of 10^5 cells/well in 2 ml of cultured medium. Cells were then treated with test compounds at the concentration of 12 µM for 24, 48, and 72 hours. Cells were suspended in 5 ml of medium and 100 µL of suspension was

added to 100 µL of Trypan Blue (Sigma Aldrich). Subsequently, 10 µL of the cell suspension was counted in a Burker chamber.

-*Western blotting.*

Proteins samples were extracted from cellular pellets using RIPA buffer (ThermoScientific) and protease cocktail inhibitor (1:100, ThermoScientific) at 4°C. After extraction, proteins were quantified by the Bradford assay method (Coomassie blue dye, Thermo Scientific) and samples were compared to a BSA (bovine serum albumin) protein standard curve at known concentrations.

For the analysis of CFTR, proteins (30 µg) were separated in 3-8% SDS-PAGE gel and transferred to a PVDF transfer membrane overnight at 4°C and 12 V (constant voltage). The membranes were blocked in non-fat dry milk 5% (1 hour at room temperature) and then incubated with primary antibody anti-CFTR (mouse, ab570, CF American Foundation 1:500) overnight at 4°C.

For the analysis of p53, Cys-C, and β2M, proteins (20 µg) were separated in 12% SDS-PAGE gel and transferred to a PVDF transfer membrane, overnight at 4°C and 12 V (constant voltage). Blotted membranes were blocked with non-fat dry milk 5% (1 hour at room temperature) and after that membranes were incubated with primary antibody anti-p53 (mouse, p53 DO-1, Santa Cruz Biotechnology, 1:2000), primary antibody anti-Cystatin-C (rabbit, Cell Signaling Biotechnology, 1:1000) or primary antibody anti-β-2-Microglobulin (rabbit, Cell SignalingBiotchnology, 1:1000), overnight at 4°C. Anti-β tubulin primary antibody (mouse, Sigma Aldrich, 1:5000) was used to detect β-tubulin as a loading control to normalize the protein bands.

After three washes (15 min on shaker) with TBS-Tween^{TM}-20 1X (ThermoScientific), membranes were incubated with anti-mouse (Invitrogen, 1:5000) or anti-rabbit (Promega, 1:2500) HRP-conjugated secondary antibodies for 1 hour. After incubation, the membranes were washed three times (15 min on a shaker) with TBS-Tween^{TM}-20 1X (ThermoScientific). The detection of the bands was performed by SuperSignal® West Femto kit (ThermoScientific) and images were acquired by ChemiDoc MP imaging system (Bio-Rad). Gel bands were quantified by ImageJ software.

-*Immunofluorescence microscopy.*

FRT and HCT116 cells were grown on round glass coverslips in 12-well plates with 1 ml of medium (without antibiotics). After removing the medium and one wash in DPBS 1X (Dulbecco's phosphate buffer saline, GIBCO), cells were fixed with cold methanol for 1 min and treated with Triton-X 0,01% for 10 min at room temperature. After washing, fixed cells were blocked in BSA (bovine serum albumin) 0,1% for 1 hour and incubated with primary antibody anti-p53 (mouse, p53 DO-1, Santa Cruz Biotechnology, 1:2000) overnight at 4°C. Coverslips were then incubated with a goat polyclonal to mouse Alexa Fluor-488 (Abcam, 1:1000) secondary antibody for 1 hour at room temperature.

For FRT cells immunofluorescence (CFTR detection), after incubation with Triton-X, cell membrane, and Golgi apparatus were stained with wheat germ agglutinin (WGA) conjugated with Alexa Fluor-594 for 10 min at room temperature. CFTR protein localization was revealed by a mouse monoclonal antibody (ab570, CF American Foundation, 1:500). Samples were incubated with a secondary antibody goat polyclonal to mouse Alexa Fluor-488 (Abcam, 1:1000), for 1 hour at room temperature.

Nuclei were stained with ProLong™ Gold antifade mounting medium with DAPI (Invitrogen). Cells were observed using a Zeiss Axioskop microscope equipped for fluorescence. Fluorescence signals were quantified by ImageJ software.

-Real-time RT-PCR.

Total RNA was extracted from the cellular pellet by using the RNeasy® Mini Kit (QIAGEN) according to the manufacturer's instructions and samples were purified by DNase Max® kit (QIAGEN). RNA was reverse transcribed in a final volume of 50 µl using the High-Capacity cDNA Reverse Transcription Kit (Applied Biosystems). For each sample, 2 µl of cDNA, corresponding to 100 ng of reverse transcribed RNA, was analyzed by real-time RT-PCR (95°C for 15 s, 60°C for 60 s, repeated for 40 cycles) in triplicate, using AB PRISM 7300 instrument (Applied Biosystems). Real-time RT-PCR was performed in a final volume of 25 µl comprising 1X Master Mix SYBR Green (Applied Biosystems) and 1 µM of forward and reverse primers, which are the following: p21(Fwd: 5'-CTG GAG ACT CTC AGG GTC GA-3'; Rev: 5'-CGG ATT AGG GCT TCC TCT TG-3') and GAPDH (Fwd: 5'-CTC ATG ACC ACA GTC CAT GCC-3'; Rev: 5'-GCC ATC CAC AGT CTT CTG GGT-3').

As regards the analysis of CFTR expression in FRT cells, we used 1 µM of forward and reverse primers mapping the exon 10 of CFTR (Fwd: 5'-ATC CAG CAA CCG CCA ACA ACT -3'; Rev: 5'-ACT TCT AAT GGT GAT GAC AGC C -3') and Actin (Fwd: 5'-ACC

GTG AAA AGA TGA CCC AGA -3'; Rev: 5'-GAG GCA TAC AGG GAC AGC ACA -3').

Data were analyzed using triplicates values of C_t (cycle threshold). Levels of RNA were determined by using the SDS software version (Applied Biosystems) according to the 2-ΔΔ C_t method and C_t values were normalized to the internal control GAPDH or mouse Actin.

-p-FLuc^{opal} transfection and measurement of luciferase activity by luminescence.

HeLa cells were seeded onto 6-well plates with 2 ml of medium (without antibiotics). After 24 hours cells were transfected using Lipofectamine™ 3000 Transfection Reagent (Invitrogen) according to the manufacturer's instructions with two vectors harboring the cDNA for FTSJ1 [Trzaska C., et al. 2020] and FLuc^{opal}. Vectors were diluted in opti-MEM (Gibco). Cells were transfected with the p-FTSJ1 vector (2.0 µg) and with 1 µg of the p-FLuc^{opal} vector. 24 hours post-transfection, HeLa cells were treated with TRIDs (NV848, NV914, and NV930) at experimental concentrations (6 µM, 12 µM, and 24 µM). Finally, cells were washed with PBS 1X and incubated with the detection mix Steady-Glo® Luciferase Assay System (Promega). 200 µl of Steady-Glo® reagent was mixed with 200 µl of Ultra Pure distilled water (DNase/RNase free; Invitrogen) and added in the samples to lysate cells. After 5 min, 200 µl of cell suspension was added in duplicate in a 96-well plate. Luciferase activity was finally measured at the GloMax®-Multi Detection System (Promega).

-Human liver microsomes.

The pool of human liver microsomes (20 mg/ml; Gibco) derived from 50 different donors, were pre-incubated with 100X NV848 (1.2 mM in H_2O), NV914, and NV930 molecules and PBS1X or TRIS-HCl (phosphate buffers, pH 7.4) phosphate buffer, at 37°C for 5 minutes. The reaction started with the addition of NADPH, respectively in the microsomes-PBS mix and in microsomes-TRIS mix. The reaction mix represented in **figure 20-A** allowed us to evaluate the metabolic activity of cytochrome-P450 (CYP).

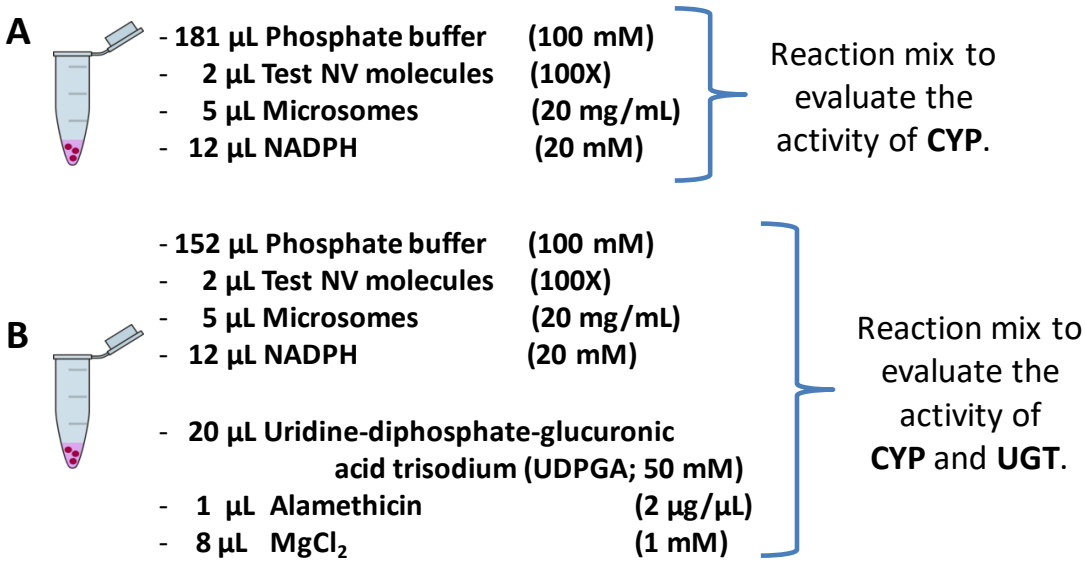

Figure 20: *Schematic representation of microsomes mixes for the evaluation of cytochrome-P450 (CYP) and UDP-glucoronyl-transferase (UGT).*

However, in order to evaluate the UDP-glucosyl-transferase (UGT) activity, the UDPGA, $MgCl_2$, and Alamethicin (pore-forming antibiotic) were added respectively in other two mixes with PBS 1X or TRIS-HCl phosphate buffer (**fig. 20-B**).

After the addition of NADPH, 30 µL of the mix was collected in a new tube and the reaction was stopped with the addition of 200 µL of acetonitrile (0-time point aliquot). The mixes were incubated for 5, 30, and 60 minutes respectively, at 37°C. Next, 30 µL of every mix was collected in a new tube, vortexed, and centrifuged (3000 rpm, 5 min). The supernatant was separated from the pellet in a new tube and analyzed by LC/MS-MS.

-CFTR activity in the organoids by FIS assay.

Briefly, organoids (between the 4th and the 20th passage) were seeded onto 96-well plates in 4µL of matrigel drops. Each drop, containing 15–60 organoids, was covered with 50 µL of growth medium. Human organoid expansion medium was replaced and then the compounds were added at 24 and 48 hours for the following treatments (**fig. 21**):

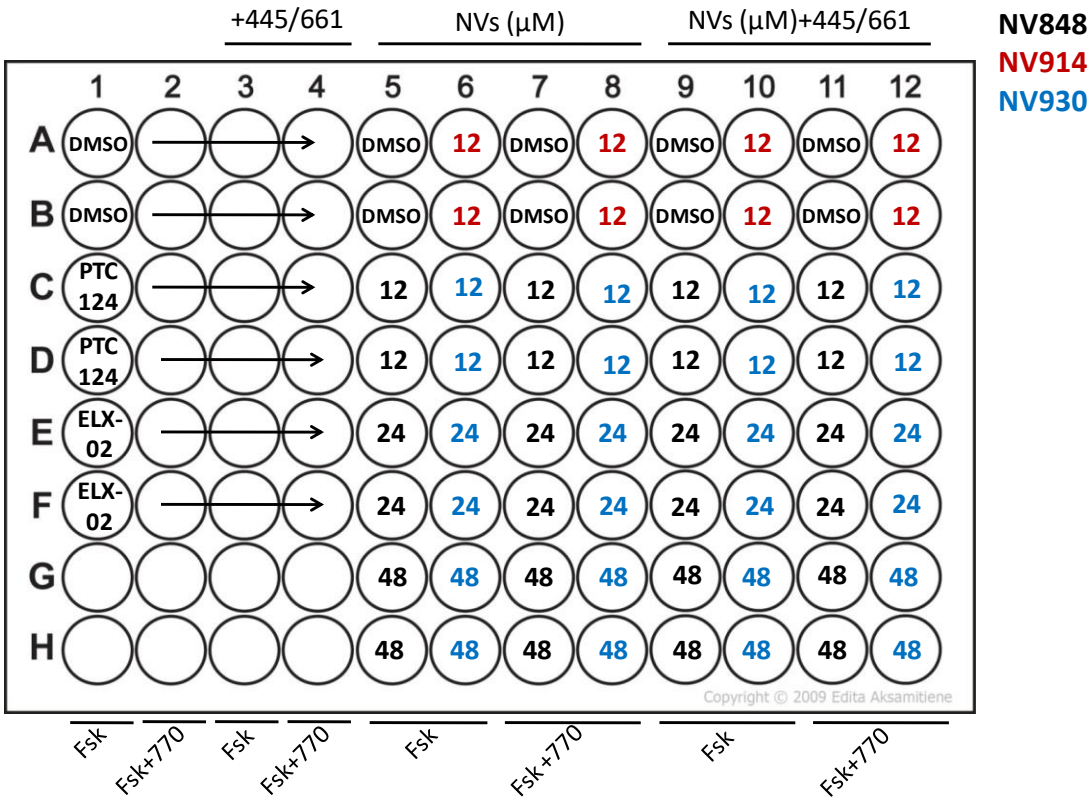

Figure 21: *Experimental representation in a 96-wells plate with compounds used for the treatments and relative concentrations. PTC124 (10 µM) and ELX-02 (80 µM) were used at non-toxic and effective doses. NV848, NV914, and NV930 (NVs) were used at different concentrations (detailed in figure; NV848: black, NV914: red, NV930: blue). Higher concentrations of NV914 (>12 µM) were not tolerated in intestinal organoids. Forskolin (5 µM; Fsk) was used in all samples as CFTR activator. Meanwhile, CFTR modulators, Elexacaftor (3µM; 445), Tezacaftor (3µM; 661), and Ivacaftor (3 µM; 770), were included to increase CFTR recovery and activity. DMSO was the vehicle of the compounds.*

Green calcein (Invitrogen) was added to stain the organoids (0.02 mg/µL). Subsequently, to stimulate CFTR activity, forskolin 5 µM was added to the organoids that were immediately analyzed by confocal live-cell microscopy (LSM800, 5× objective; Zeiss, Oberkochen, Germany). Every 10 min (from 0 to 60 min (t_0–t_{60})), the total organoid area (xy plane) was automatically quantified using Zen blue analysis software (Zeiss) and normalized to the area at t_0.

To test the rescue of CFTR function by correctors, organoids were pre-incubated for 48 hours with 3 µM Elexacaftor (VX-445; Selleckchem) and 3 µM Tezacaftor (VX-661; Selleckchem), as **figure 21** shows. Ivacaftor at a concentration of 3 µM (VX-770; Selleckchem) was added as a potentiator in combination with forskolin. Within each organoid experiment, every test condition was assessed in duplicate. Per organoid genotype, two independent experiments were performed on different days. Reported values reported correspond to the average area under the curve (AUC) calculated from plots representing the mean percentage of organoids swelling from t_0 to t_{60} (60 min) plus the standard error of the mean of the two independent experiments.

Residual CFTR function was determined from the organoid swelling after the addition of forskolin and CFTR modulators (VX-445/ VX-661/ VX-770) with DMSO (vehicle).

-Data analysis.

The experiments were performed at least in duplicate (n=2, experimental replicates) and using two (three for Real time RT-PCR and microsomal analysis) technical replicates for each analysis. All data are expressed as mean values ± standard error of the mean (SEM). Statistical analysis was performed by Student's t-test and one-way ANOVA when appropriate by GraphPad Prism software version 7.0.0 for Windows. A probability value (*p*) of less than 0.05 was regarded as significant and indicated in relevant graphs as one symbol (*) for $p< 0.05$, two symbols (**) for $p< 0.01$, three symbols (***) for $p< 0.001$, and four symbols (****) for $p< 0.0001$.

RESULTS.

TASK#1 Study of CFTR expression in the rescue of splicing mutation defects after treatment with the small molecules *kinetin* and RECTAS.

1.1 Transient transfection of the CFTR$^{N59+N510+5T12TG}$ (CFTR minigene) construction and rescue of CFTR expression after treatment with kinetin and RECTAS molecules.

To evaluate the ability of the two molecules *kinetin* and RECTAS (**fig. 9**, *Introduction Section*) to correct CFTR T_5TG_{12} mRNA splicing, a vector harboring the CFTR polymorphism T_5TG_{12} (pcDNA3.1-CFTR$^{N59+N510+5T12TG}$) was used to transfect Fischer rat thyroid cells (FTR). As a positive control, the vector containing CFTR wild-type cDNA (pcDNA3.1-CFTR^{WT}) was used.

FRT cells were chosen for the analysis because these cells do not express human CFTR protein and do not present analog cAMP-regulated protein channels that transport Cl^- ions [Sheppard D.N., et al. 1994].

24 hours post pcDNA3.1-CFTR$^{N59+N510+5T12TG}$ transfection, FRT cells were treated with *kinetin* (100 µM) or RECTAS (50 µM) for 48 hours and the total RNA was extracted to analyze CFTR expression by Real time RT-PCR.

In order to evaluate the presence of the correct CFTR mRNA, with the exon 10 inclusion promoted by *kinetin* or RECTAS treatment, two specific primers for the exon 10 sequence were used in Real time RT-PCR reaction (**fig. 22**).

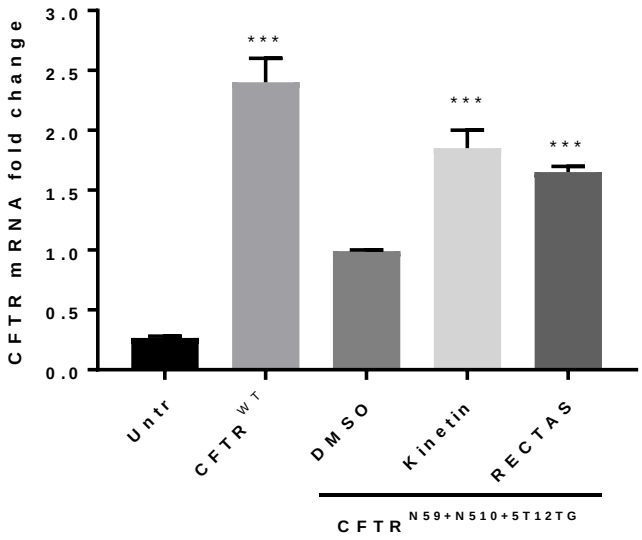

Figure 22: *Real time RT-PCR of the CFTR mRNA in FRT cells untransfected (Untr) or transfected with pcDNA3.1-CFTR$^{N59+N510+5T12TG}$ and treated with DMSO (vehicle, negative control), kinetin (100 µM), or RECTAS (50 µM). FRT cells were transfected with pcDNA3.1-CFTR^{WT} as a positive control. Data were*

analyzed by GraphPad Prism 7 software. A probability value (p) with respect to the DMSO sample: three symbols (***) for p < 0.001.

Real-time RT-PCR revealed an increase of CFTR expression in pcDNA3.1-CFTR$^{N59+N510+5T12TG}$ FRT cells treated with *kinetin* or RECTAS, with respect to untransfected cells (**fig. 22**; Untr). Moreover, the use of specific primers for exon 10 confirms the inclusion of this region in the transcript after the treatment. In contrast, also DMSO treated cells showed an increase in CFTR expression probably due to the presence of pre-splicing CFTR mRNAs.

To evaluate CFTR protein expression in pcDNA3.1-CFTR$^{N59+N510+5T12TG}$ FRT cells, 48 hours after treatment with *kinetin* or RECTAS proteins were extracted and samples were analyzed by western blot. An additional control was used for this analysis: a sample transfected with a vector containing the CFTR cDNA without the exon 10 sequence (pcDNA3.1-CFTR$^{\Delta EX10}$). This control was used to visualize the eventual different molecular weights of the CFTR protein. FRT cells were transfected with the indicated vectors and after 24 hours, treated with *kinetin* or RECTAS for 48 hours (**fig. 23**).

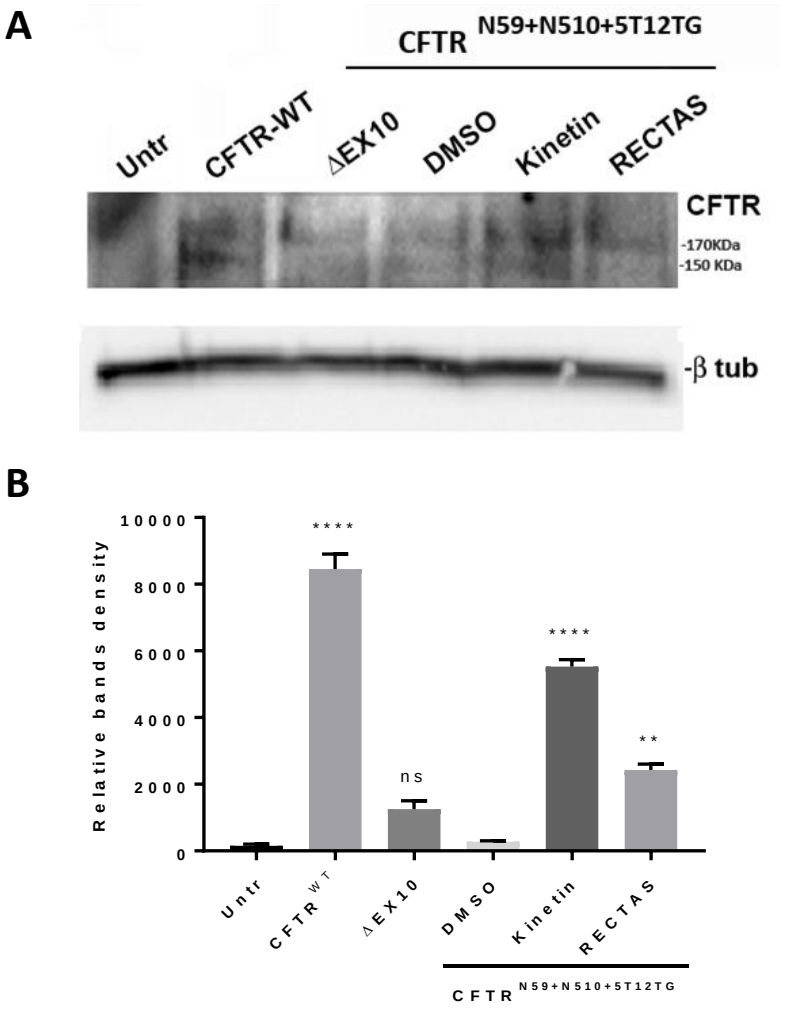

Figure 23: *A) Western blot analysis in FRT cells untransfected (Untr) or transfected with pcDNA3.1-CFTR$^{N59+N510+5T12TG}$ and treated with DMSO (vehicle, negative control), kinetin (100 µM), or RECTAS (50*

µM). FRT cells were transfected with pcDNA3.1-CFTR^{WT}(CFTR-WT) as positive control and pcDNA3.1-CFTR$^{\Delta EX10}$(ΔEX10) as a negative control of exon 10 inclusion. The two protein bands with different molecular weights (170 kDa C-band and 150 kDa B-band) represent the two forms of CFTR: glycosylated and unglycosylated CFTR forms, respectively. The band quantification was performed using the bands corresponding to the mature form of CFTR protein (170 kDa); B) Relative quantification of bands density was performed by ImageJ software. β-tubulin was used as a loading control. Data were analyzed by GraphPad Prism 7 software. A probability value (p) with respect to the DMSO sample: two symbols (**) for p < 0.01, four symbols (****) for p < 0.0001. ns= non-significant.

As shown in **figure 23**, the treatment with *kinetin* or RECTAS partially restored CFTR protein expression in pcDNA3.1-CFTR$^{N59+N510+5T12TG}$ FRT cells.

CFTR is a protein channel localized in the apical surface of the cell membrane and its correct localization is necessary for physiological osmotic regulation. To analyze the protein localization, it was evaluated by immunofluorescence assay.

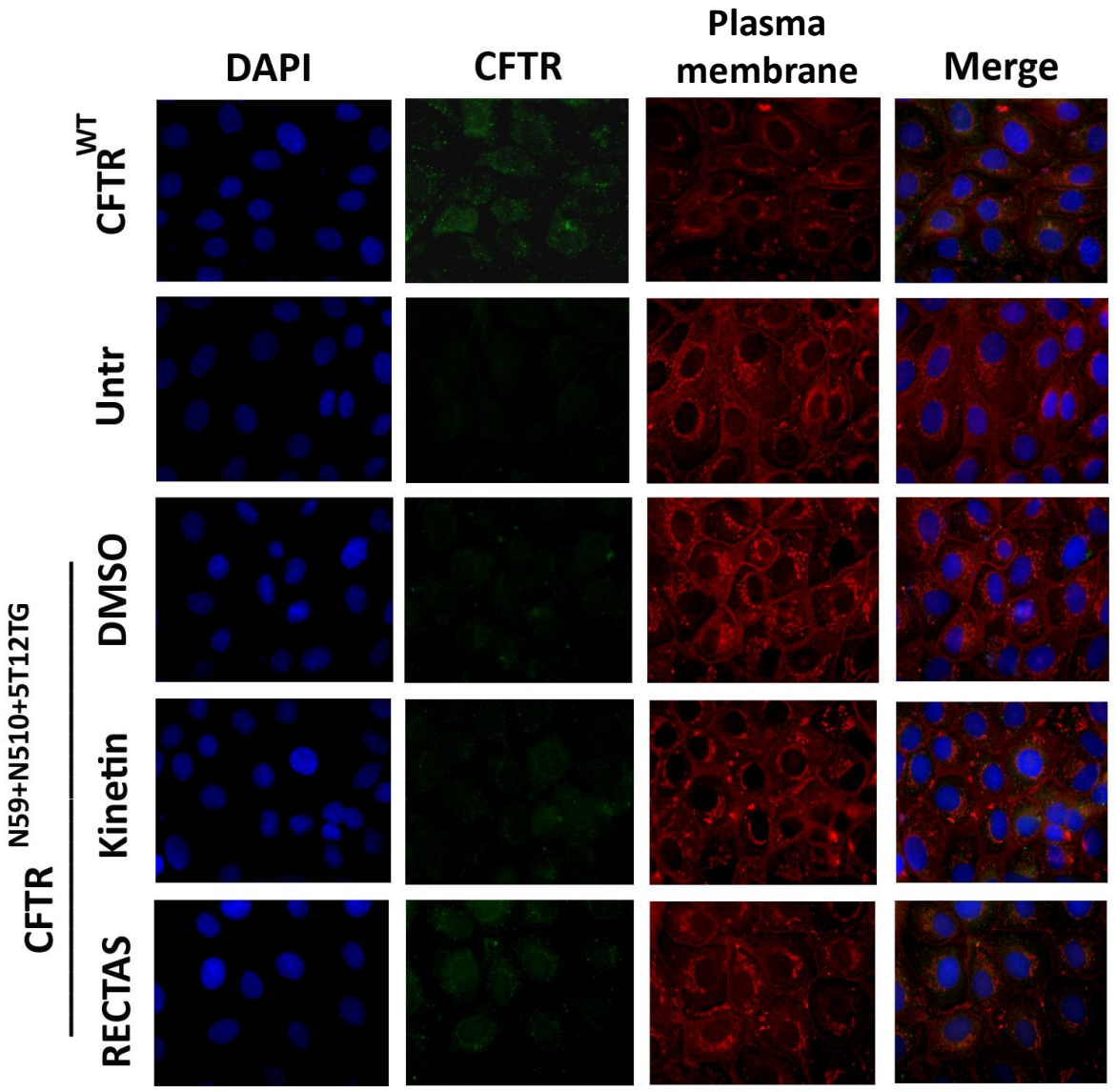

Figure 24: *Immunofluorescence analysis of FRT cells untransfected (Untr) or transfected with pcDNA3.1-CFTR^{WT} or pcDNA3.1-CFTR$^{N59+N510+5T12TG}$. Cells were treated with DMSO (vehicle, negative control), kinetin (100 µM), or RECTAS (50 µM) 48 hours after transfection. CFTR protein (green) was revealed by a*

specific primary antibody (ab570) and secondary antibody (Alexa-488). Nuclei (blue) were stained with DAPI (4',6-diamidino-2-phenylindole) and the plasma membrane (red) was stained with wheat germ agglutinin (WGA)-Alexa 594.

FRT cells were seeded on rounded glass coverslips in 12-well plates and transfected with the indicated vectors (pcDNA3.1-CFTR$^{N59+N510+5T12TG}$ or pcDNA3.1-CFTR^{WT}). 24 hours post-transfection, cells were treated with *kinetin* (100 µM) or RECTAS (50 µM) for 48 hours (**fig. 24**).

As shown in **figure 25**, CFTR protein expression was detected on cellular membranes and it results increased in 25% and 33% of the cells treated with *kinetin* or RECTAS respectively.

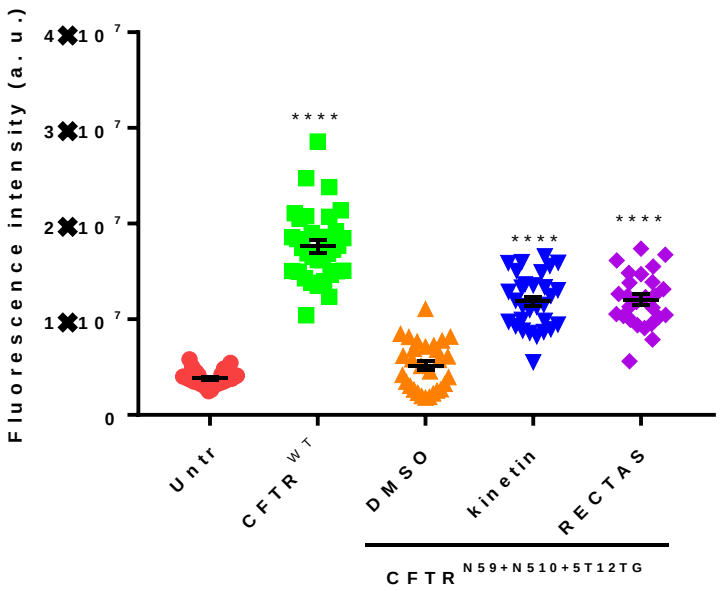

Figure 25: *Quantification of CFTR signal relative to immunofluorescence analysis. Fluorescence intensity quantification was performed by ImageJ software. Data were analyzed by GraphPad Prism 7 software. A probability value (p) with respect to the DMSO sample: four symbols (****) for p < 0.0001.*

These data support both the hypothesis that *kinetin* and RECTAS compounds are able to rescue splicing defects and induce CFTR protein recovery.

In order to improve the data obtained in transient transfections, the next step was the production of FRT cells that stably express the CFTR$^{N59+N510+5T12TG}$ *minigene* using a retroviral infection system.

1.2 Cloning CFTR^{WT} and CFTR$^{N59+N510+5T12TG}$ constructions into the retroviral vector pBPSTR1 in order to produce stably expressed FRT cells.

To increase the number of cells that express CFTR$^{N59+N510+5T12TG}$ *minigene*, the whole insert was cloned in a retroviral vector named pBPSTR1 (**fig. 19**, *Methods Section*). The

CFTR$^{N59+N510+5T12TG}$ and CFTR^{WT} inserts were recovered from pcDNA3.1 plasmids by NotI and ApaI restriction enzymes digestion.

At first, pcDNA3.1 digestion with ApaI generated a 3' protruding end, that was removed by treatment with T4 DNA polymerase in order to create a 3' blunt end. This 3' end modification was required because the consensus site for the ApaI restriction enzyme was absent in the polyclonal site of the pBPSTR1 vector. After the second digestion with NotI and dephosphorylation of the pcDNA3.1 ends, the CFTR$^{N59+N510+5T12TG}$ and CFTR^{WT} fragments were released (**fig. 26**). The consensus sites for NotI and ApaI enzymes are unique cutting sites in pcDNA3.1 plasmid, while ApaLI can generate a cut inside the sequence of CFTR cDNA. NotI and ApaI were used in order to release the CFTR$^{N59+N510+5T12TG}$ and CFTR^{WT} inserts from pcDNA3.1.

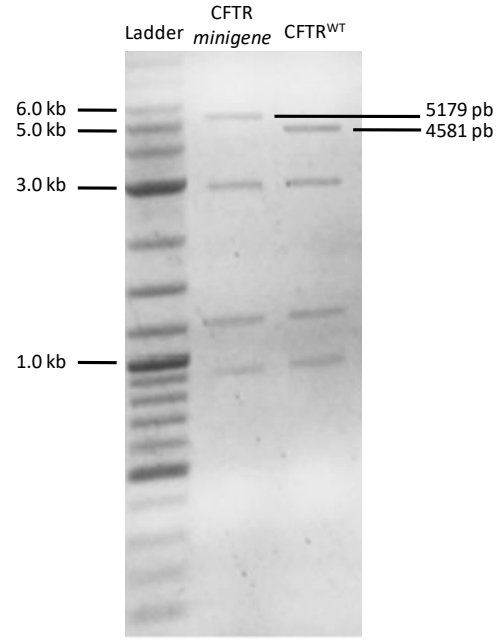

Figure 26: *Gel electrophoresis of pcDNA3.1-CFTR$^{N59+N510+5T12TG}$ (CFTR minigene) and pcDNA3.1-CFTR^{WT} (CFTR^{WT}) fragments after digestion with NotI, ApaI, and ApaLI restriction enzymes. CFTR$^{N59+N510+5T12TG}$ and CFTR^{WT} fragments present respectively a dimension of 5179 pb and 4581 pb.*

Finally, the CFTR$^{N59+N510+5T12T}$ *minigene* and CFTR^{WT} cDNA were cloned into the retroviral vector pBPSTR1 digested with NotI and PmeI.

In order to verify the correct cloning after ligation, pBPSTR1-CFTR$^{N59+N510+5T12TG}$ and pBPSTR1-CFTR^{WT} resulting vectors were digested with BamHI (**fig. 27**).

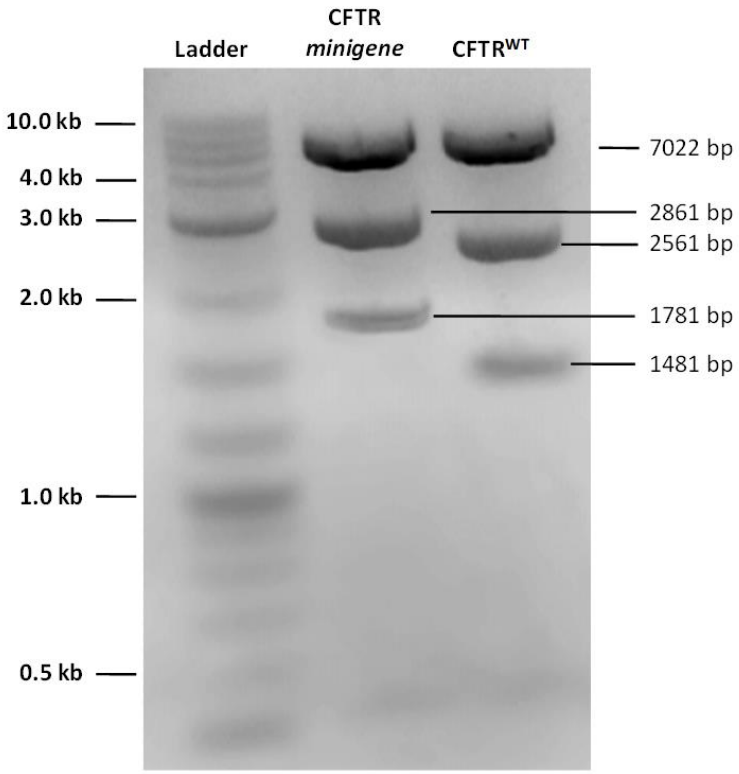

CFTR *minigene*	CFTR^{WT}
2861 bp	2561 bp
1781 bp	1481 bp
322 bp	322 bp
216 bp	216 bp

Figure 27: *Gel electrophoresis of pBPSTR1-CFTR$^{N59+N510+5T12TG}$ (CFTR minigene) and pBPSTR1-CFTR^{WT} (CFTR^{WT}) fragments after digestion with BamHI restriction enzyme. The table (right) shows the expected molecular weights of the fragments deriving from BamHI digestion. The higher bands (7022 pb) represent the pBPSTR1 vectors.*

Restriction with BamHI gave 3 cuts in pBPSTR1-CFTR$^{N59+N510+5T12TG}$ and pBPSTR1-CFTR^{WT} vectors, and that was confirmed by gel electrophoresis (the two fragments with size ≤ 322 pb are slightly visible).

The CFTR$^{N59+N510+5T12TG}$ (CFTR *minigene* in **fig. 27**) sample has a higher molecular weight with respect to CFTR^{WT} fragments because this construction harbors the two introns portions (intron 9 and intron 10) containing the T_5TG_{12} polymorphism (intron 9). The top bands correspond to the pBPSTR1 vector size.

Ligation products were then transformed into *E. coli Top10* competent cells to amplify the engineered retroviral vectors (pBPSTR1-CFTR$^{N59+N510+5T12TG}$ and pBPSTR1-CFTR^{WT}). The two retroviral vectors were transformed into *E. coli Top10* by thermal shock and plated onto LB agar plates with the addition of ampicillin, in order to isolate the positive colonies. The correct transformation of selected clones was controlled by PCR-colony (**fig.** 2**8**).

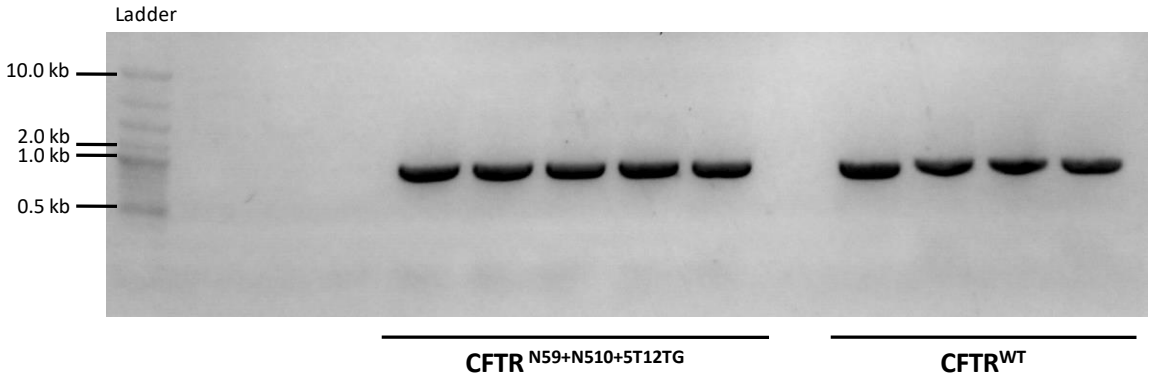

Figure 28: *Colony PCR deriving from the transformed and selected E. coli Top10. Using specific primers that mapped inside the sequence of pBPSTR1 vector and CFTR cDNA, the amplicons present a dimension of 840 pb (respectively 142 pb and 698 pb).*

Finally, the resulting extremities of pBPSTR1-CFTR$^{N59+N510+5T12TG}$ and pBPSTR1-CFTR^{WT} were sequenced (by an external company; BMR Genomics) in order to confirm the correct cloning.

1.3 Packaging cells (Phoenix) transfection with pBPSTR1-CFTR$^{N59+N510+5T12TG}$ and pBPSTR1-CFTR^{WT} and retroviral infection of FRT cells.

Phoenix (ΦNX) packaging cells can produce retroviral particles when transfected with an appropriate retroviral vector such as the pBPSTR1.

To evaluate the transfection efficacy in Phoenix cells, they were transfected with the pBPSTR1-H2BGFP retroviral vector expressing the chimeric cDNA H2BGFP [Kanda T., et al. 1998].
72 hours post-transfection 60% of the Phoenix cells showed the presence of the fluorescent protein H2BGFP (**fig. 29 A-B**).

To validate the efficacy of infection by the retroviral particles produced, the supernatant of the pBPSTR1-H2BGFP Phoenix cells was used to infect HCT116 cells (FRT cells were not used because express a fluorescent protein named YFP).
As shown in **figure 29-C**, 72 hours post-infection, HCT116 cells resulted positive to the expression of the H2BGFP protein, indicating the ability of the Phoenix cells to produce functional retroviral particles.

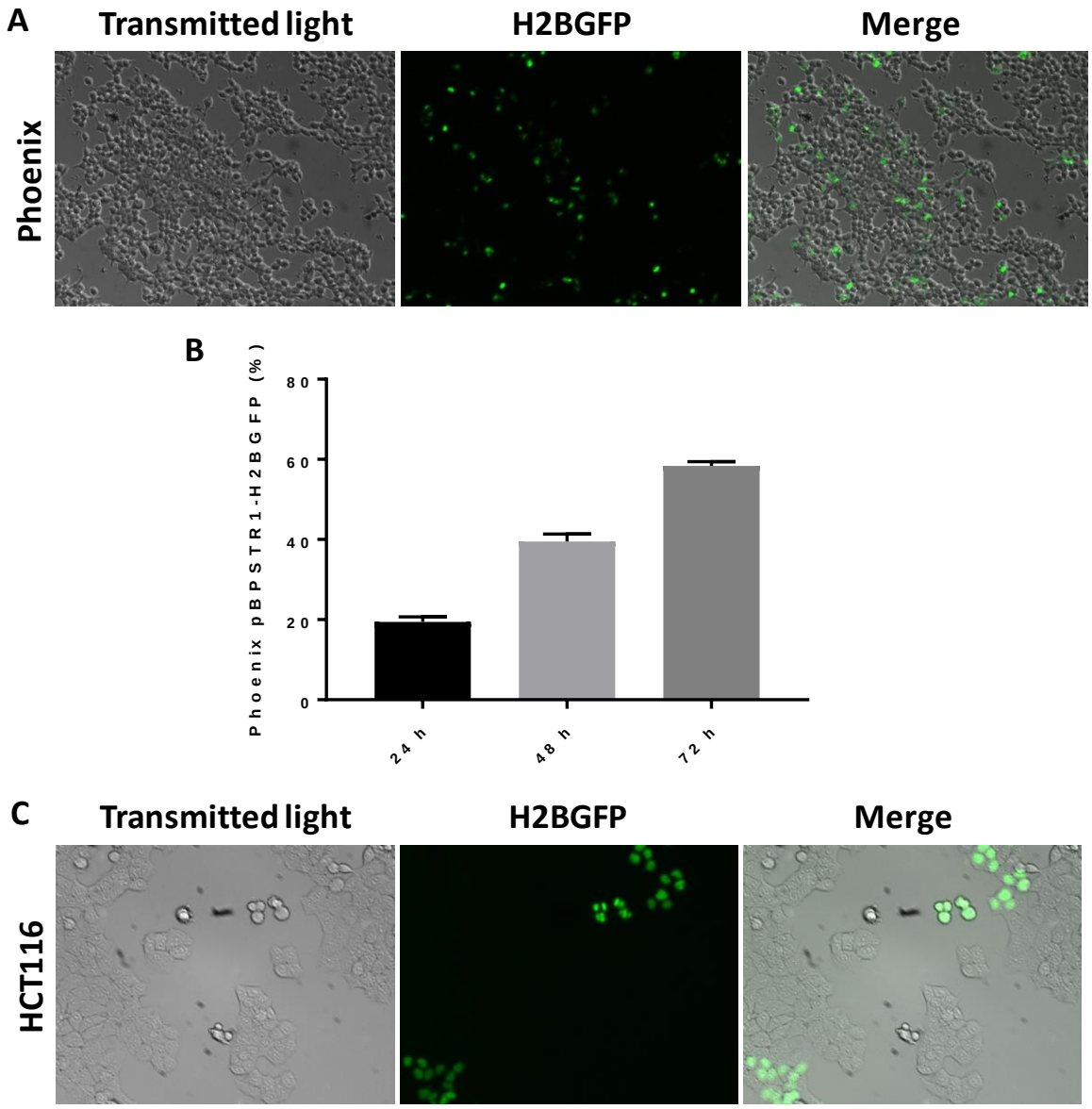

Figure 29: *A) Representative fluorescence microscopy images of Phoenix cells 72 hours after transfection with pBPSTR1-H2BGFP. B) Percentage of Phoenix after 24, 48, and 72 hours of transfection with pBPSTR1-H2BGFP. C) representative fluorescence microscopy images of HCT116 cells infected with retroviral particles derived from Phoenix transfection with pBPSTR1-H2BGFP.*

The next step was the production of retroviral particles that contain the two vectors: pBPSTR1-CFTR$^{N59+N510+5T12TG}$ or pBPSTR1-CFTR^{WT} by Phoenix cell transfection.

After the transfection, the culture medium containing the retroviral particles was collected in order to infect FRT cells.

72 hours post-infection, FRT cells were selected by puromycin for three weeks.

FRT-pBPSTR1-CFTR$^{N59+N510+5T12TG}$ and FRT-pBPSTR1-CFTR^{WT} selected cells were analyzed to confirm the expression of the CFTR$^{N59+N510+5T12TG}$ and CFTR^{WT} expression.

Total RNA was extracted from FRT-pBPSTR1-CFTR$^{N59+N510+5T12TG}$ and FRT-pBPSTR1-CFTR^{WT} and a Real-time RT-PCR analysis was performed to confirm the expression of CFTR transcript (**fig. 30**).

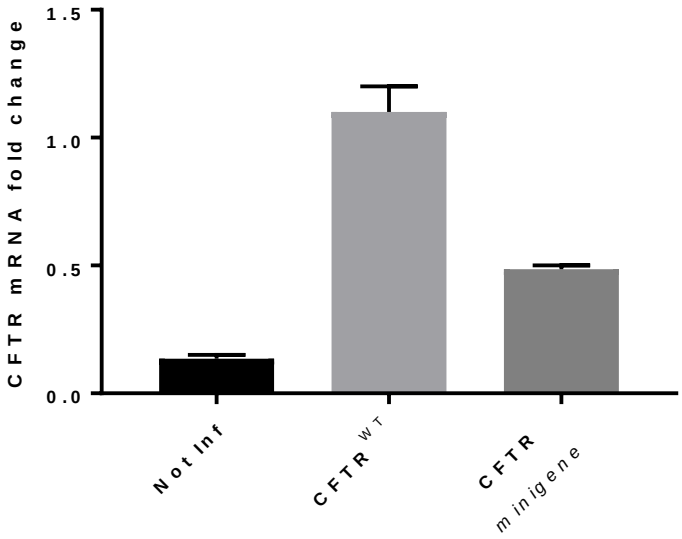

Figure 30: *Real-time RT-PCR of the CFTR mRNA in FRT cells not infected (Not Inf) or infected with retroviral particles harboring pBPSTR1-CFTR^{WT} (CFTR^{WT}) or pBPSTR1-CFTR$^{N59+N510+5T12TG}$ (CFTR minigene) constructions. Primers used in this experiment are specific for exon 10.*

As shown by real-time RT-PCR analysis, both FRT cells (FRT-pBPSTR1-CFTR$^{N59+N510+5T12TG}$ and FRT-pBPSTR1-CFTR^{WT}) express CFTR mRNA (**fig. 30**). The expression of CFTR$^{N59+N510+5T12TG}$ (CFTR *minigene*; **fig. 30**) was lower than the expression of CFTR^{WT} according to the presence of the polymorphism T_5TG_{12} mutation.

To evaluate the rescue of the CFTR protein by *kinetin* or RECTAS treatments, FRT-pBPSTR1-CFTR$^{N59+N510+5T12TG}$ were treated with *kinetin* or RECTAS for 48 hours. Immunofluorescence analysis revealed that CFTR protein expression was increased after treatment with *kinetin* or RECTAS, compared to the DMSO-treated control (**fig. 31**). Data were confirmed by fluorescence signal quantification (**fig. 32**).

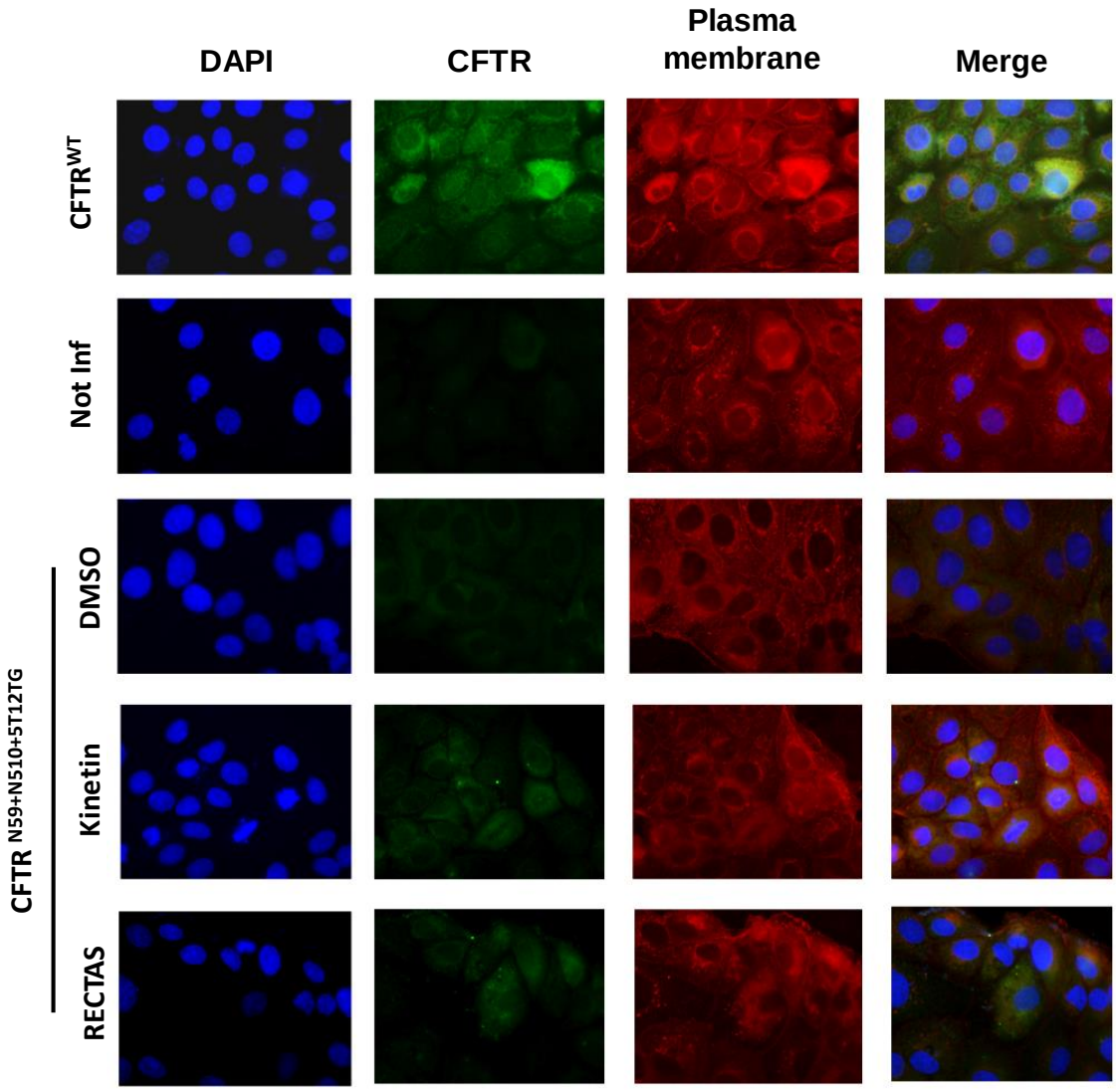

Figure 31: *Immunofluorescence analysis of FRT cells not infected (Not Inf) or infected with retroviral particles harboring pBPSTR1-CFTR^{WT} (CFTR^{WT}) or pBPSTR1-CFTR$^{N59+N510+5T12TG}$ (CFTR minigene) constructions. Cells were treated with DMSO (vehicle), kinetin (100 µM), or RECTAS (50 µM) for 48 hours. CFTR protein (green) was revealed by a specific primary antibody (ab570) and secondary antibody (Alexa-488). Nuclei (blue) were stained with DAPI (4',6-diamidino-2-phenylindole) and the plasma membrane (red) was stained with wheat germ agglutinin (WGA)-Alexa 594.*

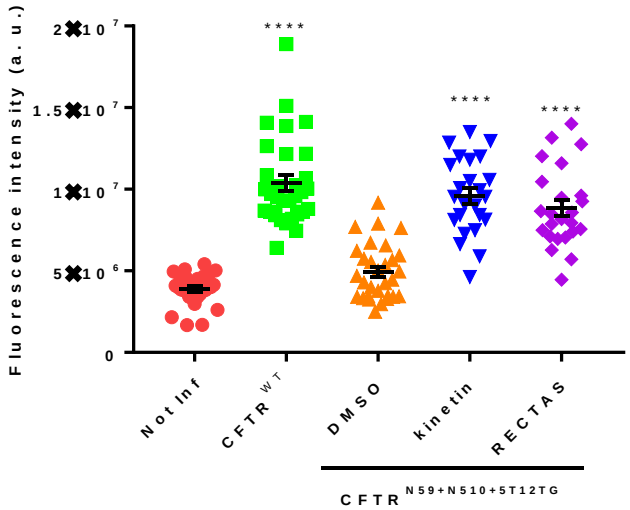

Figure 32: *Quantification of CFTR signal relative to immunofluorescence analysis. Fluorescence intensity*

quantification was performed by ImageJ software. Data were analyzed by GraphPad Prism 7 software. A probability value (p) with respect to the DMSO sample: four symbols (****) for p < 0.0001.

TASK#2 Rescue of the CFTR expression and functionality by translational readthrough inducing drugs (TRIDs) in nonsense cystic fibrosis (CF) model systems.

2.1 Dose-response activity for the evaluation of the CFTR expression in FRT cells characterized by CFTR W1282X mutation.

The second part of my Ph.D. project was based on advanced studies about the activity, functionality, and stability of three new readthrough agents as a potential treatment of nonsense-related CF.

To date, no experimental treatments specific to CF nonsense mutations are effective, but the induction of premature termination codon (PTC) translational readthrough mediated by compounds (TRIDs) can be one of the most promising and quickly available strategy to rescue *CFTR* nonsense mutations.

Three oxadiazole core molecules named NV848, NV914, and NV930 (**fig. 14**; *Introduction Section*) were identified by the research group of Pibiri I. and Lentini L. (STEBICEF Department, University of Palermo), these compounds were validated as a molecule with readthrough activity in FRT cell model system harboring two different nonsense mutations ($CFTR^{G542X}$ and $CFTR^{W1282X}$) [Pibiri I., et al. 2020].

The first step was the evaluation of the dose/response activity of the three NV molecules: NV848, NV914, and NV930 at 3, 6, 12, 24, or 48 μM (**fig. 33**).

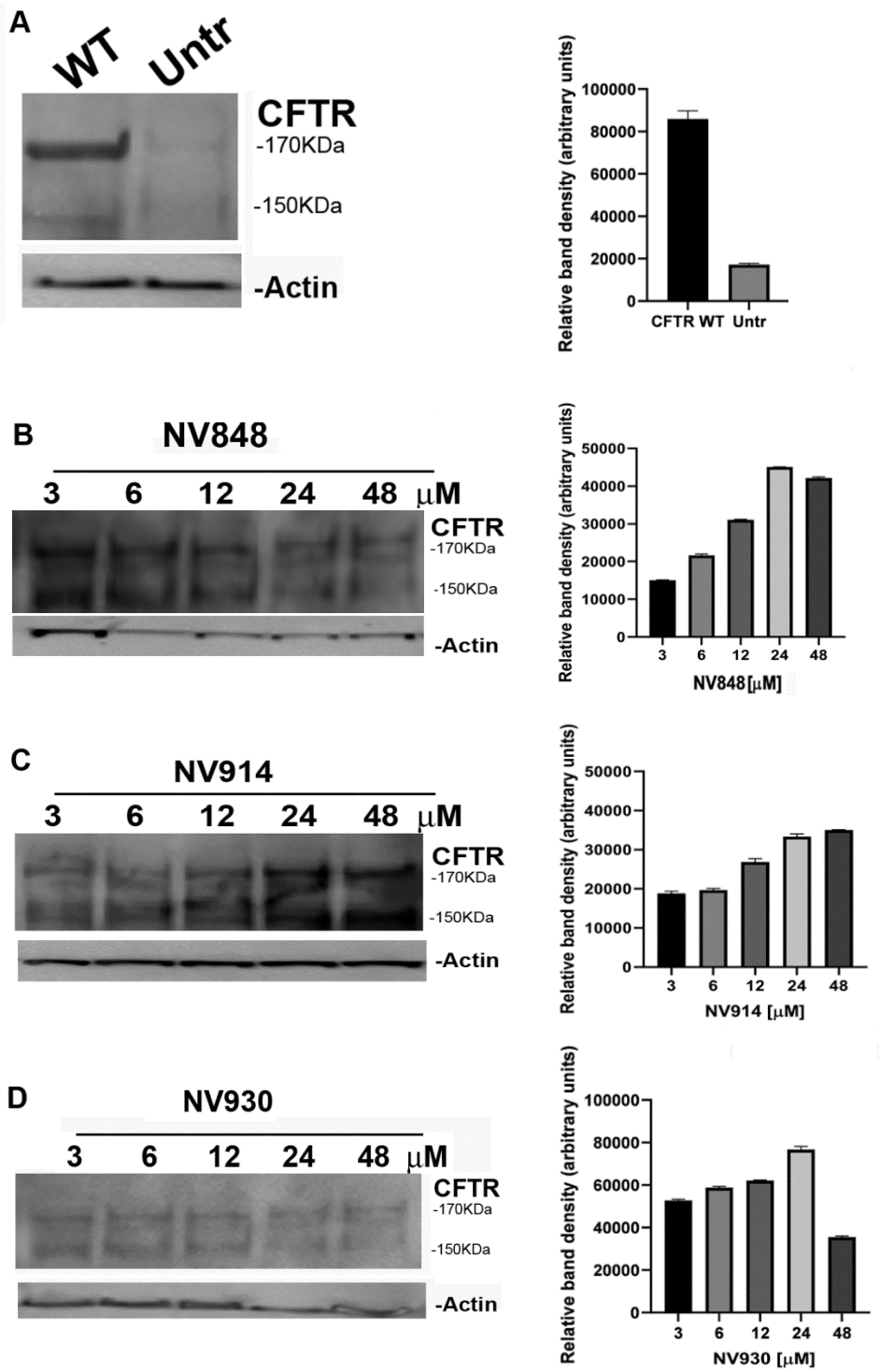

Figure 33: *(B, C, D, left) Western blot analysis to detect CFTR in FRT CFTR^{W1282X} cells 24 hours after treatment with NV molecules (NV848, NV914, and NV930) at increasing concentrations (3, 6, 12, 24, or 48 µM). (A) FRT CFTR^{WT} (WT) and untreated FRT CFTR^{W1282X} cells (Untr) were used respectively as positive and negative controls. The two protein bands with different molecular weights (170 kDa C-band and 150 kDa B-band) represent the two forms of CFTR: glycosylated and unglycosylated CFTR forms respectively. The band quantification was performed using the bands corresponding to the mature form of CFTR protein (170 kDa). Actin was used as a loading control. (right) Western blot band quantification was performed by ImageJ software.*

FRT cells expressing the p-TRACER-CFTR^{W1282X} (FRT-CFTR^{W1282X}) were treated for 24 hours with the different molecules at indicated concentrations. As shown in **figure 33**,

CFTR expression was detected in all tested concentrations. 24 μM resulted in the concentration with the highest CFTR expression.
In addition, to evaluate the potential activity of the three molecules on natural termination codons (NTCs), the presence of elongated proteins was assessed as a successive step.

2.2 Evaluation of NV molecules (NV848, NV914, and NV930) effects on the natural mRNA termination codons (NTCs) in order to confirm the specific action of new readthrough agents.

To exclude possible off-target effects on natural stop codons (NTCs) by NV molecules, another objective of the project was based on the study of NV848, NV914, and NV930 activity in different cell model systems (HCT116 and 16HBE). The rationale of these experiments was focused on the identification of specific elongated proteins such as p53 (in HCT116 cells), the Cystatin-C, and the β-2-Microglobulin (in 16HBE cells). In fact, the eventual NTCs readthrough could cause the production of proteins with different weight with respect to the normal molecular weight of the wild-type proteins.
In particular, p53 was chosen as a model of inducible protein and the other two proteins were chosen as models of housekeeping proteins with a low molecular weight. Precisely, Cystatin-C and the β-2-Microglobulin proteins were chosen because they were used in similar experiments by Crawford et al. to investigate off-target effects on NTCs by another TRID in a clinical trial (ELX-02) [Crawford D.K., et al. 2020].

2.3 Study of p53 correct translation and functionality after its translational increasing (DNA damage response) and NV molecules (NV848, NV914, and NV930) treatment.

p53 is one of the most characterized proteins in the research field, because it is involved in cell cycle arrest, DNA repair, senescence, and apoptosis, all processes to prevent cancer [Tanaka T., et al. 2018]. In order to exert its proper function, this protein needs a series of important events: aggregation in tetramer form, phosphorylation of specific aminoacidic residues, nuclear localization, and interaction with transcription promoting DNA sequence of specific genes [Gencel-Augusto J. and Lozano G. 2020].
One of the first genes activated by the p53 transcriptional factor in response to DNA damage is *CDKN1A* [Rizzotto D., et al. 2021]. This gene encodes for a cyclin-dependent kinase inhibitor also known as p21, that is fundamental to arresting the cell cycle during DNA repair response [Georgakilas A.G., et al. 2017].
After DNA damage induction, p53 mRNAs and proteins are stabilized and the translation of p53 is increased in order to accelerate DNA damage response [Grover R., et al. 2009].

p53 alterations can interfere with the functionality and correct localization of this protein in several ways [Hu J., et al. 2021].

Based on these observations, to evaluate a possible activity of the NV molecules (NV848, NV914, and NV30) on the natural termination codons (NTCs) during the translation process of the p53 protein, DNA damage was induced by Doxorubicin, in HCT116 cells in presence of NV molecules. The purpose of these experiments was to visualize the possible expression of greater molecular weight forms of p53 after treatment with NV molecules for 24 hours. Moreover, the presence of unfunctional forms of the p53 protein due to an incorrect translational process was assessed.

HTC116 are tumor and immortalized cells with a high replication rate. These cells were used for the higher translation capacity with respect to normal cells.

HCT116 cells were plated and, after 24 hours, the cells were treated with Doxorubicin to induce DNA damage and p53 translation increase, in combination with TRIDs as shown in the graphic representation in **figure 34**. p53 protein expression, functionality, and localization were analyzed after DNA damage induction in presence of NV molecules.

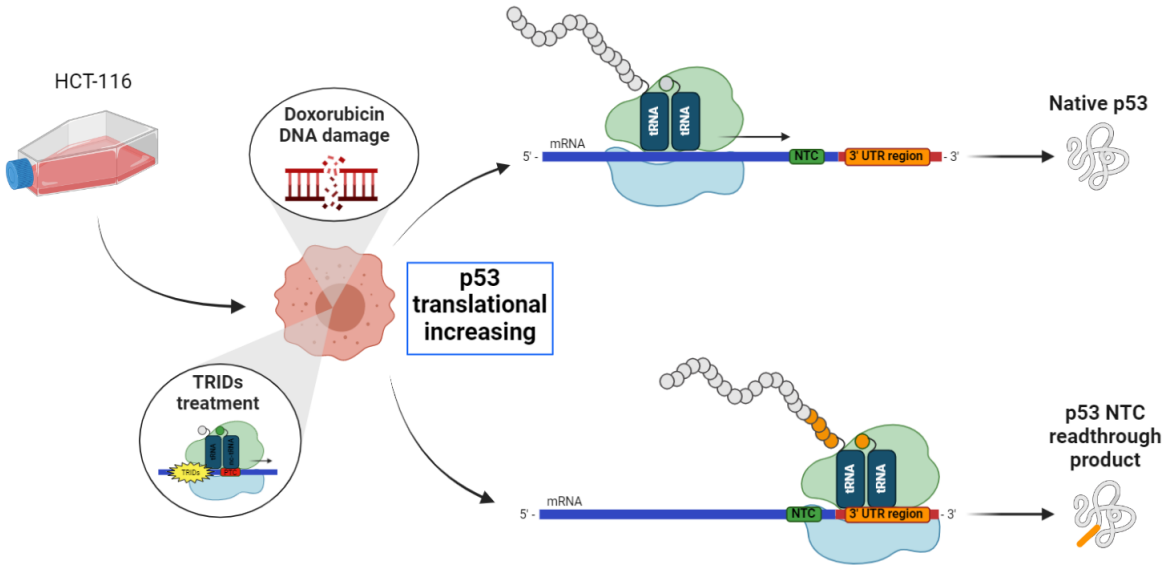

Figure 34: *Experimental scheme. Doxorubicin DNA damage induces p53 expression in HCT116 cells. TRIDs could generate translational readthrough of the natural mRNA termination codons (NTCs), even on p53 NTC. This miscoding error could result in alterations of protein expression, nuclear localization, and/or DNA/protein interaction.*

In particular, HCT116 cells were seeded in 6-well plates and treated with Doxorubicin 0,2 µg/ml in combination with G418 or NV molecules at the indicated concentrations (G418: 430 µM, 645 µM, and 1075 µM; NV848, NV914, and NV930: 3 µM, 12 µM, and 48 µM; **fig. 35**).

The G418 aminoglycoside was used as a positive control considering its capacity to induce NTCs genome-wide readthrough [Wangen J.R. and Green R. 2020].

Western blot experiments and bands quantification analysis showed a little decrease of p53 protein levels in HCT116 treated with G418 and NV914 after DNA damage compared to Doxorubicin (Dox) samples (black bars in **fig. 35-B**). However, in all analyzed samples were no visible p53 bands with greater molecular weight.

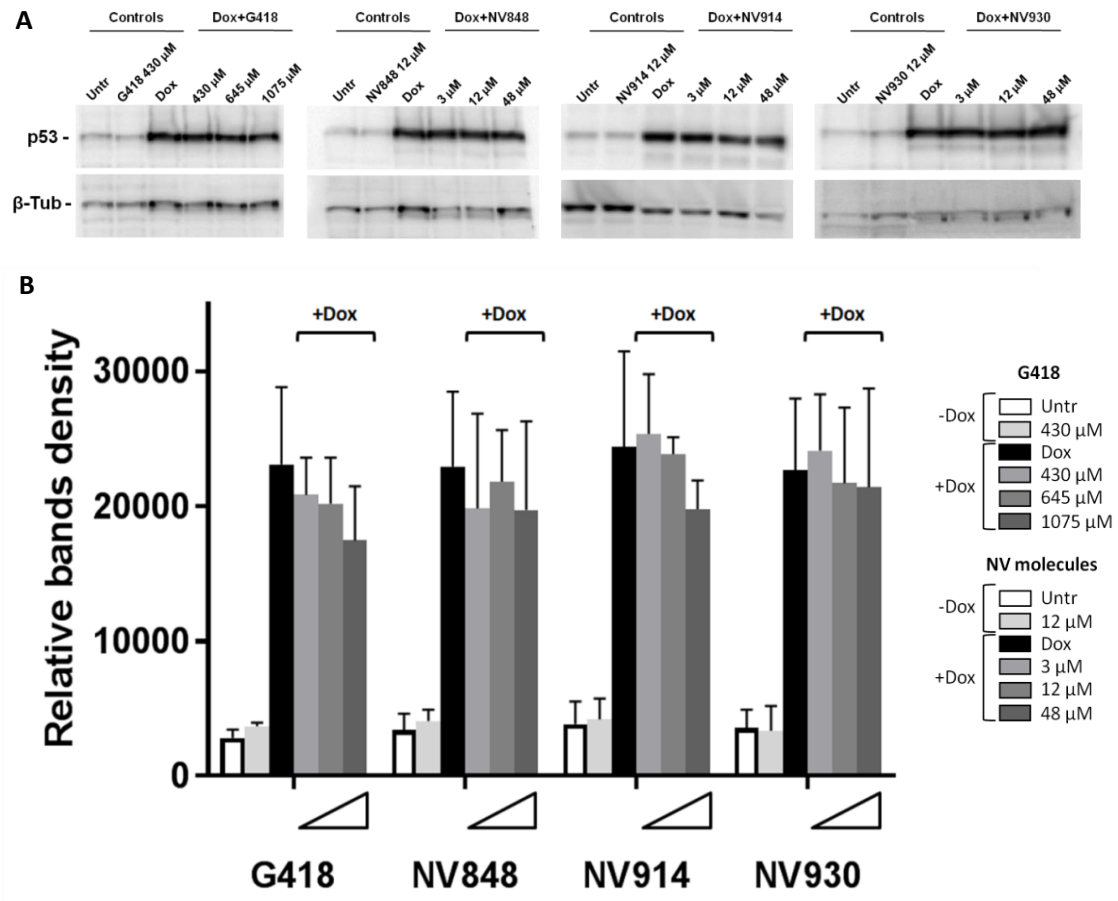

Figure 35: *(A) Western blot analysis to detect p53 in HCT116 cells 24 hours after treatment with G418 (430µM, 645 µM, and 1075 µM) or NV molecules (3 µM, 12 µM, and 48 µM) at increasing concentrations, in combination with Doxorubicin (Dox, 0,2 µg/ml). Only compound indicated the treatment without DNA damage induction (-Dox). NV or G418 samples indicated the treatment with different TRID concentrations (triangles) in combination with Doxorubicin (+Dox). β-Tubulin was used as loading control. (B) Western blot bands quantification was performed by ImageJ software.*

In response to DNA damage, p53 protein is stabilized and its protein expression is increased. Post-translational modifications and other signals are involved in p53 tetramerization and its nuclear localization to activate specific gene transcription. The nuclear translocation is a fundamental event to the correct p53 function and, in addition, this process is regulated by the presence of a protein nuclear localization sequence (NLS). Nuclear localization and export sequences together with the tetramerization domain are located in the C-terminal domain of p53. The suggestion is that: if any alteration in the p53

translational process is induced by TRID treatment, protein function would be impaired like its nuclear localization.

In order to visualize p53 protein localization after DNA damage induction and TRID treatment, an immunofluorescence assay was performed. HCT116 cells were treated with Doxorubicin and simultaneously with G418 or NV molecules at the indicated concentrations for 24 hours (**fig. 36-37**).

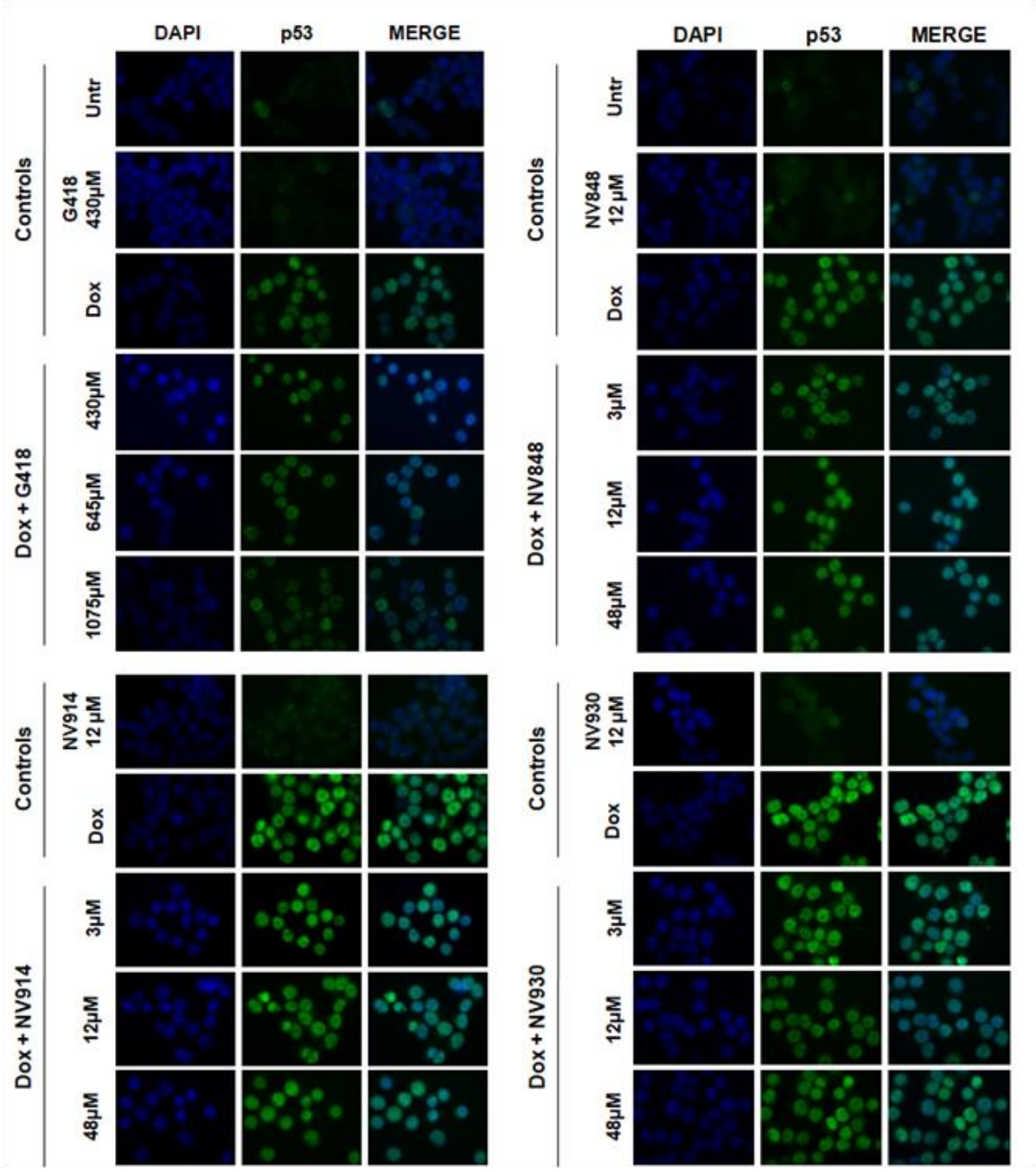

Figure 36: *Immunofluorescence analysis of HCT116 to visualize the localization of p53 (green) 24 hours after DNA damage induction by doxorubicin (0,2 µg/ml) and after 24 hours of treatment with G418, NV848, NV914, or NV930 at the indicated concentrations. p53 protein (green) was revealed by a specific primary antibody and a fluorochrome-conjugated secondary antibody (Alexa-488). Nuclei (blue) were stained with DAPI (4',6-diamidino-2-phenylindole). G418 was used as a positive control of NTCs readthrough.*

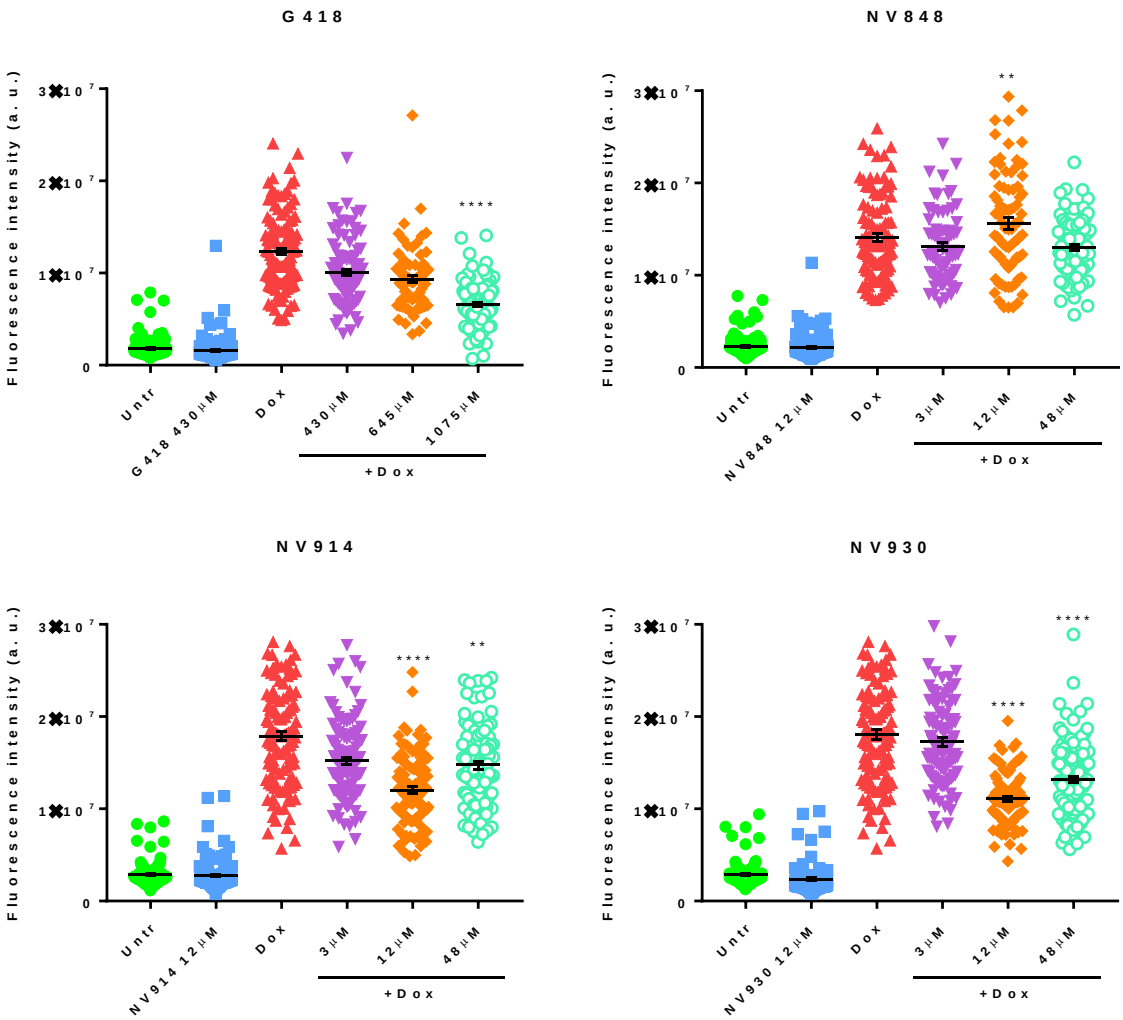

Figure 37: *Quantification of the p53 signal relative to the immunofluorescence analysis. The single shapes indicate the amount of fluorescence of a single cell. Fluorescence intensity quantification was performed by ImageJ software. Samples were analyzed compared to DNA damage controls only treated with doxorubicin (Dox). Data were analyzed by GraphPad Prism 7 software. Probability value (p): two symbols (**) for p < 0.01, four symbols (****) for p < 0.0001.*

Interestingly, the samples treated with 1075 µM of G418 showed reduced fluorescence intensity similar with respect to controls without induced DNA damage (Untr and G418 430 µM). This result could be indicative of the reduced ability of the p53 protein to respond to DNA damage as a consequence of aberrant protein production. Cells treated with NV848 and Doxorubicin showed a comparable fluorescence intensity to the DNA damage positive control sample (Dox).

On the other hand, samples treated with NV914 and NV930 showed a decreasing of fluorescence signal at 12 µM. Anyway, the p53 fluorescent signal was localized every time in the cell nuclei in all samples treated with Doxorubicin and in combination with TRIDs (G418 and NV molecules).

Since no significant change in p53 nuclear localization was revealed after treatment with Doxorubicin and NV molecules, the transcription levels of p21 (*CDKN1A*) were analyzed in order to confirm the functionality of the p53 protein.

HCT116 cells were treated with Doxorubicin and NV molecules, total mRNA was extracted and analyzed by Real time RT-PCR to determine p21 (*CDKN1A*) mRNA expression levels (**fig. 38**).

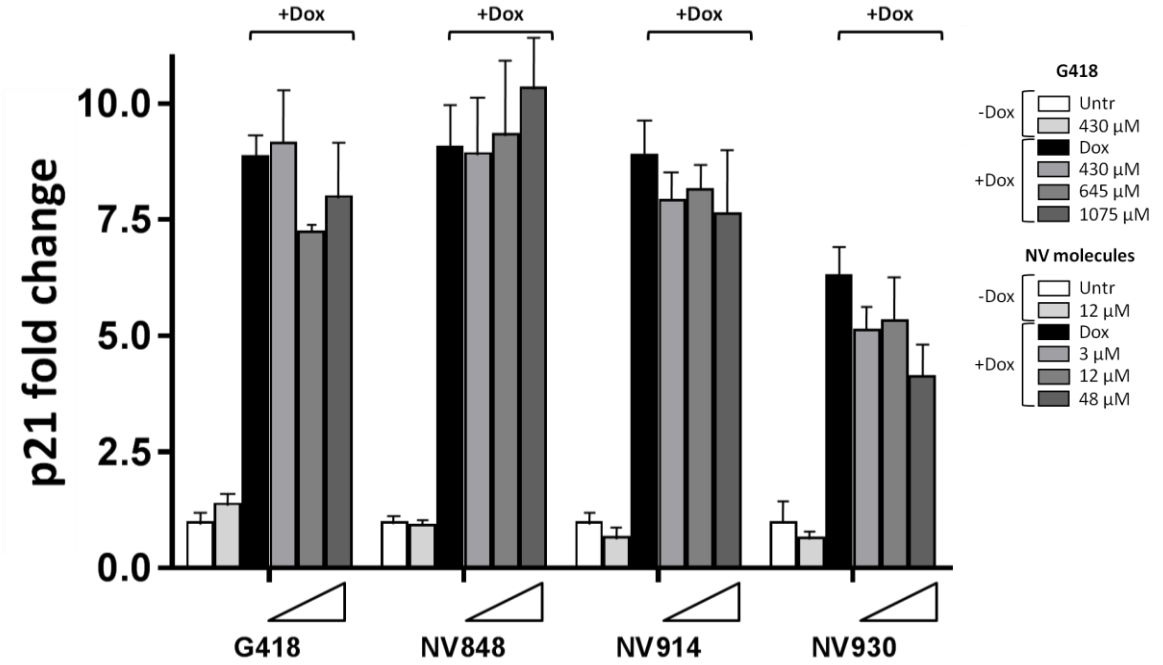

Figure 38: *Real Time RT-PCR of the p21*(*CDKN1A*) *mRNA in HCT116 cells untreated (Untr) or treated, with G418 (430 µM, 645 µM, 1075 µM) or NV molecules (3 µM, 12 µM, 48 µM) after DNA damage induction by Doxorubicin (Dox, 0,2 µg/ml). Only compound indicated the treatment without DNA damage induction (-Dox). NV or G418 samples indicated the treatment with different TRID concentrations (triangles) in combination with Doxorubicin (+Dox). Analyses were performed 24 hours after treatment conditions.*

A sensible p21 mRNA reduction (around 16%) was observed in presence of DNA damage and high concentrations of the G418 (645 µM) (**fig. 38**).

2.4 Western blot analysis of the two housekeeping proteins (Cystatin-C and β-2-Microglobulin) after treatment with NV molecules (NV848, NV914, and NV930), in order to evaluate possible NTC miscoding.

Recently a new molecule named ELX-02 has been established to be effective to treat nonsense mutations and to be safe. Furthermore, it has been shown that its targets are specifically PTCs. In fact, to demonstrate all the above-mentioned characteristics of this TRID, Crawford et al. have developed a method similar to the one shown previously for the p53 protein [Crawford D.K., et al. 2020].

Precisely, they considered two housekeeping proteins, Cystatin-C and β-2-Microglobulin, that have respectively the molecular weight of 15 kDa and 13 kDa.

The rationale of the used method is the same as described in p53. Indeed, if TRID treatment induces readthrough of NTCs in Cystatin-C and β-2-Microglobulin mRNA, a higher molecular weight can be detected by western blot analysis.

Based on the experiment by Crawford et al. human bronchial epithelial (16HBE) cells were treated with increasing concentrations of NV848, NV914, and NV930 molecules (**fig. 39**) [Crawford D.K., et al. 2020].

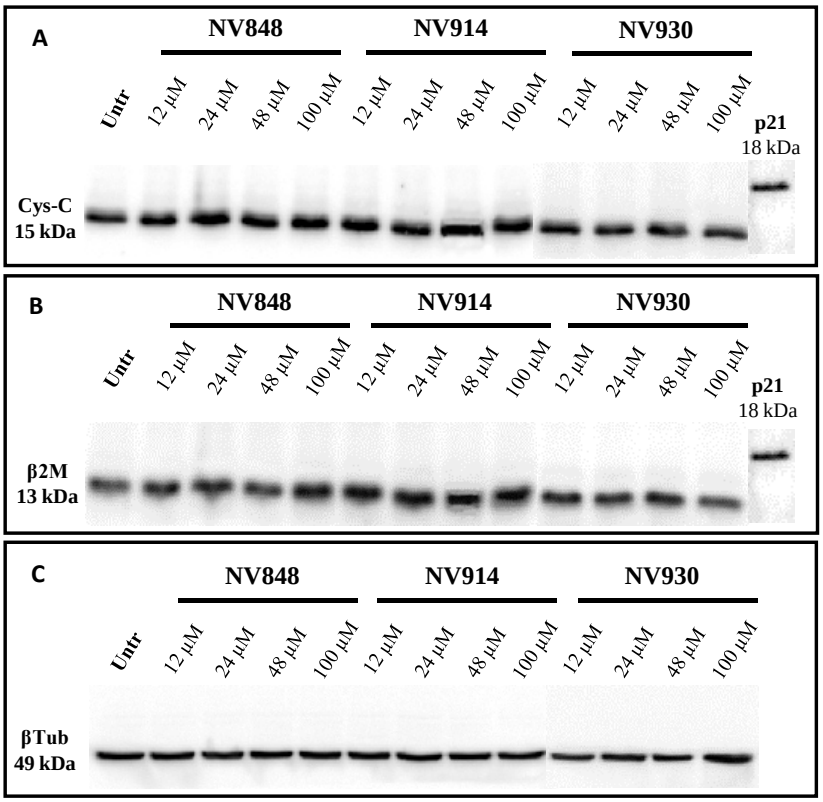

Figure 39: *Western blot analysis in 16HBE cells untreated (Untr; negative control) or treated after 24 hours with NV848, NV914, and NV930 at indicated concentrations. Images show the molecular weights of two housekeeping proteins, Cystatin-C (Cys-C; A) and β-2-Microglobulin (β2M; B). p21 protein was used as an internal control of expected high molecular weight. β-tubulin (βTub) was included as a loading control (C). Images were derived from different membranes and they were placed according to molecular weight markers migration.*

In particular, cells were treated for 24 hours at 12, 24, 48, or 100 µM and then proteins were extracted and separated by western blot analysis.

In addition, the same experiment was performed with prolonged (72 hours) treatment with TRIDs to validate the absence of NTCs readthrough (**fig. 40**).

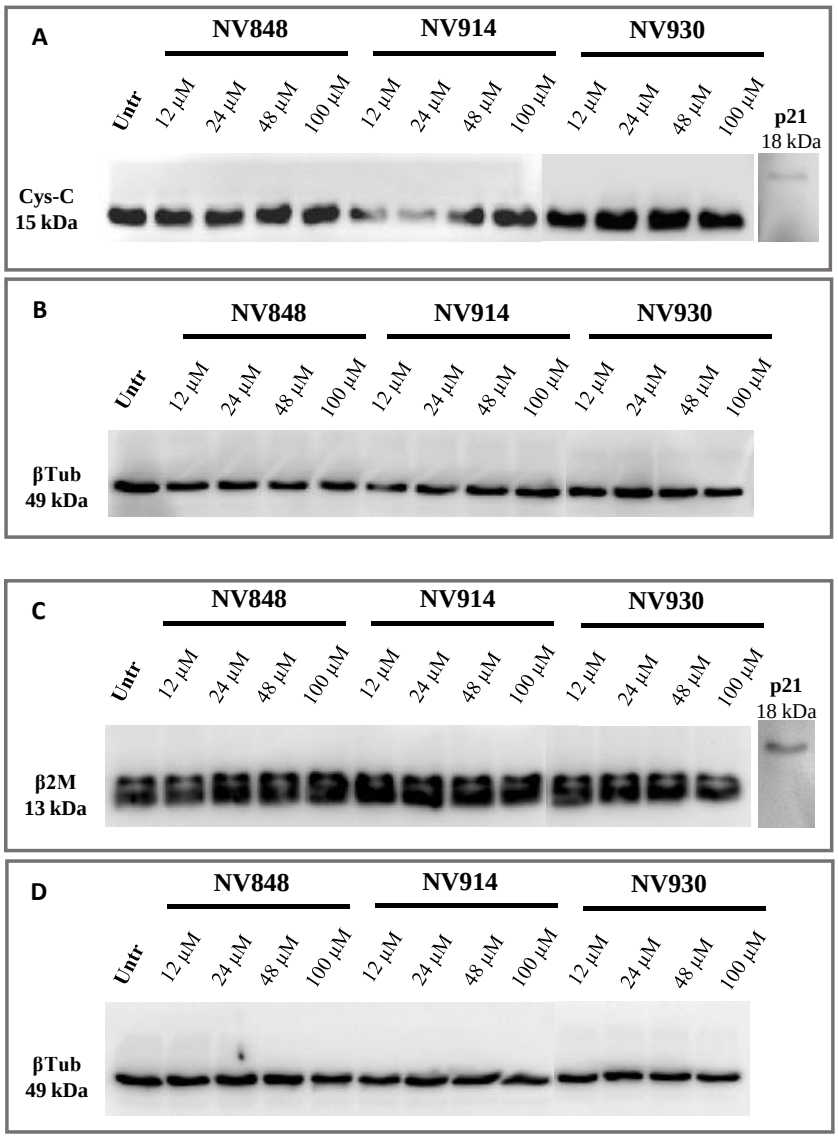

Figure 40: *Western blot analysis in 16HBE cells untreated (Untr; negative control) or treated after 72 hours with NV848, NV914, and NV930 at indicated concentrations. Every 24 hours the treatments were refreshed. Images show the molecular weights of two housekeeping proteins, Cystatin-C (Cys-C; A) and β-2-Microglobulin (β2M; C). p21 protein was used as an internal control of expected high molecular weight. β-tubulin (βTub) was included as a loading control (B-D). Images were derived from different membranes and they were placed according to molecular weight markers migration.*

No bands relative to the tested proteins with higher or abnormal molecular weight are visible, confirming the data obtained after 24 hours of treatment with NV molecules.

These experiments confirm that NV molecules did not induce appreciable readthrough on natural stop codons.

2.5 Activity study of the CFTR channel rescued by NV molecules (NV848, NV914, and NV930) in human intestinal organoids carrying CFTR nonsense mutations (G542X or W1282X).

Intestinal organoids are one of the best *in vitro* models for the estimation of CFTR protein functionality. Human intestinal organoids derived from patients carrying *CFTR* nonsense mutations were used to evaluate CFTR protein activity after treatment with NV molecules (NV848, NV914, and NV930). These experiments were performed during the external period of the Ph.D. program at the CF Organoid Research Group, University of Leuven (KU Leuven, Leuven, Belgium).

Two different genotypes were selected from intestinal organoids (derived from differentiation of adult stem cells) biobank: CFTR$^{G542X/G542X}$ and CFTR$^{W1282X/dele2,3}$. Importantly, the allele harboring dele2,3 mutation does not provide any increase of CFTR protein (class VII mutation).

In addition, in order to improve the activity of CFTR proteins, organoids were treated with CFTR modulators (Elexacaftor, Tezacaftor, and Ivacaftor) in combination with NV molecules.

CFTR$^{G542X/G542X}$ (**fig. 41-A**) and CFTR$^{W1282X/dele2,3}$ (**fig. 41-B**) organoids were treated with NV848, NV914, and NV930 alone at different concentrations and in combination with CFTR modulators for 48 hours.

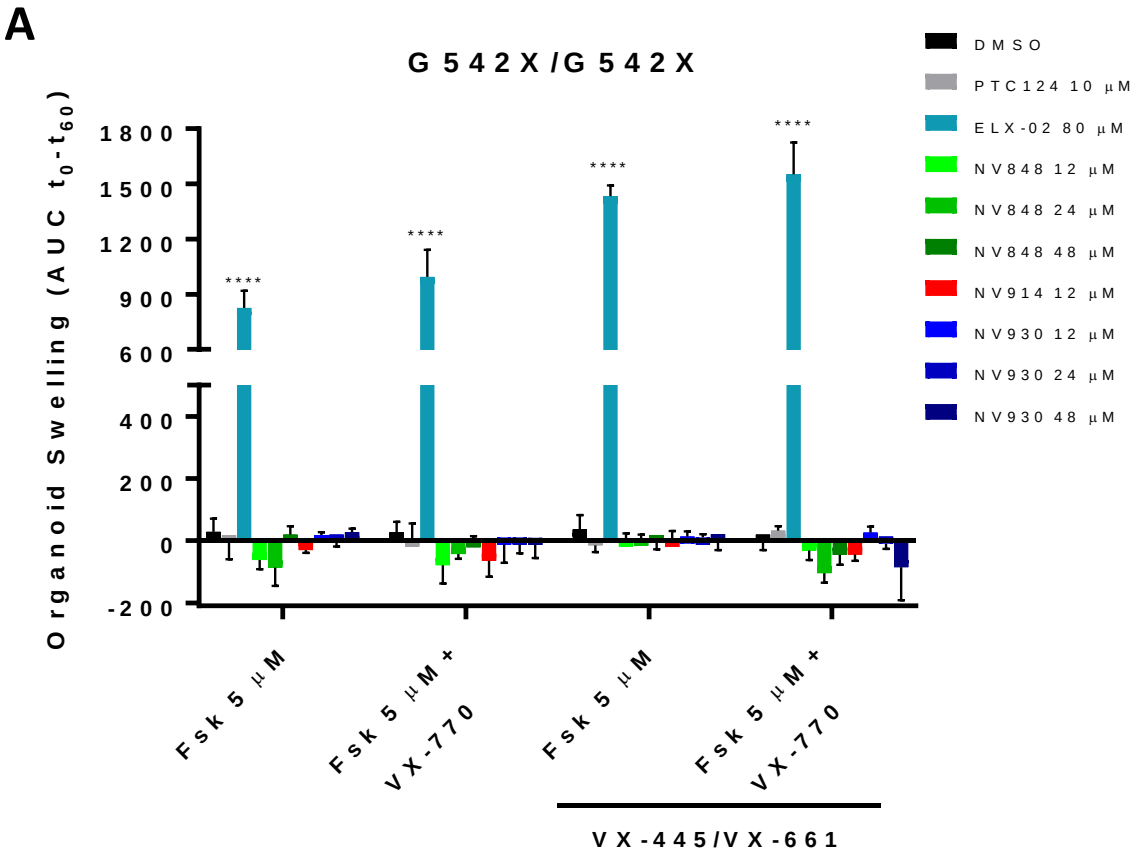

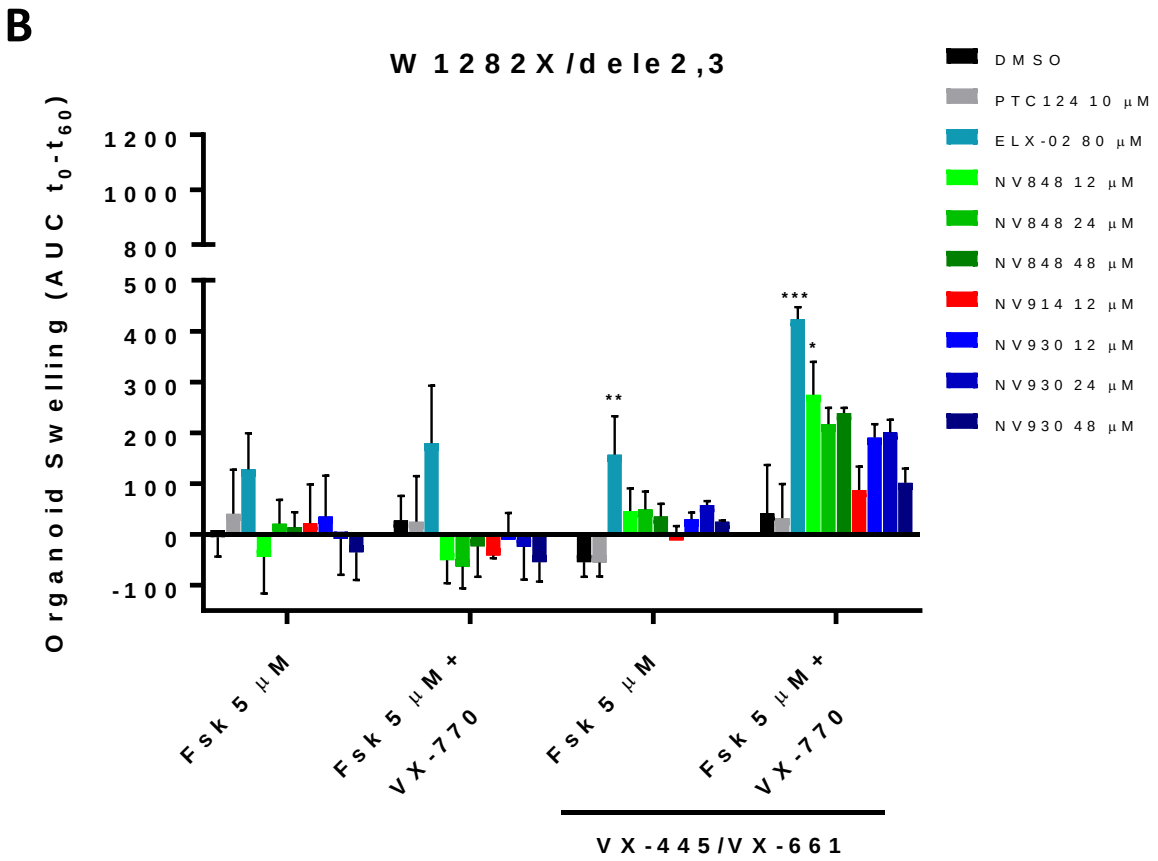

Figure 41: *$CFTR^{G542X/G542X}$ (A) and $CFTR^{W1282X/dele2,3}$(B) organoids were treated for 48 hours with DMSO (negative control), PTC124, ELX-02 (positive control), NV848, NV914, and NV930 at indicated concentrations. CFTR correctors (VX-445 Elexacaftor and VX-661 Tezacaftor; 3 µM) and CFTR potentiator (VX-770 Ivacaftor; 3 µM) were added in order to increase CFTR activity after readthrough rescue. Samples were analyzed and compared to each DMSO negative control (DMSO). Data were analyzed by GraphPad Prism 7 software. Probability value (p): one symbol (*) for p<0.05, two symbols (**) for p <0.01, three symbols (***) for p<0.001, four symbols (****) for p <0.0001.*

The forskolin-induced swelling (FIS) assay measures the increase of the organoids area (AUC; area under the curve), deriving from CFTR activity.

If CFTR protein is correctly synthesized, after the addition of forskolin (Fsk), a compound that increases the cAMP concentration and stimulates the CFTR opening, the organoids swell [Ramalho A.S., et al. 2022]. This swelling happens thanks to a water flux inside the organoid's lumen. The water enters into the lumen because the CFTR opening creates an osmotic pressure inside the organoid able to generate the swelling.

Data show two different treatment responses. In $CFTR^{G542X/G542X}$ organoids (**fig. 41-A**), the aminoglycoside ELX-02 (positive control) increased the organoids area better compared to the same treatment in $CFTR^{W1282X/dele2,3}$ organoids (**fig. 41-B**).

As regards TRIDs samples, no swelling was detected in $CFTR^{G542X/G542X}$ organoids (**fig. 41-A**). However, a visible swelling appeared in $CFTR^{W1282X/dele2,3}$ organoids (**fig. 41-B**) using TRIDs in combination with CFTR modulators (VX-445, VX-661, and VX-770). In

both genotype samples and in all experimental conditions PTC124 did not induce organoids swelling.

In order to increase the efficacy of TRIDs, the nonsense-mediated decay (NMD) pathway was inhibited in CFTR$^{G542X/G542X}$ and CFTR$^{W1282X/dele2,3}$ organoids. The NMD pathway induces the degradation of nonsense mRNAs thus limiting the NV molecule's action [Mailliot J., et al. 2022].

FIS assays were repeated in CFTR$^{G542X/G542X}$ and CFTR$^{W1282X/dele2,3}$ organoids at the previous experimental conditions (**fig. 41 A-B**), using the NMD inhibitor named NMDI14 (**fig. 42 A-B**). This compound interferes with the interaction between UPF1 and SMG7, two important NMD factors [Aksit M.A., et al. 2019].

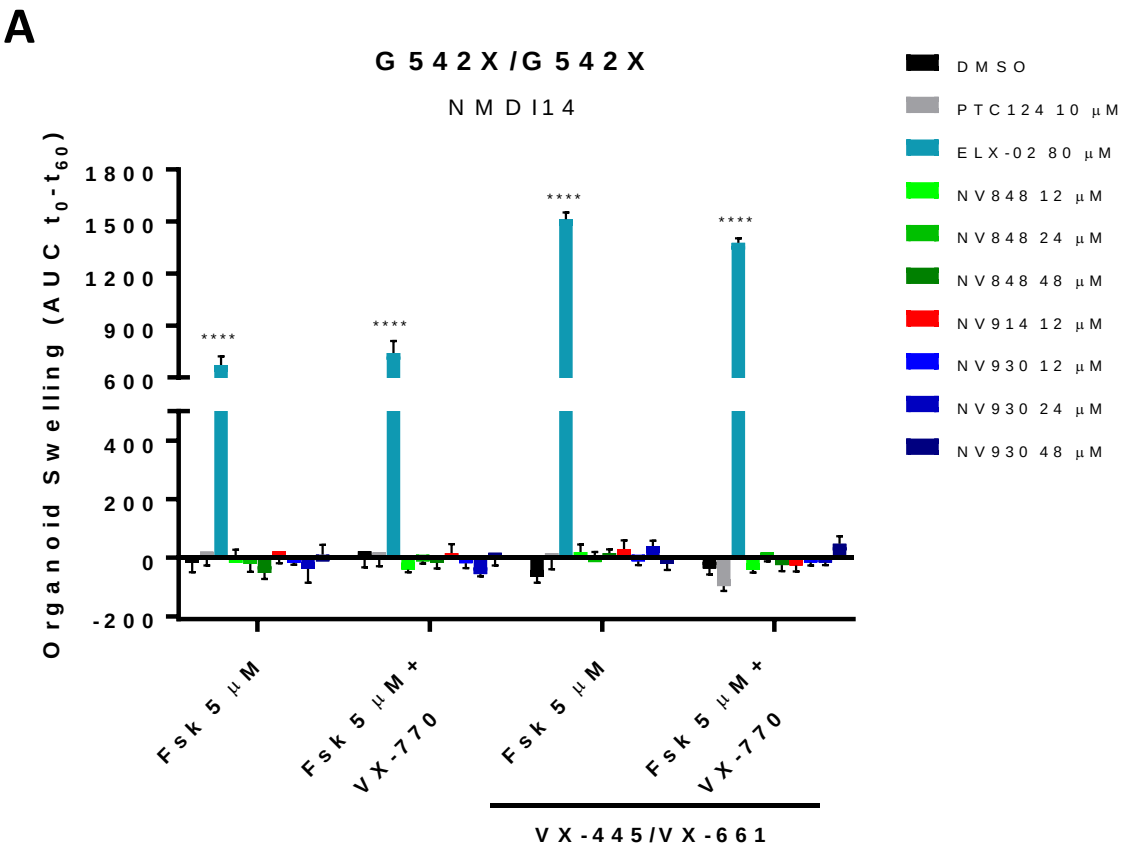

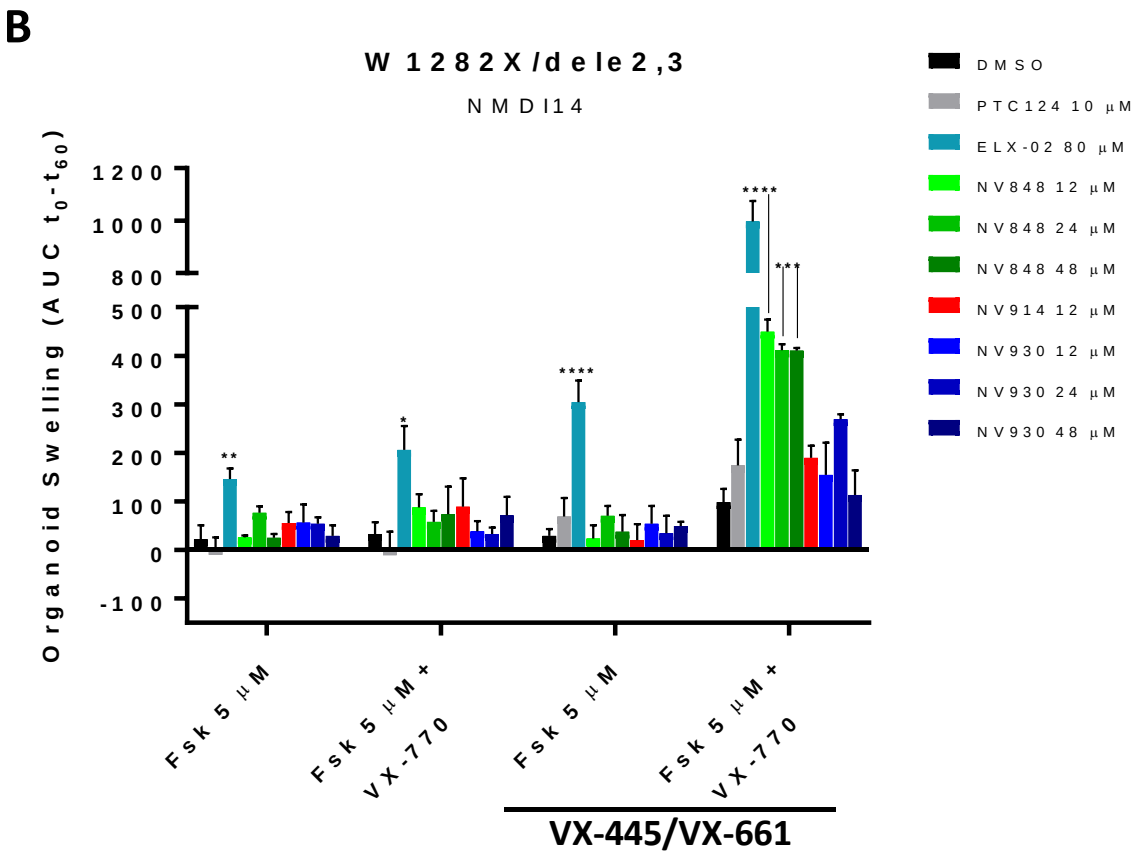

Figure 42: *CFTR$^{G542X/G542X}$ (A) and CFTR$^{W1282X/dele2,3}$(B) organoids were treated for 48 hours with DMSO (negative control), PTC124, ELX-02 (positive control), NV848, NV914, and NV930 at indicated concentrations. All samples were treated with NMD inhibitor NMDI14 (0.625 µM). CFTR correctors (VX-445 Elexacaftor and VX-661 Tezacaftor; 3 µM) and CFTR potentiator (VX-770 Ivacaftor; 3 µM) were added in order to increase CFTR activity after readthrough rescue. Samples were analyzed and compared to each DMSO negative control (DMSO). Data were analyzed by GraphPad Prism 7 software. Probability value (p):one symbol (*) for p<0.05, two symbols (**) for p <0.01, three symbols (***) for p<0.001, four symbols (****) for p <0.0001.*

Data show a little variation of AUC between the experiment without NMDI14 (**fig. 41-A**) and with the addition of the NMD inhibitor (**fig. 42-A**), as regards ELX-02. Anyway, NV molecules treatment did not induce organoid swelling also in presence of NMDI14 (**fig. 42-A**) in CFTR$^{G542X/G542X}$ organoids.

However, by inhibiting the NMD pathway through NMDI14 in CFTR$^{W1282X/dele2,3}$ organoids, it is possible to see an increase of AUC in samples treated with TRIDs and CFTR modulators (VX-445, VX-661, and VX-770; **fig. 42-B**), compared to the FIS assay without NMDI14 (**fig. 41-B**). Thus, NMD inhibition synergized with the induction of translational readthrough via TRIDs, at least in CFTR$^{W1282X/dele2,3}$ organoids.

Finally, the percentage of the increasing area during FIS assays in CFTR$^{W1282X/dele2,3}$ organoids evidenced the difference between the CFTR rescue mediated by NV848 and PTC124 treatment in combination with CFTR modulators (VX-445, VX-661, and VX-770; **fig. 43 A-B**). The same result was visible using the NMD inhibitor NMDI14 (**fig. 43 C-D**).

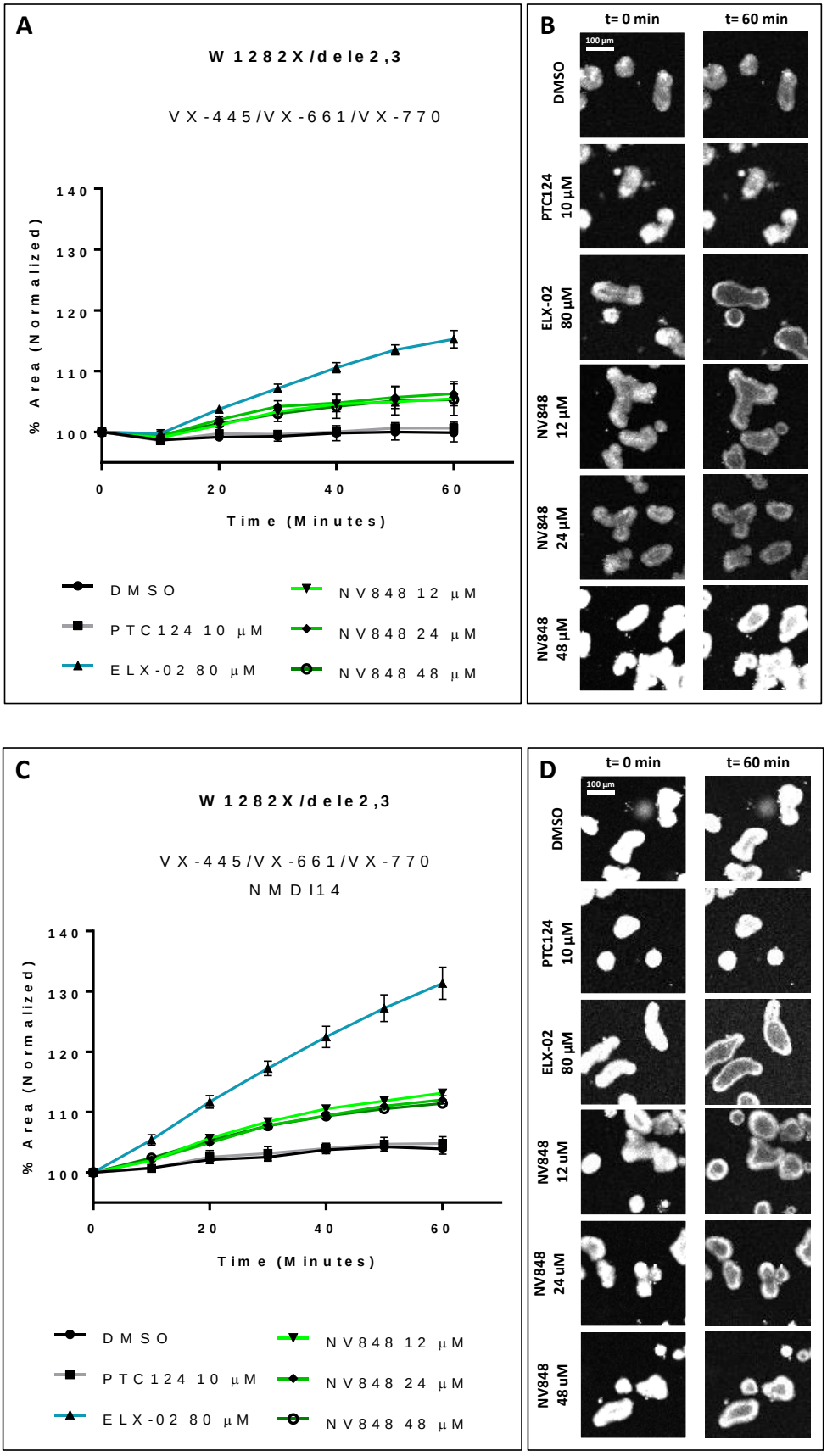

Figure 43: *(A-C) Percentage of total CFTR$^{W1282X/dele2,3}$ organoids area (1 hour of FIS), 48 hours after treatment with DMSO (negative control), PTC124, ELX-02 (positive control), and NV848 at indicated concentrations in combination with CFTR modulators (VX-445 Elexacaftor; VX-661 Tezacaftor; VX-770 Ivacaftor; 3 µM). NMD pathway inhibitor NMDI14 (0.625 µM) was used in order to increase TRIDs efficacy*

(C). (B-D) Representative confocal images (calcein staining) of human intestinal organoids (W1282X/dele2,3) during FIS assay (0 min to 60 min). Scale bar = 100 µm.

TASK#3 NV848, NV914, and NV930 molecule metabolic stability and mechanism of action (MOA) studies.

An important step to evaluate the metabolic stability of the three compounds NV848, NV914, and NV930 was the study of the three molecules amount after incubation with human liver microsomes (HLM). In fact, HLM can be used to investigate cytochrome-P450 (CYP) and UDP-glucuronyl-transferase (UGT) activity (in addition to other enzymes activity such as flavin monooxygenase and epoxide hydrolase), and to evaluate the consumption of exogenous drugs, mimicking the liver biotransformation ability *in vitro*. The human liver vesicles used were derived from 50 different donors in order to collect more enzyme isoforms in a single microsomes mix. In the used system, all donors were equally represented for a truer population sample (25 female and 25 male donors; mixed gender). The metabolism products were analyzed by LC-MS/MS (in collaboration with Prof. Pibiri I., STEBICEF Department, University of Palermo) in order to clarify the amount of compound that was metabolized after incubation.

3.1 Evaluation of NV848 metabolic stability in human liver microsomes (HLM).

HLM (30 µg) were incubated with PTC124 or NV848 in two different buffers (DPBS and Tris) at 37°C. A phosphate buffer (DPBS) and another one without phosphate components (Tris), were used to understand eventual alteration in HLM efficiency.

Every mix contained the necessary cofactors and substrates for the evaluation of the metabolic activity of cytochrome-P450 alone (CYP) or contemporary the UGT and CYP activity (CYP/UGT). A single reaction was stopped by adding acetonitrile (organic solvent) after 0, 5, 30, and 60 minutes (**fig. 44**).

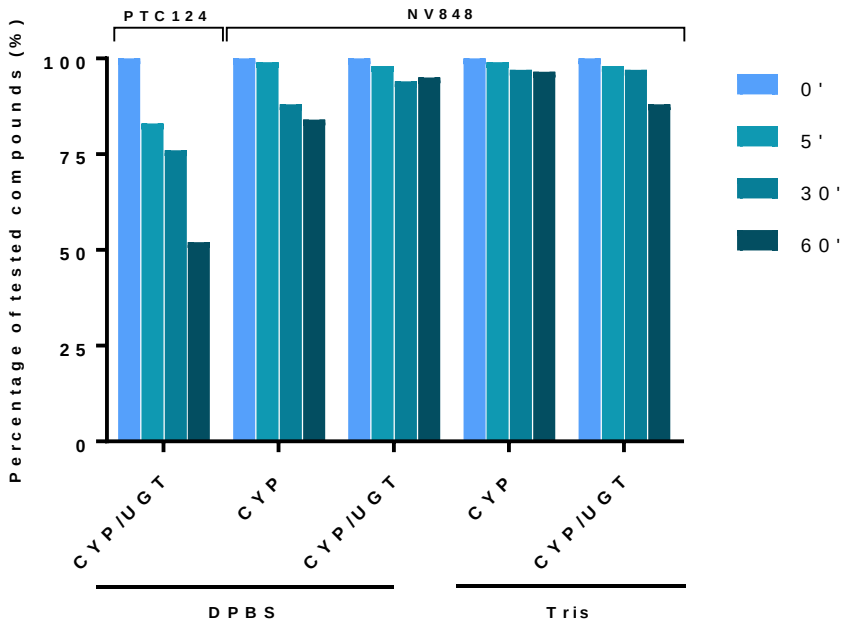

Figure 44: *Percentage of tested compounds after 0, 5, 30, and 60 minutes incubated with human liver microsomes (HLM). Samples have been distinguished with respect to enzymatic activity (CYP or CYP/UGT) and phosphate buffers used (DPBS and Tris).*

The samples were collected and analyzed by LC-MS/MS (in collaboration with Prof. Pibiri I., STEBICEF Department, University of Palermo).

We used PTC124 (Ataluren; oxadiazole readthrough agent) to verify the compound consumption observed by Kong et al. as a control [Kong R., et al. 2020]. PTC124 incubation with HLM confirmed the metabolic consumption of the compound which reached about 50% after 60 minutes, while the corresponding formation of its glucuronate derivative as the main metabolite was observed.

On the other hand, NV848 showed higher metabolic stability with its major consumption reaching 16% or 11% after 60 minutes in CYP-DPBS or CYP/UGT-Tris conditions, respectively, while no metabolite was detected. Irrelevant NV848 consumption (around 5%) was observed in the other experimental conditions, CYP/UGT-DPBS and CYP-Tris.

In general, NV848 is more stable against biotransformation mediated by CYP, UGT, and other liver microsome enzymes compared to PTC124. Interestingly, no glucuronate metabolites were detected after incubation of NV848 in presence of the cofactors needed for the evaluation of UGT activity (also in two different buffers).

3.2 Evaluation of NV914 metabolic stability in human liver microsomes (HLM).

Regarding NV914, the compound's consumption was detected by HPLC (LC-MS/MS) analysis as previously described for the NV848 test (**fig. 44**). Microsome assays were

performed only in phosphate buffer (DPBS) because the HLM experiments using NV848 did not show any significant difference between DPBS and Tris buffer analysis (**fig. 45**).

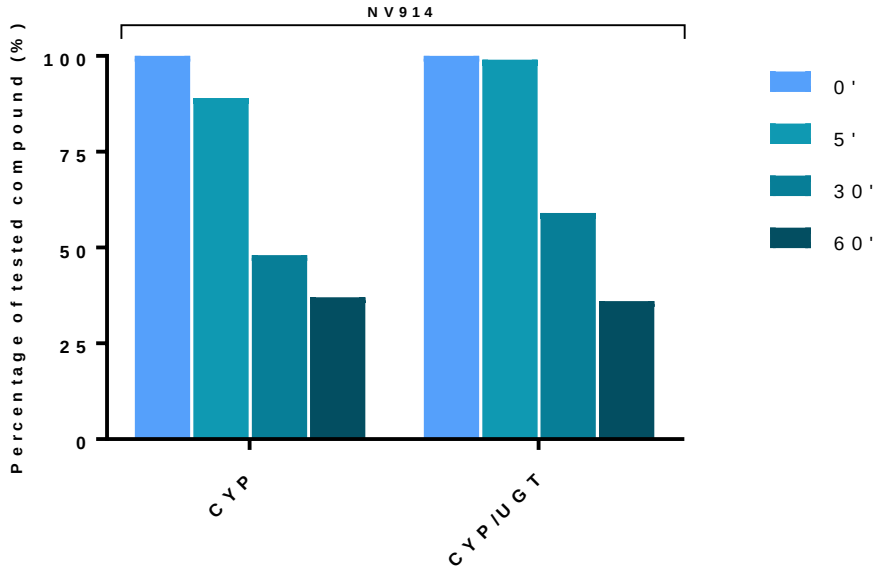

Figure 45: *Percentage of the tested compound after 0, 5, 30, and 60 minutes incubated with human liver microsomes (HLM). Samples have been distinguished with respect to enzymatic activity (CYP or CYP/UGT).*

In contrast to NV848 stability in HLM, the consumption of NV914 was comparable to that observed in PTC124 CYP/UGT samples (**fig. 44**). Furthermore, NV914 probably was metabolized by cytochrome-P450 (CYP) and fewer by UDP-glucuronyl-transferase (UGT).

These experiments suggested that NV914 stability in HLM was different with respect to the stability of NV848. Although, the readthrough activity *in vitro* of NV914 was confirmed by previous tests.

3.3 Evaluation of NV930 metabolic stability in human liver microsomes (HLM).

The metabolic stability of NV930 was performed according to the experimental conditions of NV848 and NV914 analysis.

As regards NV930 metabolization, its specific mass was detected only at the first two time points (0' and 5') and with a very low percentage (around 10%). Since the molecule cannot be metabolized at time 0 min, a possible rearrangement has been proposed (**fig. 46**). The NV930 HPLC analysis revealed a specific peak corresponding to benzoyl cyanamide mass and for this reason, the rearrangement was suggested.

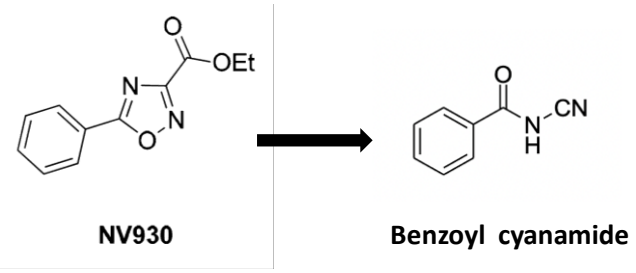

Figure 46: *Proposed NV930 rearrangement and chemical structure of the resulting compound. NV930 formula: $C_{10}H_{11}N_2O_3$. Benzoyl cyanamide formula: $C_8H_6N_2O$.*

At this point, a new experiment using a benzoyl cyanamide solution was made. HLM were incubated with benzoyl cyanamide (37°C) and the reactions were stopped using acetonitrile. After HPLC analysis, benzoyl cyanamide seems very stable in metabolism since the concentration registered after 60 minutes was similar respect to the initial one.

In order to clarify a possible benzoyl cyanamide readthrough activity, HeLa cells were transfected using a vector harboring the cDNA of firefly luciferase with a nonsense mutation (UGA) in the FLuc cDNA (p-FLuc^{opal}). HeLa cells were plated onto 6-well plates and 24 hours after transfection cells were treated with different concentrations (6, 12, or 24 µM) of benzoyl cyanamide for 24 hours. As a positive control, 12 µM PTC124 was used (**fig. 47**).

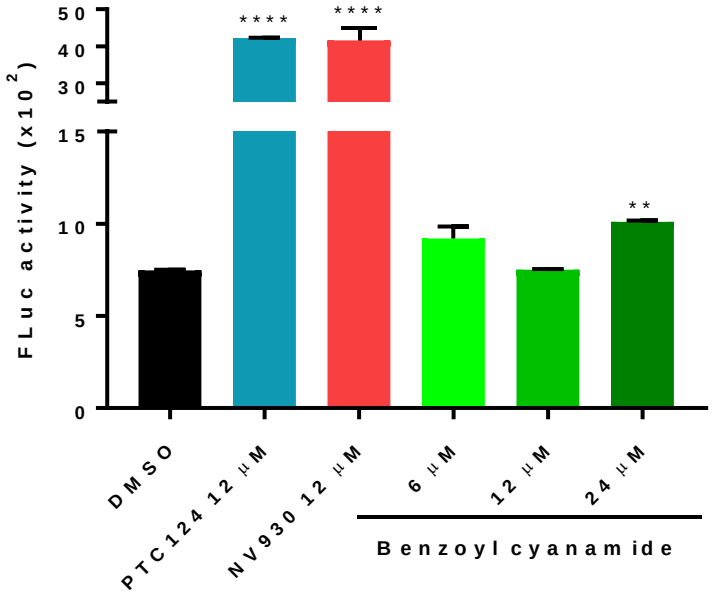

Figure 47: *Luciferase activity in HeLa cells transfected with luciferase^{UGA} vector (p-FLuc^{opal}; 1,0 µg). Cells were treated 24 hours after transfection with DMSO (negative control), PTC124 12µM (positive control), NV930 12 µM and benzoyl cyanamide (6 µM, 12 µM, and 24 µM). Data were analyzed by GraphPad Prism 7 software. A probability value (p) with respect to the DMSO sample: two symbols (**) for $p < 0.01$; four symbols (****) for $p < 0.0001$.*

PTC124 was used at the optimum concentration (12 µM), the same concentration of NV molecules [Pibiri I., et al 2020].

Data show a small increase of FLuc activity after treatment with benzoyl cyanamide 24 µM (around 34% compared to DMSO sample). However, the rescue of luminescence signal after treatment with PTC124 or NV930 was more efficient (around 4 fold) with respect to benzoyl cyanamide (24 µM).

3.4 NV molecules (NV848, NV914, and NV930) interact with the methyltransferase FTSJ1 as a potential mechanism of action (MOA).

Nowadays, as regards translational readthrough, only the molecular target of aminoglycoside antibiotics is supported by several evidence [Prokhorova I., et al., 2017].
In recent work, Trzaska C. and Lejeune F. have identified a new molecular target for the compound 2,6-diamino purine (DAP), a molecule that possesses translational readthrough activity [Trzaska C., et al. 2020]. One of the most commonly incorporated tRNAs at the PTC position (UGA stop codon) is the $tRNA^{Trp}$ (Tryptophan). This specific $tRNA^{Trp}$ can be modified by the methyltransferase named FTSJ1, that methylates the cytosine at position 34 of $tRNA^{Trp}$. The inhibition of FTSJ1 is associated with an increase of UGA stop codon recognition by $tRNA^{Trp}$. This mechanism enhances the translational readthrough probability.

The hypothesis is thus to understand if NV molecules could interact with FTSJ1 as the DAP compound does. If it is possible, when the concentration of FTSJ1 increases in the cells, the readthrough activity of NV molecules is altered because their concentration is not enough to inhibit all FTSJ1 proteins.

In order to evaluate the possible interaction between FTSJ1 and NV848, NV914, and NV930 molecules, HeLa cells were co-transfected with a vector harboring the UGA premature stop codon in the firefly luciferase cDNA and another vector harboring FTSJ1 cDNA (kindly provided by F. Lejeune, Institut de Biologie de Lille, France). The cells were then treated 24 hours after transfection with NV848, NV914, NV930, or DAP (**fig. 48**).

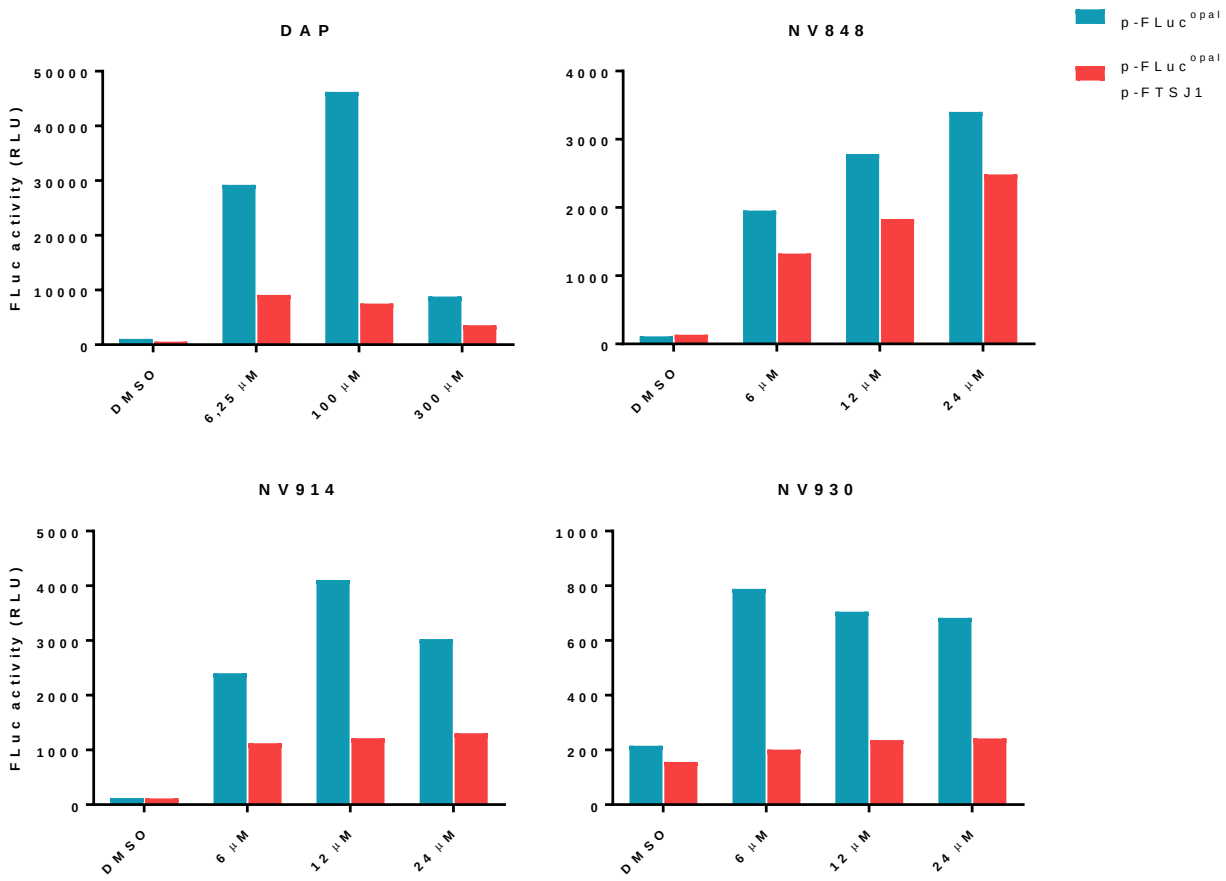

Figure 48: *Luciferase activity in HeLa cells co-transfected with luciferase^{UGA} vector (p-FLuc^{opal}; 1,0 µg) and FTSJ1 vector (p-FTSJ1; 2,0 µg). Cells were treated 24 hours after transfection with DAP (6,25 µM, 100 µM, and 300 µM), NV848, NV914, and NV930 at the indicated concentrations (6 µM, 12 µM, and 24 µM).*

As shown in **figure 48**, NV848 inhibited weakly FTSJ1 with respect to DAP. These results indicate that the FTSJ1 protein probably is not an NV848 target.

However, the treatment with NV914 and NV930 decrease strongly the luminescence signal after co-transfection of the p-FTSJ1 vector, compared to the samples only transfected with p-FLuc^{opal}. The similar FLuc decreasing activity pattern between DAP, NV914, and NV930 suggests that these NV compounds could interact with the methyltransferase FTSJ1.

Moreover, computational experiments performed by Prof. Tutone M. (STEBICEF department, University of Palermo; Carollo P.S., et al. manuscript in preparation) confirmed these results. NV914 and NV930 showed more affinity for FTSJ1 methyltransferase catalytic site compared to NV848, during a quantitative structure-activity relationship (QSAR) simulation.

3.5 Non-oxadiazolic TRIDs (NV2899, NV2909, NV2913, and NV2907) treatment in order to rescue CFTR expression.

The last aim of the project was to test other potential readthrough compounds in view of a possible failure of the three NV molecules studied. Therefore, in parallel, the aim was to study four new non-oxadiazole compounds: NV2899, NV2909, NV2913, and NV2907 (**fig. 49**)

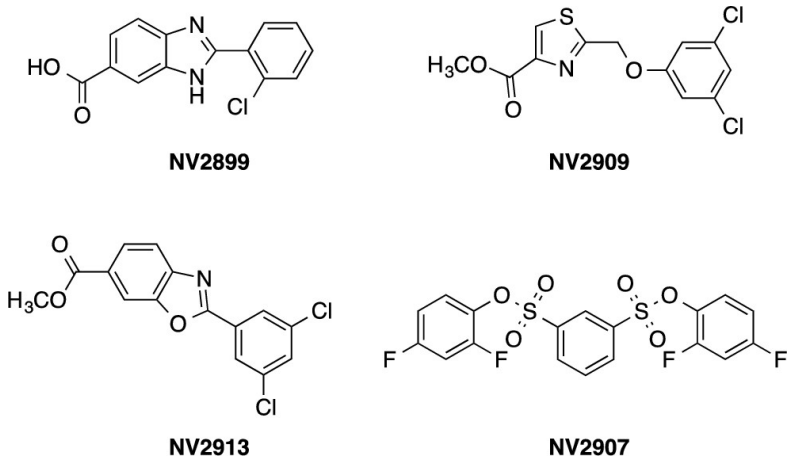

Figure 49: *Four non-oxadiazole compound structures. Also, the chemical core and substituents are different with respect to PTC124 (Ataluren) chemical characteristics.*

Firstly, the four non-oxadiazole core compounds cytotoxicity was tested in FRT cells after 24, 48, and 72 hours of treatment with NV2899, NV2909, NV2907, or NV2913 compounds at 12 µM and stained with trypan blue to quantify live and dead cells (**fig. 50**).

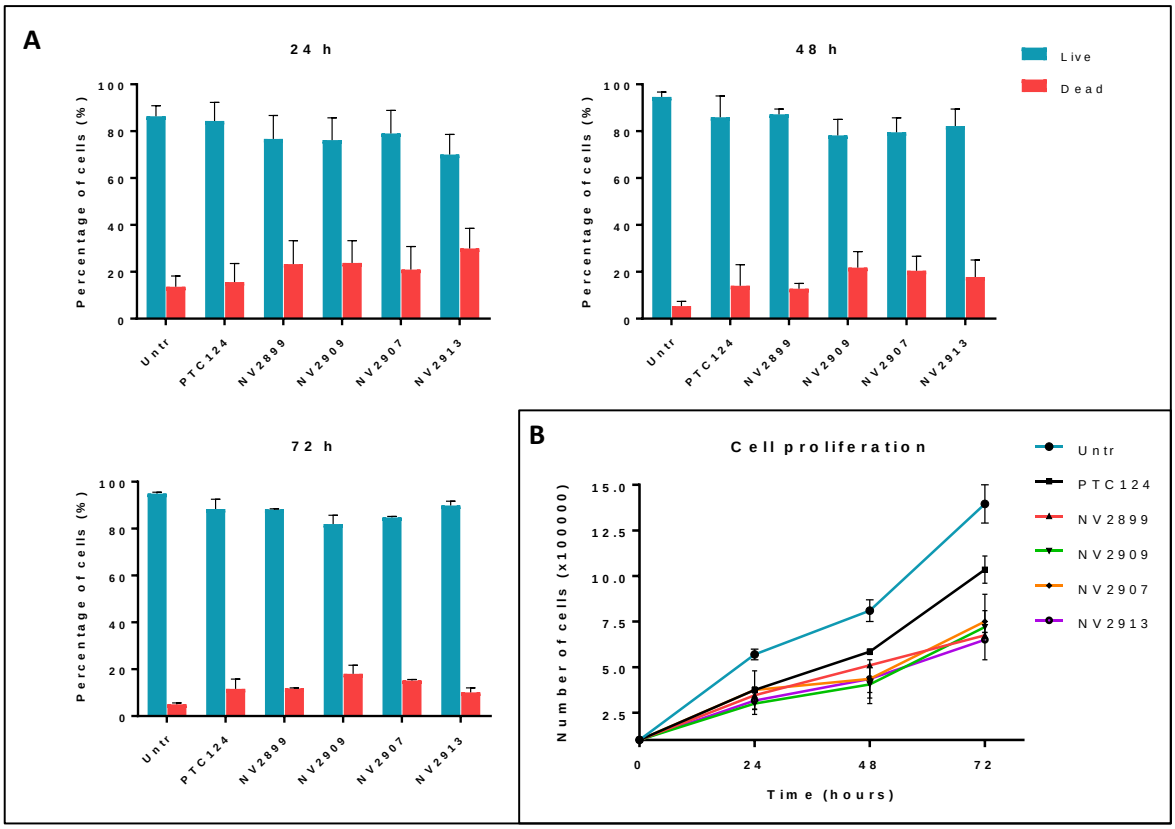

Figure 50: *(A) Percentage of live and dead FRT cells after 24, 48, and 72 hours of treatment with NV2899,*

NV2909, NV2907, or NV2913 (12 µM) readthrough compounds. (B) Cell proliferation at 24, 48, and 72 hours of treatment with indicated compounds. PTC124 was used as a non-toxic readthrough agent control.

The concentration used to treat FRT cells (12 µM) is the optimum concentration used for NV848, NV914, and NV930 experiments [Pibiri I., et al. 2020].

The new four non-oxadiazole core compounds showed a similar percentage of dead cells in analyzed samples. All treated FRT cells (with NV molecules or PTC124) presented a decrease in cell proliferation with respect to untreated cells (Untr). This could be attributed to the compound's solvent (DMSO) that shares all treatments.

Translational readthrough efficiency was evaluated in FRT cells stably transfected with a plasmid harboring the cDNA of the human CFTR gene with the most diffuse nonsense mutation G542X (UGA stop codon) [Laselva O., et al. 2022]. CFTR protein rescue was detected by immunofluorescence assay. FRT-CFTR^{G542X} cells were seeded on rounded glass coverslips in 12-well plates and treated with NV2899, NV2907, NV2909, or NV2913 molecules at 12 µM for 24 hours (**fig. 51**).

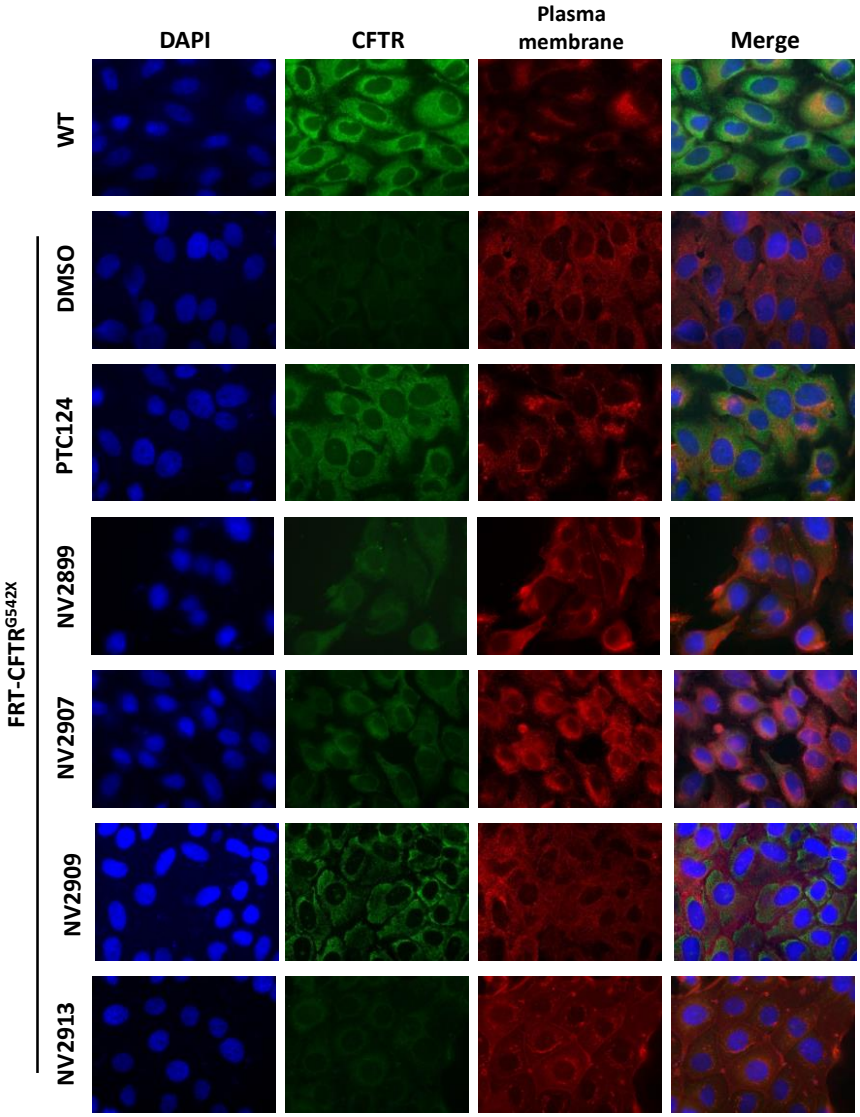

Figure 51: *Immunofluorescence analysis of FRT cells stable transfected with a plasmid harboring CFTR*

cDNA with nonsense mutation (FRT-CFTR^{G542X}), treated with DMSO (vehicle, negative control; DMSO) or NV2899, NV2907, NV2909, or NV2913 (12 µM) for 24 hours. FRT cells stable transfected with a plasmid harboring CFTR WT cDNA (WT) were used as a positive control. PTC124 sample represents the translational readthrough positive control. CFTR protein (green) was revealed by a specific primary antibody (ab570) and a fluorochrome-conjugated secondary antibody (Alexa-488). Nuclei (blue) were stained with DAPI (4',6-diamidino-2-phenylindole) and the plasma membrane (red) was stained with wheat germ agglutinin (WGA)-Alexa 594.

PTC124 was used as translational readthrough control (positive control). Immunofluorescence images (**fig. 51**) showed CFTR rescue in samples treated with NV2899 and NV2909 compared to the negative control (DMSO). In contrast, FRT-CFTR^{G542X} treated with NV2907 and NV2913 did not show protein rescue after 24 hours of treatment. These data were confirmed by immunofluorescence signal quantification (**fig. 52**).

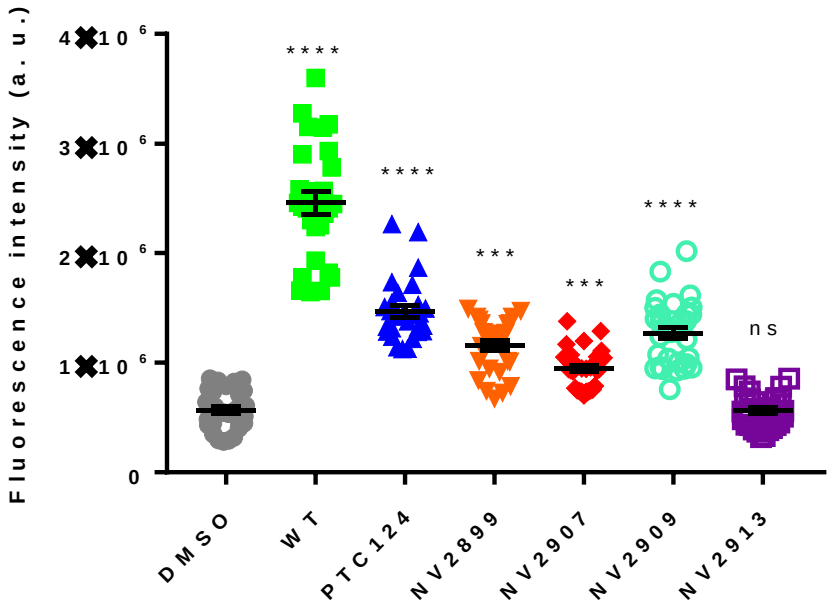

Figure 52: *Quantification of the CFTR signal relative to the immunofluorescence analysis. The single shapes indicate the amount of fluorescence of a single cell. Fluorescence intensity quantification was performed by ImageJ software. Samples were analyzed and compared to DMSO control (DMSO). Data were analyzed by GraphPad Prism 7 software. Probability value (p): three symbols (***) for p < 0.001, four symbols (****) for p < 0.0001. ns= not significant.*

DISCUSSION.

CF is one of the most adverse genetic pathologies caused by several different mutations in the *CFTR* gene. The heterogeneity among *CFTR* mutations makes the identification of a unique CF cure a complicated challenge. In terms of finding a target therapy for every mutation, this research project was based on the study of the CFTR expression rescue in presence of splicing and nonsense mutations.

Splicing defects in CFTR mRNAs are not widely investigated, especially some polymorphisms such as the T_5TG_{12} polymorphism located into the intron 9.
In this work, the treatment with two small molecules *kinetin* and RECTAS was proposed as a pharmacological approach to restoring CFTR expression in cell systems harboring splicing mutation (T_5TG_{12} polymorphism).
Using a CFTR vector that contains the CFTR *minigene* characterized by T_5TG_{12} polymorphism and part of the two introns 9 and 10 ($CFTR^{N59+N510+5T12TG}$), the rescue of mRNAs splicing and protein recovery was studied.
After transient expression of $CFTR^{N59+N510+5T12TG}$ in FRT cells, the treatment with *kinetin* and RECTAS partially corrected the aberrant CFTR mRNAs splicing and increased the amount of exon 10 inclusion. As demonstrated by the use of specific primers that map into the exon 10. It can be hypothesized that *kinetin* and RECTAS modulate the splicing of mutated CFTR mRNAs interacting with the spliceosome components in order to avoid the exon 10 skipping. Presumably, the *kinetin* and RECTAS mechanism of action is specific for mRNAs with mutations in splicing *cis*-elements (e.g. T_5TG_{12} polymorphism) and not for CFTR transcript.
In addition, this was associated with increased CFTR protein expression and localization in the plasma membrane of the transfected FRT cells.

In order to generate stable cells expressing the $CFTR^{N59+N510+5T12TG}$ *minigene*, it was successfully cloned in the retroviral vector pBPSTR1 (pBPSTR1-$CFTR^{N59+N510+5T12TG}$).
After the transfection of Phoenix packaging cells and retroviral infection, FRT cells were used to generate $CFTR^{N59+N510+5T12TG}$ stable expressing cells.
The experiments performed in FRT stable expressing $CFTR^{N59+N510+5T12TG}$ confirmed the partial rescue of CFTR protein expression after treatment with *kinetin* or RECTAS. These two molecules represent an important and potential treatment of the *CFTR* gene splicing mutations.

In the second part of my project, I focalized the attention on *CFTR* nonsense mutations (class I). Nonsense mutations lead to an aggressive form of CF, caused by the complete absence of functional CFTR proteins in the cells. To date, no one experimental treatments specific to CFTR nonsense mutations are effective, but the inducing of PTC translational readthrough mediated by compounds (TRIDs) can be one of the most promising and quickly available strategies to rescue this class of CFTR mutations.

Advanced studies of three new TRIDs named NV848, NV914, and NV930 obtained in this project, have added original evidence regarding their specificity, functionality, stability, and mechanism of action [Pibiri I., et al. 2020].

In my project, the specificity of NV848, NV914, and NV930 against premature stop codons (PTCs) was confirmed using two different *in vitro* systems. In fact, to exclude the possibility that the NV molecules induced the readthrough of the NTCs, three different translation products were analyzed with the intent to identify increased forms of molecular weight.

As proteins model the Cys-C and β2M were chosen because ubiquitous proteins and above all they were used previously to demonstrate the absence of the readthrough on the NTC by ELX-02 [Crawford D.K., et al. 2020].

In particular, by using *in silico* translation (ExPASy translate tool), it was observed that the amino acids included between the first stop codon (NTC) and the second one in the sequence encoding for the Cys-C protein, are 60. Through a theoretical calculation, these amino acids hypothetically add about 7,32 kDa to the Cys-C protein. For β2M resulted 49 amino acids between the two stop codons and a theoretical addition of 5,71 KDa to the molecular weight of the proteins reported in **figure 53**.

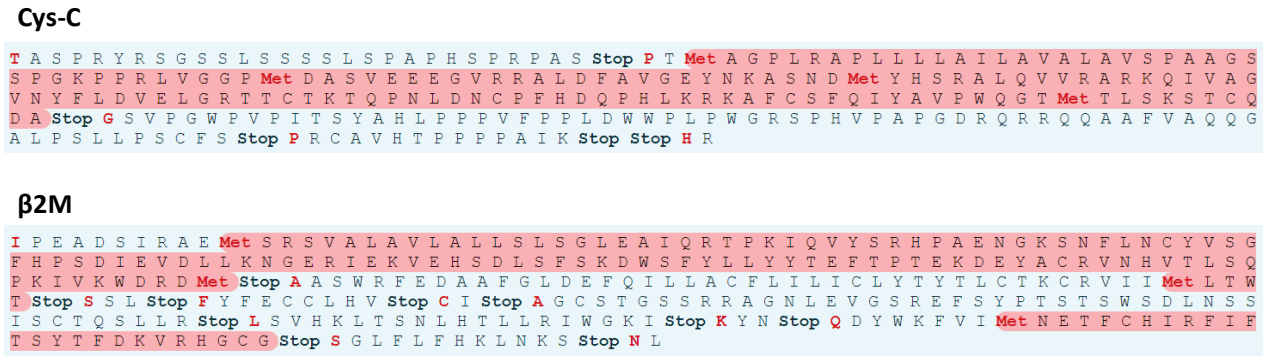

Figure 53: *In silico translation of Cystatin C (Cys-C) and β-2-Microglobulin (β2M) mRNAs. Open riding frames are highlighted in red.*

Western blot analysis did not show any translational products with higher molecular weight after treatment with NV848, NV914, and NV930 (**fig. 39-40**).

In addition, a similar study using p53 protein as a model system was performed. The treatment with NV848, NV914, and NV930 molecules did not show molecular weight alteration or a functional alteration of p53, except using the aminoglycoside G418 (protein localization decreasing after DNA damage). Moreover, these results are consistent with a recent work in which the data show that the ribosome could reach the UTR region of mRNAs (over the NTCs) after treatment with G418 (1075 μM = 500 μg/mL) in HEK293T cells [Wangen J.R. and Green R. 2020].

An important goal of this project was the study of the activity of the three NV molecules in CF human organoids harboring nonsense mutation of the CFTR gene. Human CF intestinal organoids represent an important preclinical *in vitro* system for the estimation of drug activity.

NV molecules were tested on two different organoid genotypes (G542X/G542X and W1282X/dele2,3) in combination with CFTR modulators or NMD pathway inhibitor. In all conditions, NV848, NV914, and NV930 did not work in $CFTR^{G542X/G542X}$ organoids, but the combination of NV molecules and CFTR modulators, restored partially the CFTR activity in $CFTR^{W1282X/dele2,3}$ organoids, especially using NV848.

Moreover, the treatment with NV848, NV914, and NV93, associated with CFTR modulators, in combination with NMD inhibitor (NMDI14), enhanced the effect of NV molecules in $CFTR^{W1282X/dele2,3}$organoids.

These results are relevant for the research of new readthrough agents, especially because the major promising compound's clinical trial (ELX-02) failed the clinical trial (ClinicalTrials.gov Identifier: NCT04135495).

Finally, the project was extended in the evaluation of the effective stability of the NV molecules in a system that mimics liver metabolism *in vivo*. Molecule stability is fundamental for their correct activity in biological systems. One of the best *in vitro* systems for the evaluation of compound stability is the use of human liver microsomes (HLM). Studies of NV848, NV914, and NV930 stability in HLM are important preliminary steps for *in vivo* administration.

In particular, the NV848 molecule revealed good metabolic stability in HLM compared to commercial readthrough agent PTC124 (Ataluren).

In contrast, the HLM metabolic stability of NV914 appeared similar to that of PTC124, with a consumption of 36% at 60 min (CYP/UGT activity evaluation).

Interestingly, NV930 appeared to change in a compound (benzoyl cyanamide) that showed low readthrough activity in HeLa cells transfected with $p\text{-}FLuc^{opal}$. Probably, a minimal

percentage of NV930 could be converted into benzoyl cyanamide, because NV930 rescues *CFTR* nonsense mutation in cells.

Finally, the mechanism of action (MOA) of NV848, NV914, and NV930 was investigated. It was suggested that NV molecules could interact with protein factors during translation and not with the ribosome as aminoglycoside antibiotics (e.g. G418) [Huang S., et al. 2022].

One of the most interesting targets of NV914 and NV930 (deriving from computational analysis performed by Prof. Tutone M., STEBICEF Department, University of Palermo) could be the catalytic site of the methyltransferase FTSJ1. In my experiments, the co-transfection with p-FTSJ1 and p-FLuc^{opal} plasmids and contemporary treatment with NV914 and NV930, revealed a similar decrease in luminescence signal as observed by readthrough agent (DAP) that inhibits FTSJ1 and promotes translational readthrough [Trzaska C., et al. 2020].

However, NV848 showed a different response suggesting that this compound could not interact with the methyltransferase catalytic site but probably with other factors (e.g. DDX19 or eRF factors; **fig. 54**).

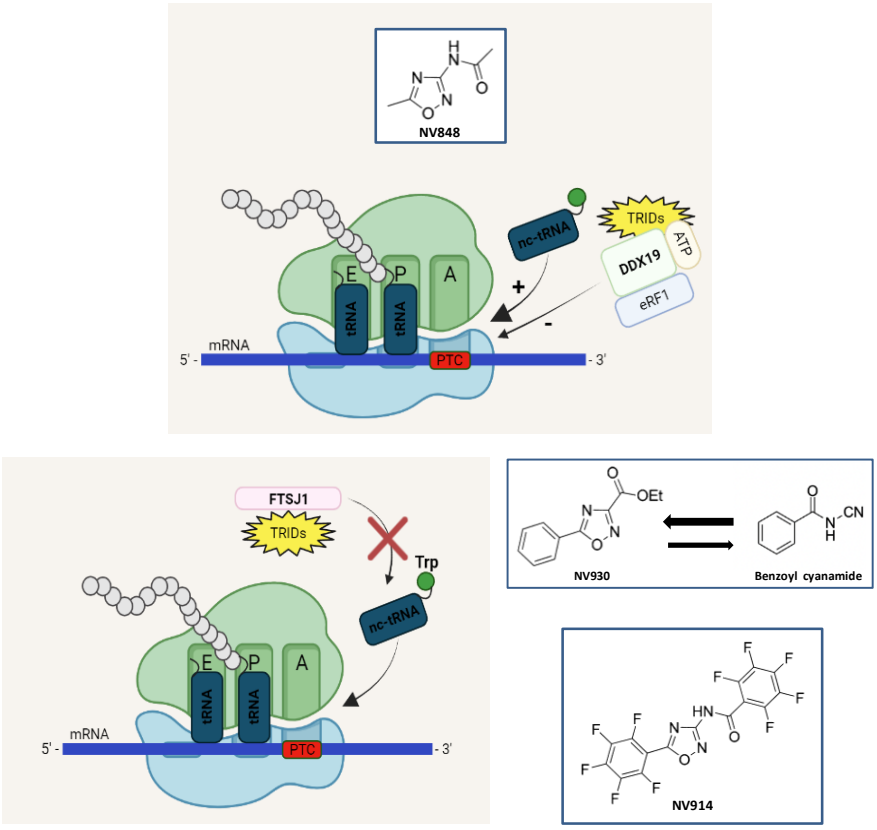

Figure 54: *NV848, NV914, and NV930 proposed models of the mechanism of action (MOA). NV848 could not interact directly with the ribosome, but it could interfere with translation termination factors such as DDX19 or eRFs. Moreover, NV914 and NV930 appear to inhibit the methyltransferase FTSJ1, and that increases the recognition probability of the UGA stop codon by tRNA^{Trp}. nc-tRNA: near-cognate tRNA.*

As regards, the final step of this work, four new TRIDs (non-oxadiazole core structures) named NV2899, NV2909, NV2913, and NV2907 were studied to have other eventual readthrough agents if the above-cited molecules will be not functional in the future applications. These new TRIDs exhibited low toxicity and readthrough capacity (except for NV2913), in order to rescue CFTR localization in FRT-CFTR^{G542X} cells.
Validation and selection of new TRIDs are central goals for the research of effective cure of nonsense-related CF. In fact, the efficiency of readthrough agents in CF patients could be different with respect to *in vitro* experimental evidence.

CONCLUSIONS.

In conclusion, the treatment with *kinetin* and RECTAS appears to be a good strategy in order to modulate the correct splicing of CFTR mRNAs with the T_5TG_{12} polymorphism. The results obtained in FRT cells transfected with two different vectors harboring CFTR cDNA with the T_5TG_{12} polymorphism confirm the recovery of CFTR expression in this cellular CF model system.

On the other hand, the advanced studies about NV848, NV914, and NV930 resulted in a series of important findings for the pharmacological treatment of nonsense-related CF. NV848 compound showed good metabolic stability in HLM and positive activity in order to restore CFTR functionality in human intestinal organoids CFTR$^{W1282X/dele2,3}$ by combining it with CFTR modulators.
The NV914 HLM consumption was higher compared to that of NV848, and NV930 metabolic stability was not completely clarified. A metabolite with minimal readthrough activity was found for NV930 (benzoyl cyanamide). However, NV914 and NV930 seem to show rescue activity of CFTR in CFTR$^{W1282X/dele2,3}$ human intestinal organoids, in combination with CFTR modulators.
All NV molecules would induce translational readthrough of PTCs without generating abnormal translational products as regards Cys-C and β2M, or induced p53.
Finally, the catalytic site of the methyltransferase FTSJ1 could be the target of NV914 and NV930 but not of NV848. MOA is an important aspect of the design of performing compounds in order to increase the functionality effect of readthrough agents.

This work added important evidence for what concerns the study of small molecules in the fight against CF nonsense and splicing mutations.

The possibility to use compounds, that could become drugs in the coming years, for the treatment of target and specific CF mutations, could be a significant expectation for all patients without an effective cure.

REFERENCES.

1. Ajiro M, Awaya T, Kim YJ, Iida K, Denawa M, Tanaka N, Kurosawa R, Matsushima S, Shibata S, Sakamoto T, Studer L, Krainer AR, Hagiwara M. ***Therapeutic manipulation of IKBKAP mis-splicing with a small molecule to cure familial dysautonomia***. Nat Commun. 2021 Jul 23;12(1):4507. doi: 10.1038/s41467-021-24705-5. Erratum in: Nat Commun. 2021 Oct 12;12(1):6039. PMID: 34301951; PMCID: PMC8302731.
2. Aksit MA, Bowling AD, Evans TA, Joynt AT, Osorio D, Patel S, West N, Merlo C, Sosnay PR, Cutting GR, Sharma N. ***Decreased mRNA and protein stability of W1282X limits response to modulator therapy.*** J Cyst Fibros. 2019 Sep;18(5):606-613. doi: 10.1016/j.jcf.2019.02.009. Epub 2019 Feb 23. PMID: 30803905; PMCID: PMC6706327.
3. Andersen DH. ***Cystic fibrosis of the pancreas and its relation to celiac disease: a clinical and pathologic study.*** *Am J Dis Child.* 1938;56(2):344–399. doi:10.1001/archpedi.1938.01980140114013.
4. Argent BE, Gray MA, Steward MC, Case RM (2012) ***Cell physiology of pancreatic ducts***. In: Physiology of the gastrointestinal tract, Elsevier Inc, pp 1399–1424.
5. Asha S, Vidyavathi M. ***Role of human liver microsomes in in vitro metabolism of drugs-a review***. ApplBiochemBiotechnol. 2010 Mar;160(6):1699-722. doi: 10.1007/s12010-009-8689-6. Epub 2009 Jul 7. PMID: 19582595.
6. Awatade NT, Wong SL, Hewson CK, Fawcett LK, Kicic A, Jaffe A, Waters SA. ***Human Primary Epithelial Cell Models: Promising Tools in the Era of Cystic Fibrosis Personalized Medicine***. Front Pharmacol. 2018 Dec 7;9:1429. doi: 10.3389/fphar.2018.01429. PMID: 30581387; PMCID: PMC6293199.
7. Banning A, Schiff M, Tikkanen R. ***Amlexanox provides a potential therapy for nonsense mutations in the lysosomal storage disorder Aspartylglucosaminuria***. BiochimBiophys Acta Mol Basis Dis. 2018 Mar;1864(3):668-675. doi: 10.1016/j.bbadis.2017.12.014. Epub 2017 Dec 13. PMID: 29247835.
8. Bell SC, Mall MA, Gutierrez H, Macek M, Madge S, Davies JC, Burgel PR, Tullis E, Castaños C, Castellani C, Byrnes CA, Cathcart F, Chotirmall SH, Cosgriff R, Eichler I, Fajac I, Goss CH, Drevinek P, Farrell PM, Gravelle AM, Havermans T, Mayer-Hamblett N, Kashirskaya N, Kerem E, Mathew JL, McKone EF, Naehrlich L, Nasr SZ, Oates GR, O'Neill C, Pypops U, Raraigh KS, Rowe SM, Southern KW, Sivam S, Stephenson AL, Zampoli M, Ratjen F.***The future of cystic fibrosis care: a global perspective***. Lancet Respir Med. 2020 Jan;8(1):65-124. doi: 10.1016/S2213-2600(19)30337-6. Epub 2019 Sep 27. Erratum in: Lancet Respir Med. 2019 Dec;7(12):e40. PMID: 31570318; PMCID: PMC8862661.
9. Benhabiles H, Gonzalez-Hilarion S, Amand S, Bailly C, Prévotat A, Reix P, Hubert D, Adriaenssens E, Rebuffat S, Tulasne D, Lejeune F. ***Optimized approach for the identification of highly efficient correctors of nonsense mutations in human diseases***. PLoS One. 2017 Nov 13;12(11):e0187930. doi: 10.1371/journal.pone.0187930. PMID: 29131862; PMCID: PMC5683606.
10. Bergougnoux A, Délétang K, Pommier A, Varilh J, Houriez F, Altieri JP, Koenig M, Férec C, Claustres M, Lalau G, Bienvenu T, Audrézet MP, Pagin A, Girodon E, Raynal C, Taulan-Cadars M. ***Functional characterization and phenotypic spectrum of three recurrent disease-causing deep intronic variants of the CFTR gene***. J Cyst Fibros. 2019 Jul;18(4):468-475. doi: 10.1016/j.jcf.2018.10.012. Epub 2018 Oct 30. PMID: 30389601.
11. Berkers G, van Mourik P, Vonk AM, Kruisselbrink E, Dekkers JF, de Winter-de Groot KM, Arets HGM, Marck-van der Wilt REP, Dijkema JS, Vanderschuren MM, Houwen RHJ, Heijerman HGM, van de Graaf EA, Elias SG, Majoor CJ, Koppelman GH, Roukema J, Bakker M, Janssens HM, van der Meer R, Vries RGJ, Clevers HC, de Jonge HR, Beekman JM, van der Ent CK. ***Rectal Organoids Enable Personalized Treatment of Cystic Fibrosis***. Cell Rep. 2019 Feb 12;26(7):1701-1708.e3. doi: 10.1016/j.celrep.2019.01.068. PMID: 30759382.
12. Boyle MP, De Boeck K. ***A new era in the treatment of cystic fibrosis: correction of the underlying CFTR defect.*** Lancet Respir Med. 2013 Apr;1(2):158-63. doi: 10.1016/S2213-2600(12)70057-7. Epub 2013 Jan 30. Erratum in: Lancet Respir Med. 2013 Apr;1(2):101. PMID: 24429096.
13. Burke JF, Mogg AE**.** ***Suppression of a nonsense mutation in mammalian cells in vivo by the aminoglycoside antibiotics G-418 and paromomycin***. Nucleic Acids Res. 1985 Sep 11;13(17):6265-72. doi: 10.1093/nar/13.17.6265. PMID: 2995924; PMCID: PMC321951.

14. ClinicalTrials.gov Identifier: NCT04135495. ***A phase 2 study to evaluate the safety, tolerability, PK and PD of ELX-02 in cystic fibrosis patients with G542X allele***.
15. Corrao F, Zizzo MG, Tutone M, Melfi R, Fiduccia I, Carollo PS, Leonardo AD, Caldara G, Perriera R, Pace A, Belmonte B, Sammataro S, Pibiri I, Lentini L. ***Nonsense codonssuppression. An acute toxicity study of threeoptimizedTRIDs in murine model, safety and tolerabilityevaluation***. BiomedPharmacother. 2022 Oct18;156:113886. doi: 10.1016/j.biopha.2022.113886. Epubahead of print. PMID: 36265311.
16. Crawford DK, Alroy I, Sharpe N, Goddeeris MM, Williams G. ***ELX-02 Generates Protein via Premature Stop Codon Read-Through without Inducing Native Stop Codon Read-Through Proteins***. J PharmacolExpTher. 2020 Aug;374(2):264-272. doi: 10.1124/jpet.120.265595. Epub 2020 May 6. PMID: 32376628.
17. Crawford DK, Mullenders J, Pott J, Boj SF, Landskroner-Eiger S, Goddeeris MM. ***Targeting G542X CFTR nonsense alleles with ELX-02 restores CFTR function in human-derived intestinal organoids***. J Cyst Fibros. 2021 May;20(3):436-442. doi: 10.1016/j.jcf.2021.01.009. Epub 2021 Feb 5. PMID: 33558100.
18. Cutting GR. ***Cystic fibrosis genetics: from molecular understanding to clinical application***. Nat Rev Genet. 2015 Jan;16(1):45-56. doi: 10.1038/nrg3849. Epub 2014 Nov 18. PMID: 25404111; PMCID: PMC4364438.
19. Davies JC, Van de Steen O, van Koningsbruggen-Rietschel S, Drevinek P, Derichs N, McKone EF, Kanters D, Allamassey L, Namour F, de Kock H, Conrath K. ***GLPG1837, a CFTR potentiator, in p.Gly551Asp (G551D)-CF patients: An open-label, single-arm, phase 2a study (SAPHIRA1)***. J Cyst Fibros. 2019 Sep;18(5):693-699. doi: 10.1016/j.jcf.2019.05.006. Epub 2019 May 27. PMID: 31147302.
20. De Boeck K. ***Cystic fibrosis in the year 2020: A disease with a new face***. Acta Paediatr. 2020 May;109(5):893-899. doi: 10.1111/apa.15155. Epub 2020 Jan 22. PMID: 31899933.
21. Deletang K, Taulan-Cadars M. ***Splicing mutations in the CFTR gene as therapeutic targets***. Gene Ther. 2022 Aug;29(7-8):399-406. doi: 10.1038/s41434-022-00347-0. Epub 2022 Jun 2. PMID: 35650428; PMCID: PMC9385490.
22. Donaldson SH, Pilewski JM, Griese M, Cooke J, Viswanathan L, Tullis E, Davies JC, Lekstrom-Himes JA, Wang LT; VX11-661-101 Study Group. ***Tezacaftor/Ivacaftor in Subjects with Cystic Fibrosis and F508del/F508del-CFTR or F508 del/G551D-CFTR***. Am J Respir Crit Care Med. 2018 Jan 15;197(2):214-224. doi: 10.1164/rccm.201704-0717OC. PMID: 28930490; PMCID: PMC5768901.
23. Elborn JS. ***Adult Care in Cystic Fibrosis***. Semin Respir Crit Care Med. 2019 Dec;40(6):857-868. doi: 10.1055/s-0039-3400289. Epub 2019 Dec 30. PMID: 31887770.
24. Floquet C, Hatin I, Rousset JP, Bidou L. ***Statistical analysis of readthrough levels for nonsense mutations in mammalian cells reveals a major determinant of response to gentamicin***. PLoS Genet. 2012;8(3):e1002608. doi: 10.1371/journal.pgen.1002608. Epub 2012 Mar 29. PMID: 22479203; PMCID: PMC3315467.
25. Fukuda R, Okiyoneda T. ***Cystic Fibrosis Transmembrane Conductance Regulator (CFTR) Ubiquitylation as a Novel Pharmaceutical Target for Cystic Fibrosis***. Pharmaceuticals (Basel). 2020 Apr 22;13(4):75. doi: 10.3390/ph13040075. PMID: 32331485; PMCID: PMC7243099.
26. Gabel ME, Galante GJ, Freedman SD. ***Gastrointestinal and Hepatobiliary Disease in Cystic Fibrosis***. Semin Respir Crit Care Med. 2019 Dec;40(6):825-841. doi: 10.1055/s-0039-1697591. Epub 2019 Oct 28. PMID: 31659728.
27. Galietta LV, Jayaraman S, Verkman AS. ***Cell-based assay for high-throughput quantitative screening of CFTR chloride transport agonists.*** Am J Physiol Cell Physiol. 2001 Nov;281(5):C1734-42. doi: 10.1152/ajpcell.2001.281.5.C1734. PMID: 11600438.
28. Gencel-Augusto J, Lozano G. ***p53 tetramerization: at the center of the dominant-negative effect of mutant p53***. GenesDev. 2020 Sep 1;34(17-18):1128-1146. doi: 10.1101/gad.340976.120. PMID: 32873579; PMCID: PMC7462067.
29. Gentzsch M, Mall MA. ***Ion Channel Modulators in Cystic Fibrosis***. Chest. 2018 Aug;154(2):383-393. doi: 10.1016/j.chest.2018.04.036. Epub 2018 May 8. PMID: 29750923; PMCID: PMC6113631.
30. Georgakilas AG, Martin OA, Bonner WM**.** ***p21: A Two-Faced Genome Guardian***. Trends Mol Med. 2017 Apr;23(4):310-319. doi: 10.1016/j.molmed.2017.02.001. Epub 2017 Mar 7. PMID: 28279624.
31. Gill KL, Houston JB, Galetin A. ***Characterization of in vitro glucuronidation clearance of a range of drugs in human kidney microsomes: comparison with liver and intestinal glucuronidation and impact***

of albumin. Drug MetabDispos. 2012 Apr;40(4):825-35. doi: 10.1124/dmd.111.043984. Epub 2012 Jan 24. PMID: 22275465; PMCID: PMC3310423.

32. Grover R, Candeias MM, Fåhraeus R, Das S. ***p53 and little brother p53/47: linking IRES activities with protein functions***. Oncogene. 2009 Jul 30;28(30):2766-72. doi: 10.1038/onc.2009.138. Epub 2009 Jun 1. PMID: 19483723.
33. Guiu J, Jensen KB. ***In Vivo Studies Should Take Priority When Defining Mechanisms of Intestinal Crypt Morphogenesis***. Cell Mol Gastroenterol Hepatol. 2022;13(1):1-3. doi: 10.1016/j.jcmgh.2021.06.028. Epub 2021 Sep 22. PMID: 34562638; PMCID: PMC8600083.
34. Haggie PM, Phuan PW, Tan JA, Xu H, Avramescu RG, Perdomo D, Zlock L, Nielson DW, Finkbeiner WE, Lukacs GL, Verkman AS. ***Correctors and Potentiators Rescue Function of the Truncated W1282X-Cystic Fibrosis Transmembrane Regulator (CFTR) Translation Product***. J Biol Chem. 2017 Jan 20;292(3):771-785. doi: 10.1074/jbc.M116.764720. Epub 2016 Nov 28. PMID: 27895116; PMCID: PMC5247652.
35. Hegyi P, Wilschanski M, Muallem S, Lukacs GL, Sahin-Tóth M, Uc A, Gray MA, Rakonczay Z Jr, Maléth J. ***CFTR: A New Horizon in the Pathomechanism and Treatment of Pancreatitis***. RevPhysiolBiochemPharmacol. 2016;170:37-66. doi: 10.1007/112_2015_5002. PMID: 26856995; PMCID: PMC5232416.
36. Heijerman HGM, McKone EF, Downey DG, Van Braeckel E, Rowe SM, Tullis E, Mall MA, Welter JJ, Ramsey BW, McKee CM, Marigowda G, Moskowitz SM, Waltz D, Sosnay PR, Simard C, Ahluwalia N, Xuan F, Zhang Y, Taylor-Cousar JL, McCoy KS; VX17-445-103 Trial Group. ***Efficacy and safety of the elexacaftor plus tezacaftor plus ivacaftor combination regimen in people with cystic fibrosis homozygous for the F508del mutation: a double-blind, randomised, phase 3 trial.*** Lancet. 2019 Nov 23;394(10212):1940-1948. doi: 10.1016/S0140-6736(19)32597-8. Epub 2019 Oct 31. Erratum in: Lancet. 2020 May 30;395(10238):1694. PMID: 31679946; PMCID: PMC7571408.
37. Heijerman HGM, McKone EF, Downey DG, Van Braeckel E, Rowe SM, Tullis E, Mall MA, Welter JJ, Ramsey BW, McKee CM, Marigowda G, Moskowitz SM, Waltz D, Sosnay PR, Simard C, Ahluwalia N, Xuan F, Zhang Y, Taylor-Cousar JL, McCoy KS; VX17-445-103 Trial Group. ***Efficacy and safety of the elexacaftor plus tezacaftor plus ivacaftor combination regimen in people with cystic fibrosis homozygous for the F508del mutation: a double-blind, randomised, phase 3 trial***. Lancet. 2019 Nov 23;394(10212):1940-1948. doi: 10.1016/S0140-6736(19)32597-8. Epub 2019 Oct 31. Erratum in: Lancet. 2020 May 30;395(10238):1694. PMID: 31679946; PMCID: PMC7571408.
38. Hu J, Cao J, Topatana W, Juengpanich S, Li S, Zhang B, Shen J, Cai L, Cai X, Chen M**.** ***Targeting mutant p53 for cancer therapy: direct and indirect strategies*****.**JHematolOncol. 2021 Sep 28;14(1):157. doi: 10.1186/s13045-021-01169-0. PMID: 34583722; PMCID: PMC8480024.
39. Huang S, Bhattacharya A, Ghelfi MD, Li H, Fritsch C, Chenoweth DM, Goldman YE, Cooperman BS. ***Ataluren binds to multiple protein synthesis apparatus sites and competitively inhibits release factor-dependent termination***. Nat Commun. 2022 May 6;13(1):2413. doi: 10.1038/s41467-022-30080-6. PMID: 35523781; PMCID: PMC9076611.
40. Kanda T, Sullivan KF, Wahl GM. ***Histone-GFP fusion proteinenables sensitive analysis of chromosome dynamics in living mammaliancells***. CurrBiol. 1998 Mar 26;8(7):377-85. doi: 10.1016/s0960-9822(98)70156-3. PMID: 9545195.
41. Kerem B, Rommens JM, Buchanan JA, Markiewicz D, Cox TK, Chakravarti A, Buchwald M, Tsui LC. ***Identification of the cystic fibrosis gene: genetic analysis***. Science. 1989 Sep 8;245(4922):1073-80. doi: 10.1126/science.2570460. PMID: 2570460.
42. Kerem E, Konstan MW, De Boeck K, Accurso FJ, Sermet-Gaudelus I, Wilschanski M, Elborn JS, Melotti P, Bronsveld I, Fajac I, Malfroot A, Rosenbluth DB, Walker PA, McColley SA, Knoop C, Quattrucci S, Rietschel E, Zeitlin PL, Barth J, Elfring GL, Welch EM, Branstrom A, Spiegel RJ, Peltz SW, Ajayi T, Rowe SM; Cystic Fibrosis Ataluren Study Group. ***Ataluren for the treatment of nonsense-mutation cystic fibrosis: a randomised, double-blind, placebo-controlled phase 3 trial***. Lancet Respir Med. 2014 Jul;2(7):539-47. doi: 10.1016/S2213-2600(14)70100-6. Epub 2014 May 15. PMID: 24836205; PMCID: PMC4154311.
43. Kleizen B, Hunt JF, Callebaut I, Hwang TC, Sermet-Gaudelus I, Hafkemeyer S, Sheppard DN. ***CFTR: New insights into structure and function and implications for modulation by small molecules***. J Cyst Fibros. 2020 Mar;19 Suppl1:S19-S24. doi: 10.1016/j.jcf.2019.10.021. Epub 2019 Nov 21. PMID: 31759907.

44. Knowles MR, Boucher RC. ***Mucus clearance as a primary innate defense mechanism for mammalianairways***. J Clin Invest. 2002 Mar;109(5):571-7. doi: 10.1172/JCI15217. PMID: 11877463; PMCID: PMC150901.
45. Kong R, Ma J, Hwang S, Moon YC, Welch EM, Weetall M, Colacino JM, Almstead N, Babiak J, Goodwin E. ***In vitro metabolism, reaction phenotyping, enzyme kinetics, CYP inhibition and induction potential of ataluren.***Pharmacol Res Perspect. 2020 Apr;8(2):e00576. doi: 10.1002/prp2.576. PMID: 32196986; PMCID: PMC7083565.
46. Laselva O, Eckford PD, Bartlett C, Ouyang H, Gunawardena TN, Gonska T, Moraes TJ, Bear CE. ***Functional rescue of c.3846G>A (W1282X) in patient-derived nasal cultures achieved by inhibition of nonsense mediated decay and protein modulators with complementary mechanisms of action***. J Cyst Fibros. 2020 Sep;19(5):717-727. doi: 10.1016/j.jcf.2019.12.001. Epub 2019 Dec 9. PMID: 31831337.
47. Laselva O, Guerra L, Castellani S, Favia M, Di Gioia S, Conese M. ***Small-molecule drugs for cystic fibrosis: Where are we now?***PulmPharmacolTher. 2022 Feb;72:102098. doi: 10.1016/j.pupt.2021.102098. Epub 2021 Nov 15. PMID: 34793977.
48. Leubitz A, Frydman-Marom A, Sharpe N, van Duzer J, Campbell KCM, Vanhoutte F. ***Safety, Tolerability, and Pharmacokinetics of Single Ascending Doses of ELX-02, a Potential Treatment for Genetic Disorders Caused by Nonsense Mutations, in Healthy Volunteers***. Clin Pharmacol Drug Dev. 2019 Nov;8(8):984-994. doi: 10.1002/cpdd.647. Epub 2019 Jan 16. PMID: 30650260.
49. Leushacke M, Barker N. ***Ex vivo culture of the intestinal epithelium: strategies and applications***. Gut. 2014 Aug;63(8):1345-54. doi: 10.1136/gutjnl-2014-307204. Epub 2014 May 19. PMID: 24841573.
50. Linsdell P. ***Architecture and functional properties of the CFTR channel pore***. Cell Mol Life Sci. 2017 Jan;74(1):67-83. doi: 10.1007/s00018-016-2389-5. Epub 2016 Oct 3. PMID: 27699452.
51. Liu F, Zhang Z, Csanády L, Gadsby DC, Chen J. ***Molecular Structure of the Human CFTR Ion Channel***. Cell. 2017 Mar 23;169(1):85-95.e8. doi: 10.1016/j.cell.2017.02.024. PMID: 28340353.
52. Loughran G, Jungreis I, Tzani I, Power M, Dmitriev RI, Ivanov IP, Kellis M, Atkins JF. Stop codon readthrough generates a C-terminally extended variant of the human vitamin D receptor with reduced calcitriol response. J Biol Chem. 2018 Mar 23;293(12):4434-4444. doi: 10.1074/jbc.M117.818526. Epub 2018 Jan 31. PMID: 29386352; PMCID: PMC5868278.
53. Mailliot J, Vivoli-Vega M, Schaffitzel C. ***No-nonsense: insights into the functional interplay of nonsense-mediated mRNA decay factors***. Biochem J. 2022 May 13;479(9):973-993. doi: 10.1042/BCJ20210556. PMID: 35551602; PMCID: PMC9162471.
54. McHugh DR, Cotton CU, Hodges CA. ***Synergy between Readthrough and Nonsense Mediated Decay Inhibition in a Murine Model of Cystic Fibrosis Nonsense Mutations***. Int J Mol Sci. 2020 Dec 31;22(1):344. doi: 10.3390/ijms22010344. PMID: 33396210; PMCID: PMC7794695.
55. Middleton PG, Mall MA, Dřevínek P, Lands LC, McKone EF, Polineni D, Ramsey BW, Taylor-Cousar JL, Tullis E, Vermeulen F, Marigowda G, McKee CM, Moskowitz SM, Nair N, Savage J, Simard C, Tian S, Waltz D, Xuan F, Rowe SM, Jain R; VX17-445-102 Study Group. ***Elexacaftor-Tezacaftor-Ivacaftor for Cystic Fibrosis with a Single Phe508del Allele***. N Engl J Med. 2019 Nov 7;381(19):1809-1819. doi: 10.1056/NEJMoa1908639. Epub 2019 Oct 31. PMID: 31697873; PMCID: PMC7282384.
56. Mihályi C, Iordanov I, Töröcsik B, Csanády L. ***Simple binding of proteinkinase A prior to phosphorylationallows CFTR anionchannels to be opened by nucleotides***. Proc NatlAcad Sci U S A. 2020 Sep 1;117(35):21740-21746. doi: 10.1073/pnas.2007910117. Epub 2020 Aug 17. PMID: 32817533; PMCID: PMC7474675.
57. Morkous SS. ***Treatment with Ataluren for Duchene Muscular Dystrophy***. PediatrNeurol Briefs. 2020 Dec 4;34:12. doi: 10.15844/pedneurbriefs-34-12. PMID: 33304086; PMCID: PMC7718099.
58. Neu-Yilik G, Raimondeau E, Eliseev B, Yeramala L, Amthor B, Deniaud A, Huard K, Kerschgens K, Hentze MW, Schaffitzel C, Kulozik AE. ***Dual function of UPF3B in early and late translation termination***. EMBO J. 2017 Oct 16;36(20):2968-2986. doi: 10.15252/embj.201797079. Epub 2017 Sep 12. PMID: 28899899; PMCID: PMC5641913.
59. Palma M, Lejeune F. ***Deciphering the molecular mechanism of stop codon readthrough***. Biol Rev CambPhilos Soc. 2021 Feb;96(1):310-329. doi: 10.1111/brv.12657. Epub 2020 Oct 22. PMID: 33089614.
60. Paulus W, Baur I, Boyce FM, Breakefield XO, Reeves SA. ***Self-contained, tetracycline-regulated retroviral vector system for gene delivery to mammalian cells***. J Virol. 1996;70(1):62-67. doi:10.1128/JVI.70.1.62-67.1996.

61. Pear WS, Nolan GP, Scott ML, Baltimore D. ***Production of high-titerhelper-free retroviruses by transienttransfection***. Proc NatlAcad Sci U S A. 1993 Sep 15;90(18):8392-6. doi: 10.1073/pnas.90.18.8392. PMID: 7690960; PMCID: PMC47362.
62. Pibiri I, Lentini L, Melfi R, Tutone M, Baldassano S, Ricco Galluzzo P, Di Leonardo A, Pace A. ***Rescuing the CFTR protein function: Introducing 1,3,4-oxadiazoles as translational readthrough inducing drugs***. Eur J Med Chem. 2018 Nov 5;159:126-142. doi: 10.1016/j.ejmech.2018.09.057. Epub 2018 Sep 26. PMID: 30278331.
63. Pibiri I, Melfi R, Tutone M, Di Leonardo A, Pace A, Lentini L. Targeting Nonsense: ***Optimization of 1,2,4-Oxadiazole TRIDs to Rescue CFTR Expression and Functionality in Cystic Fibrosis Cell Model Systems***. Int J Mol Sci. 2020 Sep 3;21(17):6420. doi: 10.3390/ijms21176420. PMID: 32899265; PMCID: PMC7504161.
64. Pierandrei S, Blaconà G, Fabrizzi B, Cimino G, Cirilli N, Caporelli N, Angeloni A, Cipolli M, Lucarelli M. ***Two novel and correlated CF-causing insertions in the (TG)mTn tract of the CFTR gene***. PLoS One. 2019 Oct 8;14(10):e0222838. doi: 10.1371/journal.pone.0222838. PMID: 31593572; PMCID: PMC6782095.
65. Pranke I, Golec A, Hinzpeter A, Edelman A, Sermet-Gaudelus I. ***Emerging Therapeutic Approaches for Cystic Fibrosis. From Gene Editing to Personalized Medicine***. Front Pharmacol. 2019 Feb 27;10:121. doi: 10.3389/fphar.2019.00121. PMID: 30873022; PMCID: PMC6400831.
66. Prokhorova I, Altman RB, Djumagulov M, Shrestha JP, Urzhumtsev A, Ferguson A, Chang CT, Yusupov M, Blanchard SC, Yusupova G. ***Aminoglycoside interactions and impacts on the eukaryotic ribosome***. Proc Natl Acad Sci U S A. 2017 Dec 19;114(51):E10899-E10908. doi: 10.1073/pnas.1715501114. Epub 2017 Dec 5. PMID: 29208708; PMCID: PMC5754804.
67. Ramalho AS, Boon M, Proesmans M, Vermeulen F, Carlon MS, Boeck K. ***Assays of CFTR Function In Vitro, Ex Vivo and In Vivo***. Int J Mol Sci. 2022 Jan 27;23(3):1437. doi: 10.3390/ijms23031437. PMID: 35163362; PMCID: PMC8836180.
68. Ridley K, Condren M. Elexacaftor-Tezacaftor-Ivacaftor: ***The First Triple-Combination Cystic Fibrosis Transmembrane Conductance Regulator Modulating Therapy***. J PediatrPharmacolTher. 2020;25(3):192-197. doi: 10.5863/1551-6776-25.3.192. PMID: 32265602; PMCID: PMC7134581.
69. Riordan JR, Rommens JM, Kerem B, Alon N, Rozmahel R, Grzelczak Z, Zielenski J, Lok S, Plavsic N, Chou JL, et al. ***Identification of the cystic fibrosis gene: cloning and characterization of complementary DNA***. Science. 1989 Sep 8;245(4922):1066-73. doi: 10.1126/science.2475911. Erratum in: Science 1989 Sep 29;245(4925):1437. PMID: 2475911.
70. Rizzotto D, Englmaier L, Villunger A. ***At a Crossroads to Cancer: How p53-Induced Cell Fate Decisions Secure Genome Integrity***. Int J Mol Sci. 2021 Oct 8;22(19):10883. doi: 10.3390/ijms221910883. PMID: 34639222; PMCID: PMC8509445.
71. Rommens JM, Iannuzzi MC, Kerem B, Drumm ML, Melmer G, Dean M, Rozmahel R, Cole JL, Kennedy D, Hidaka N, et al. ***Identification of the cystic fibrosis gene: chromosome walking and jumping***. Science. 1989 Sep 8;245(4922):1059-65. doi: 10.1126/science.2772657. PMID: 2772657.
72. Roy B, Friesen WJ, Tomizawa Y, Leszyk JD, Zhuo J, Johnson B, Dakka J, Trotta CR, Xue X, Mutyam V, Keeling KM, Mobley JA, Rowe SM, Bedwell DM, Welch EM, Jacobson A. ***Ataluren stimulates ribosomal selection of near-cognate tRNAs to promote nonsense suppression***. Proc Natl Acad Sci U S A. 2016 Nov 1;113(44):12508-12513. doi: 10.1073/pnas.1605336113. Epub 2016 Oct 4. PMID: 27702906; PMCID: PMC5098639.
73. Saint-Criq V, Gray MA**.** ***Role of CFTR in epithelial physiology***. Cell Mol Life Sci. 2017 Jan;74(1):93-115. doi: 10.1007/s00018-016-2391-y. Epub 2016 Oct 6. PMID: 27714410; PMCID: PMC5209439.
74. Salani M, Urbina F, Brenner A, Morini E, Shetty R, Gallagher CS, Law EA, Sunshine S, Finneran DJ, Johnson G, Minor L, Slaugenhaupt SA**.** ***Development of a Screening Platform to Identify Small Molecules That Modify ELP1 Pre-mRNA Splicing in Familial Dysautonomia***. SLAS Discov. 2019 Jan;24(1):57-67. doi: 10.1177/2472555218792264. Epub 2018 Aug 7. PMID: 30085848.
75. Sheppard DN, Carson MR, Ostedgaard LS, Denning GM, Welsh MJ. ***Expression of cystic fibrosis transmembrane conductance regulator in a model epithelium.*** Am J Physiol. 1994 Apr;266(4 Pt 1):L405-13. doi: 10.1152/ajplung.1994.266.4.L405. PMID: 7513963.
76. Strong TV, Boehm K, Collins FS**.** ***Localization of cystic fibrosis transmembrane conductance regulator mRNA in the human gastrointestinal tract by in situ hybridization***. J Clin Invest. 1994 Jan;93(1):347-54. doi: 10.1172/JCI116966. PMID: 7506713; PMCID: PMC293778.

77. Strub MD, McCray PB Jr. ***Transcriptomic and Proteostasis Networks of CFTR and the Development of Small Molecule Modulators for the Treatment of Cystic Fibrosis Lung Disease***. Genes (Basel). 2020 May 13;11(5):546. doi: 10.3390/genes11050546. PMID: 32414011; PMCID: PMC7288469.
78. Taelman J, Diaz M, Guiu J**. *Human Intestinal Organoids: Promise and Challenge***. Front Cell Dev Biol. 2022 Mar 11;10:854740. doi: 10.3389/fcell.2022.854740. PMID: 35359445; PMCID: PMC8962662.
79. Tanaka T, Watanabe M, Yamashita K. ***Potential therapeutic targets of TP53 gene in the context of its classically canonical functions and its latest non-canonical functions in human cancer***. Oncotarget. 2018 Mar 23;9(22):16234-16247. doi: 10.18632/oncotarget.24611. PMID: 29662640; PMCID: PMC5882331.
80. Taylor-Cousar JL, Mall MA, Ramsey BW, McKone EF, Tullis E, Marigowda G, McKee CM, Waltz D, Moskowitz SM, Savage J, Xuan F, Rowe SM**. *Clinical development of triple-combination CFTR modulators for cystic fibrosis patients with one or two F508del alleles***. ERJ Open Res. 2019 Jun 17;5(2):00082-2019. doi: 10.1183/23120541.00082-2019. PMID: 31218221; PMCID: PMC6571452.
81. Tewkesbury DH, Robey RC, Barry PJ. ***Progress in precision medicine in cystic fibrosis: a focus on CFTR modulator therapy***. Breathe (Sheff). 2021 Dec;17(4):210112. doi: 10.1183/20734735.0112-2021. PMID: 35035569; PMCID: PMC8753614.
82. Trzaska C, Amand S, Bailly C, Leroy C, Marchand V, Duvernois-Berthet E, Saliou JM, Benhabiles H, Werkmeister E, Chassat T, Guilbert R, Hannebique D, Mouray A, Copin MC, Moreau PA, Adriaenssens E, Kulozik A, Westhof E, Tulasne D, Motorin Y, Rebuffat S, Lejeune F. ***2,6-Diaminopurine as a highly potent corrector of UGA nonsense mutations***. Nat Commun. 2020 Mar 20;11(1):1509. doi: 10.1038/s41467-020-15140-z. PMID: 32198346; PMCID: PMC7083880.
83. Tutone M, Pibiri I, Perriera R, Campofelice A, Culletta G, Melfi R, Pace A, Almerico AM, Lentini L. ***Pharmacophore-Based Design of New Chemical Scaffolds as Translational Readthrough-Inducing Drugs (TRIDs).*** ACS Med Chem Lett. 2020 Feb 18;11(5):747-753. doi: 10.1021/acsmedchemlett.9b00609. PMID: 32435380; PMCID: PMC7236267.
84. Van Mourik P, Beekman JM, van der Ent CK. ***Intestinal organoids to model cystic fibrosis***. Eur Respir J. 2019 Jul 4;54(1):1802379. doi: 10.1183/13993003.02379-2018. PMID: 31023844.
85. Venturini A, Borrelli A, Musante I, Scudieri P, Capurro V, Renda M, Pedemonte N, Galietta LJV. Comprehensive ***Analysis of Combinatorial Pharmacological Treatments to Correct Nonsense Mutations in the CFTR Gene***. Int J Mol Sci. 2021 Nov 4;22(21):11972. doi: 10.3390/ijms222111972. PMID: 34769402; PMCID: PMC8584557.
86. Vonk AM, van Mourik P, Ramalho AS, Silva IAL, Statia M, Kruisselbrink E, Suen SWF, Dekkers JF, Vleggaar FP, Houwen RHJ, Mullenders J, Boj SF, Vries R, Amaral MD, de Boeck K, van der Ent CK, Beekman JM. ***Protocol for Application, Standardization and Validation of the Forskolin-Induced Swelling Assay in Cystic Fibrosis Human Colon Organoids***. STAR Protoc. 2020 Jun 3;1(1):100019. doi: 10.1016/j.xpro.2020.100019. PMID: 33111074; PMCID: PMC7580120.
87. Wainwright CE, Elborn JS, Ramsey BW, Marigowda G, Huang X, Cipolli M, Colombo C, Davies JC, De Boeck K, Flume PA, Konstan MW, McColley SA, McCoy K, McKone EF, Munck A, Ratjen F, Rowe SM, Waltz D, Boyle MP; TRAFFIC Study Group; TRANSPORT Study Group. ***Lumacaftor-Ivacaftor in Patients with Cystic Fibrosis Homozygous for Phe508del CFTR***. N Engl J Med. 2015 Jul 16;373(3):220-31. doi: 10.1056/NEJMoa1409547. Epub 2015 May 17. PMID: 25981758; PMCID: PMC4764353.
88. Wangen JR, Green R. ***Stop codon context influences genome-wide stimulation of termination codon readthrough by aminoglycosides***. Elife. 2020 Jan 23;9:e52611. doi: 10.7554/eLife.52611. PMID: 31971508; PMCID: PMC7089771.
89. Wine JJ. ***How the sweatglandrevealslevels of CFTR activity***. J CystFibros. 2022 May;21(3):396-406. doi: 10.1016/j.jcf.2022.02.001. Epub 2022 Feb 17. PMID: 35184981.
90. Xue X, Mutyam V, Thakerar A, Mobley J, Bridges RJ, Rowe SM, Keeling KM, Bedwell DM. ***Identification of the amino acids inserted during suppression of CFTR nonsense mutations and determination of their functional consequences***. Hum Mol Genet. 2017 Aug 15;26(16):3116-3129. doi: 10.1093/hmg/ddx196. PMID: 28575328; PMCID: PMC5886253.
91. Yeh HI, Sohma Y, Conrath K, Hwang TC. A common mechanism for CFTR potentiators. J Gen Physiol. 2017 Dec 4;149(12):1105-1118. doi: 10.1085/jgp.201711886. Epub 2017 Oct 27. PMID: 29079713; PMCID: PMC5715911.

92. Yeh JT, Yu YC, Hwang TC. ***Structural mechanisms for defective CFTR gating caused by the Q1412X mutation, a severe Class VI pathogenic mutation in cystic fibrosis***. J Physiol. 2019 Jan;597(2):543-560. doi: 10.1113/JP277042. Epub 2018 Dec 2. PMID: 30408177; PMCID: PMC6332826.
93. Yoon JC, Casella JL, Litvin M, Dobs AS. ***Male reproductive health in cystic fibrosis***. J Cyst Fibros. 2019 Oct;18 Suppl2:S105-S110. doi: 10.1016/j.jcf.2019.08.007. PMID: 31679721.
94. Yoshida M, Kataoka N, Miyauchi K, Ohe K, Iida K, Yoshida S, Nojima T, Okuno Y, Onogi H, Usui T, Takeuchi A, Hosoya T, Suzuki T, Hagiwara M. ***Rectifier of aberrant mRNA splicing recovers tRNA modification in familial dysautonomia*.** Proc Natl Acad Sci U S A. 2015 Mar 3;112(9):2764-9. doi: 10.1073/pnas.1415525112. Epub 2015 Feb 9. PMID: 25675486; PMCID: PMC4352824.
95. Zaher A, ElSaygh J, Elsori D, ElSaygh H, Sanni A. ***A Review of Trikafta: Triple CysticFibrosis Transmembrane ConductanceRegulator (CFTR) Modulator Therapy***. Cureus. 2021 Jul 3;13(7):e16144. doi: 10.7759/cureus.16144. PMID: 34268058; PMCID: PMC8266292.